UNDERSTANDING FLUID GELS AND HYDROCOLLOID TRIBOLOGY

BY

DAVID GARREC

A thesis submitted to
The University of Birmingham
for the degree of
DOCTOR OF ENGINEERING

Department of Chemical Engineering
College of Physical and Engineering Sciences
The University of Birmingham

June 2013

Abstract

This thesis seeks to expand the knowledge on fluid gels and hydrocolloid tribology from a microstructural perspective. This aim was based on recent research which has highlighted the significance of tribology for in-mouth fat-related textural analysis during oral processing and the use of hydrocolloids, including fluid gels, for the development of reduced-fat liquid and semi-solid foods. This thesis considers the microstructure of hydrocolloids in terms of understanding how fluid gel structures are controlled from their ingredients and processing conditions, and how hydrocolloid structures influence their material properties and ability to provide lubrication.

To conduct this research, preliminary work was initially carried out to develop tribometry surfaces that mimic saliva-coated oral mucosa; and, experimental procedures were developed to minimise the error margins of tribological data whilst maximising the discrimination between different lubricant structures. From that basis, the influence of hydrocolloid structure on lubrication was investigated for hydrocolloids formulated into polymeric and particulate structures.

It was shown that the microstructure of a fluid between two-rubbing surfaces determines the tribological response which cannot necessarily be predicted from that fluid's rheology. This suggests that food microstructures influence fat-related textural attributes and that tribology is an important field to study alongside rheology for the designed formulation of low-fat foods with acceptable mouth-feel. More specifically, the ability of polymeric thickeners to entrain a rubbing contact and provide lubrication was shown to be determined by chain conformation where random coils are excluded and expanded chains are entrained. For hydrocolloids formulated into particulate structures, the stiffness of the particles as well as their volume fraction were characterised and tested for their influence on lubrication. The

particles were formulated to ~ 1 μm in diameter which was similar to the tribometer surface roughness dimensions. The particles were small enough that they were not perceived as ‘grainy’ during oral consumption whilst also being large enough to provide lubrication. Friction was shown to decrease with particle stiffness suggesting that the particles lubricate the contact by separating the mating tribological surfaces where less deformable particles have the greatest effect. Additionally, the effect of salts was studied where friction was demonstrated to be dependent on salt concentration and position within the Hofmeister series. In water/salt solutions, this was shown to be a result of surface-bound hydrated ions; and, for hydrocolloid/salt solutions it was due to salt-induced adsorption of hydrated hydrocolloids to the tribometry surfaces.

From the characterisation of kappa carrageenan fluid gels, they are hypothesised to consist of particles with ‘hairs’, that is, disordered polymer chains, resultant from a disruption of the coil to helix process caused by the applied shear during their formation. This causes particle aggregation at low volume fractions and a rheological behaviour between that typical for linear-polymers and hard-spheres.

Acknowledgments

I would like to express my gratitude towards Prof. Ian Norton, Prof. Peter Lillford and Dr. Brian Guthrie for their support, guidance, encouragement and for providing me with unique opportunities and, above all, for inspiring me to value research for its significance and excitement. I would also like to thank Brian Guthrie for making me so welcome during my time spent in Minneapolis.

Within Cargill, I would also like to thank Dr. Didier Bonnet and Dr. Danièle Karleskind for their keen interest in this project, useful conversations and constant support. Additionally, I would like to thank Pat Moran and Adam Steinbach for useful discussions, help in Cargill's laboratories and for all the good memories.

Within the University of Birmingham, I would also like to thank Dr. Richard Greenwood for continued guidance, encouragement and support throughout the EngD scheme; and also to the support staff, particularly John Hooper and Lynn Draper. My thanks go to Dr. James Bowen and Theresa Morris for training and assistance with the Science City and STEM equipment, respectively.

My gratitude also goes to Cargill for funding and permission to publish research articles and this thesis; and also to the Royal Commission for the Exhibition of 1851 for funding and awarding me with an Industrial Fellowship. I would also like to thank the EPSRC for sponsorship.

I thank my friends at the University of Birmingham for all the useful as well as useless discussions, great memories, support and friendship which I will treasure forever. I thank Mum, Momo, Alan and James for their continued interest and tongue-in-cheek remarks! Finally, and most importantly, Lauren, thank you for making my EngD possible with your continued encouragement and love and for making our time in Birmingham so special.

Table of Contents

List of Figures

List of Tables

Nomenclature

Rheology

η	Apparent viscosity
$[\eta]$	Intrinsic viscosity
η_0	Zero shear viscosity
η_∞	Infinite shear viscosity
η_{rel}	Relative viscosity ($\eta_{0\ suspension}$ / $\eta_{0\ solvent}$)
η_{sp}	Relative viscosity (η_{rel} - 1)
η_s	Viscosity of solvent
$\dot{\gamma}$	Shear rate
σ	Shear stress
K	Arbitrary constant for the Ellis equation
n	Power law index for the Ellis equation
C	Arbitrary constant for the Cross equation
m	Exponent for the Cross equation
G'	Storage (elastic) modulus
G''	Loss (viscous) modulus
δ	Phase angle ($\tan^{-1} G''/G'$)
K_H	Huggins constant
K_K	Kraemer constant
p	Viscosity ratio ($\eta_{\text{ oil phase}}/\eta_{\text{ aqueous phase}}$)

Tribology

W	Normal load (N)
F_t	Tangential friction force (N)
μ	Friction coefficient (dimensionless) (F_t/W)
U_{disc}	Disc speed
U_{ball}	Ball speed
U	Entrainment speed
SRR	Slide to roll ratio [$(U_{disc} - U_{ball})/U$]
K	Arbitrary shift factor

τ	Interfacial shear strength
A	Area
a	Radius of contact area
A_r	Real area of contact
A_a	Apparent area contact
R^*	Reduced radius
E^*	Reduced elastic modulus
v	Poisons ratio

Other

R_q or RMS	Root mean square
R_a	Centre line average
o/w	Oil in water emulsion
M	Molecular weight
K'	Arbitrary constant for Mark-Houwink equation
α	Chain expansion coefficient
C^*	Critical overlap concentration
C	Concentration
g	Gravitational acceleration (9.81 mm s^{-2})
T_m	Midpoint temperature
T_{exit}	Pin stirrer exit temperature
T_{in}	Pin stirrer inlet temperature
E	Young's modulus
$\Delta H_{m\,FG}$	Enthalpy of melting a fluid gel
$\Delta H_{m\,QG}$	Enthalpy of melting a quiescent gel
ΔG_{hyd}	Gibbs free energy of hydration
N	Lyotropic number
R_{hyd}	Hydrated anion radius
θ	Water contact angle
$M_{FG.0}$	Mass of fluid gel prior to centrifugation
$M_{FG.s}$	Mass of solid component of fluid gel after centrifugation
φ_{FG}	Fluid gel solid phase volume after centrifugation

$M_{QG.0}$	Mass of quiescent gel prior to centrifugation
$M_{QG.s}$	Mass of solid component of quiescent gel after centrifugation
φ_{QG}	Quiescent gel solid phase volume after centrifugation
φ_{syn}	Syneresis phase volume
Φ	Volume fraction
Φ_{FG}	Fluid gel particle phase volume (φ_{FG} + [(1 - φ_{QG}) - φ_{syn}])
Φ_{eff}	Effective volume fraction (= kc)
k	Specific volume in mL/g
c	Concentration in g/mL
Φ_m	Maximum volume fraction
Φ_c	Critical volume fraction
h	Heat transfer coefficient
~	Approximately
wt.%	Concentration on a weight for weight basis
k_{CH}	Rate of coil to helix transition

Abbreviations

GG	Guar gum
LBG	Locust bean gum
SCL	Scleroglucan
λC	Lambda carrageenan
κC	Kappa carrageenan
XG	Xanthan gum
AFM	Atomic force microscope (microscopy)
CTS	Cargill Texturizing Solutions
DSC	Dynamic scanning calorimetry
FG	Fluid gel
IEHL	Iso-elastic hydrodynamic lubrication
Inc.	Incorporated
KD	Krieger-Dougherty
LVR	Linear viscoelastic region
MTM2	Mini Traction Machine (2nd Edition)

PDMS	Polydimethyl siloxane
HL-PDMS	Hydrophilic PDMS
NMR	Nuclear Magnetic Resonance
PEG	Poly(ethylene glycol)
PEO	poly(ethylene oxide)
PEP	poly(ethylene propylene)
PGM	Pig gastric mucin
PNIPAM	poly(*N*-isopropylacrylamide)
PPO	poly(propylene oxide)
PTFE	Polytetrafluoroethylene
QCM	Quartz crystal microbalance
QG	Quiescent gel
SAM	Self assembled monolayer
SPR	Surface Plasmon resonance
US	United States of America
USD	US Dollars
WPI	Whey protein isolate

Chapter 1.

Introduction

1.1. Background

The consumer response of food products are largely a function of their material properties. These properties are dependent on the foods' microstructure which is determined by the ingredients and the processing conditions used in the formulation. This forms the basis of a microstructural approach to food formulation engineering and is depicted schematically in Fig. 1.1. Using this approach, food products can be designed from healthy ingredients to form microstructures and material properties that provide a determined consumer response.

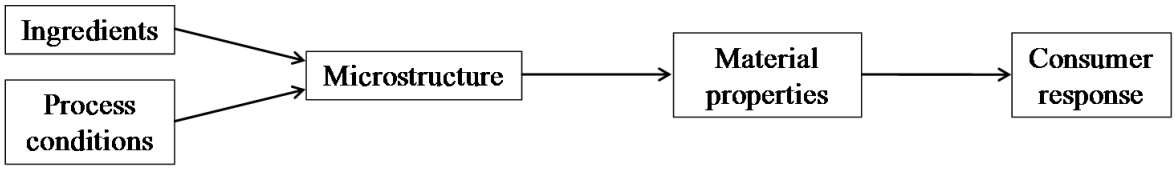

Fig. 1.1. A microstructural approach to food formulation engineering

Hydrocolloids are a class of high molecular weight polysaccharides and proteins that are widely used in aqueous solvents to impart a vast number of functions including texture, stability and thickness for use in semi-solid and liquid foods. Considering the microstructure approach for hydrocolloids, much is known on the influence of their processing on their structures and material properties. This includes the influence of sourcing and purification techniques on their structure. There is also a plethora of literature on mixing hydrocolloids with other ingredients and processing them to form thickened liquids and gels with specific material properties. For example, the rheological properties of such thickened liquids are known to depend on the hydrocolloid microstructure in terms of polymeric molecular weight, chain conformation and inter-chain interactions (Tombs and Harding, 1998; Morris *et al.*, 1981); and, the mechanical properties of gels are known to depend on the structures of the polymeric networks formed (Morris *et al.*, 1980b). This ability of hydrocolloids to structure water has been manipulated for the purpose of fat replacements in foods. This has been

achieved from a range of structures including the use of xanthan gum as a polymeric thickener in mayonnaise products (Barbara, 1998), microparticulated whey protein particles in the fat replacer Simplesse® (Singer *et al.*, 1988) and phase separated hydrocolloid mixtures of gelatin and maltoxtrin in low-fat spreads (Kasapis *et al.*, 1993b; Chronakis and Kasapis, 1995).

A relatively new application for hydrocolloids is 'fluid gels' which are formed under conditions of sheared gelation. The effect of the shear is to restrict the molecular ordering process to within discrete entities which forms gelled particles; conversely, under quiescent conditions, bulk gels are formed from the macroscopic ordering of an 'infinite' network. Fluid gels have the potential to replace a significant portion of fat in emulsion based foods without detriment to the consumer response provided the aqueous particles can be formulated to provide similar material properties to the high-fat products. This will rely on a detailed understanding of the structure of the fluid gel particles, how they are controlled and how they influence performance. Whilst significant progress has been made in this area, there is still much to be learnt.

Completing the microstructural approach to formulating hydrocolloids in food products requires the dependence of their material properties on consumer response to be well understood. An example of where this has been successful is in relating the viscosity of hydrocolloid solutions to their 'thickness' perceived during oral consumption. However, many attributes, such as 'creaminess', are more elusive to define and require data from numerous instrumental techniques for correlations between properties and perception to be made. The creaminess attribute has been ascribed as a function of thickness (viscosity), smoothness (determined by a lack of detection of the structural composition *e.g.* particulates) and slipperiness (which relates to tribology).

Tribology is the study of lubrication, friction, wear and contact mechanics and, in recent years, has emerged as a useful tool in determining fat-related textural attributes. As an example, it has been shown (Malone *et al.*, 2003) that friction measured between the rotating surfaces of a contacting ball and disc correlate well with the perception of slipperiness. It is anticipated that this strong correlation is due to the thin-film of fluid measured between the ball and disc being of similar dimensions to the films perceived during the late stages of oral processing, that is, when the tongue pushes against the hard-palate before swallowing.

In spite of the relevance of tribology in determining fat-related textural attributes and the use of hydrocolloids in reduced-fat foods, the dependence of hydrocolloid structure on tribology is poorly understood.

1.2. Objectives

Given the aforementioned gaps in the knowledge required for texturally acceptable low-fat foods using hydrocolloids, the aim of this thesis is to advance the understanding of fluid gel formation and properties, and hydrocolloid tribology. Specifically, the influence of ingredients and processing conditions on hydrocolloid microstructure, and the influence of those structures on tribology, is investigated.

To achieve this objective, fluid gels were produced and their structure and properties were thoroughly analysed using a wide range of techniques. The results of this analysis will be discussed in accordance with their formation process which was explored by controlling the ratio of sheared to quiescent gelation, thereby also probing the influence of processing conditions on fluid gel structures and properties.

The tribology of hydrocolloids will be discussed for both polymeric and particulate structures which represent two principle classes of hydrocolloid thickener (Mitchell, 2008).

Products thickened with polymers behave differently to those with particulates due to their structurally attributable flow behaviour and mixing efficiencies with saliva; the latter of which influences mass transfer and therefore the perceptions of taste and aroma. In spite of this knowledge, the influence of polymer and particulate structures on tribology, which influences texture perception, is poorly understood.

In this work, polysaccharides in a non gelled state were employed to represent polymeric thickeners and fluid gels represented particulate thickeners. The structurally attributable tribological response of polymers was explored by probing the influence of chain conformation and concentration (which influence chain entanglement) on friction. For particulate fluid gels, the effect of particle stiffness and volume fraction on friction was explored. Additionally, the influence of salts on tribology was investigated. Salts are used in foods for taste, preservation and to control rheology (*e.g.* salt induced gelation). However, the influence of salt on hydrocolloid tribology is poorly understood and so was explored by testing a range of concentrations of salts of the Hofmeister series.

1.3. Relevance to Cargill

Cargill Inc., the industrial collaborator of this study, is a privately held multinational conglomerate that primarily trades, develops and markets food and agricultural commodities. A family owned company that started business in 1865, they are now world leaders in commodity distribution employing 142,000 people in 65 countries with an annual revenue of ~ $130 billion (USD) (Cargill, 2012b). Cargill's business can be identified as five key market segments: food ingredients; agricultural services; industrial; risk management and financial; and, origination and processing. Within the food ingredients sector, Cargill Texturizing

Solutions (CTS) is a Business Unit that distributes hydrocolloids to the global food and beverage industry.

Diets high in levels of fat, salt and sugar increase the likelihood of the development of health conditions such as type II diabetes, cardiovascular diseases, strokes and increased blood pressure. Consequently, there has recently been increased pressure on the producers of processed foods to lower these levels. This pressure has come from both governmental recommendations on diets and a consumer desire for healthy alternatives (*e.g.* low-fat) to many foods. However, reduced fat alternatives are often of inferior quality and are less favoured by consumers. This is particularly problematic for the western world where consumers tend not to comprise their short-term eating pleasure for their long term health benefits.

As discussed in the previous section, hydrocolloids have the potential to structure water in a way that mimics the role of fat in determining food material properties. Additionally, understanding hydrocolloid tribology is expected to benefit the development of reduced-fat foods with desired consumer response. Therefore, since Cargill distribute hydrocolloids, the results of this thesis are of their benefit as they are in a prime position to provide the food industry's requirements of reduced fat foods with acceptable mouth-feel. Cargill's mission statement states that their "purpose is to be the global leader in nourishing people" and that their "mission is to create distinctive value"; Cargill Texturizing Solutions also state that they "provide solutions for customer success" (Cargill, 2012a). Thus, Cargill have an interest in tackling global obesity in addition to providing their customers with a detailed scientific understanding of their ingredients' uses and properties. Specifically, the results discussed in this thesis allow Cargill to advise their customers on appropriate ingredients and processes for optimising product performance.

1.4. Thesis layout

The following Chapter (Chapter 2 - Literature Review) provides a comprehensive review of relevant literature on three major topics: hydrocolloids, particulates and tribology. Then, Chapter 3 describes the materials used and the methodology conducted for the experimental analysis which is then presented in the results chapters of this thesis (Chapters 4 – 6). Chapter 3 also includes a discussion on tribometer surfaces and contains results obtained for the development of soft hydrophilic surfaces (for mimicking oral mucosa) and on a study conducted to ascertain appropriate tribometer surfaces for maximising data reproducibility and lubricant discrimination.

The results chapters then begin with Chapter 4 which discusses the results obtained in understanding the formation and properties of fluid gels. This begins with a discussion on the influence of potassium ions on fluid gel production, and then a comprehensive characterisation of fluid gels is provided on their properties and structure using data obtained from a wide range of instrumental techniques. This characterisation of fluid gels also includes their particle volume fraction, where the development of a method for determining this parameter is described. Finally, Chapter 4 concludes with a discussion on an experiment designed to control the ratio of sheared to quiescent gelation thereby probing fluid gel formation and the influence of processing on properties and structure.

Chapter 5 discusses the tribology of hydrocolloids as polymeric thickeners both with and without salts. For this, a range of polysaccharides was used that varies in chain expansion coefficient from random coils to extended chains. These were then tested tribologically as a function of their concentration in two regimes of lubrication. Thus, the influence of polysaccharide chain conformation and concentration (which also influences the structure in terms of chain overlap behaviour) on tribology is probed. The tribological dependence of salt

concentration and position within the Hofmeister series is then tested for water and polysaccharide solutions.

Chapter 6, the final results chapter, probes fluid gel properties and structures further by conducting a thorough rheological examination as a function of their volume fraction and particle stiffness. Hydrocolloid tribology is also analysed further in this chapter by studying the tribology of fluid gels, again, as a function of volume fraction and particle stiffness.

Finally, the conclusions of this thesis are summarised together with recommendations for future work (Chapter 7). Chapter 8 then gives a complete list of the sources for information used throughout the thesis.

1.5. Publications and presentations

Results obtained throughout this study have been published as follows:

Publications:

- Garrec, D. A. & Norton, I. T. 2012. The influence of hydrocolloid hydrodynamics on lubrication. *Food Hydrocolloids,* 26, 389-397.
- Garrec, D. A. & Norton, I. T. 2012. On the lubricating behaviour of kappa carrageenan gelled networks. *Gums and stabilisers for the food industry,* 16, 183-190.
- Garrec, D. A. & Norton, I. T. 2012. Boundary lubrication by sodium salts: A Hofmeister series effect. *Journal of Colloid and Interface Science*, 379, 33-40.
- Garrec, D. A. & Norton, I. T. 2012. Understanding fluid gel formation and properties. *Journal of Food Engineering*, 112, 175-182.
- Garrec, D. A., Frasch-Melnik, S., Henry, J. V. L., Spyropoulos, F. & Norton, I. T. 2012. Designing colloidal structures for micro and macro nutrient content and release in foods. *Faraday Discussions*, 158, 37-49.
- Garrec, D. A., Guthrie, B. & Norton, I. T. 2013. Kappa carrageenan fluid gel material properties. Part 1: Rheology. *Food Hydrocolloids,* 33, 151-159.
- Garrec, D. A. & Norton, I. T. 2013. Kappa carrageenan fluid gel material properties. Part 2: Tribology. *Food Hydrocolloids*, 33, 160-167.

Poster presentation:

- Garrec, D. A., Norton, I. T., Spyropoulos, F., Lillford, P. J. & Guthrie, B. Develop and test a reformulation model for in-mouth lubrication by emulsion based foods, based on time dependent rheology and tribology. *15th Gums and Stabilisers for the Food Industry*, Wrexham 2009.

Oral presentations (speaker underlined):

- Garrec, D. A., Guthrie, B., Cox, P. W. & Norton, I. T. The Influence of Hydrocolloid Structure and Bulk-Rheology on Soft-Tribology, *10th International Hydrocolloids Conference*, Shanghai 2010.
- Garrec, D. A., Guthrie, B. & Norton, I. T. Characterisation and Control of Fluid Gel Properties, *16th Gums and Stabilisers for the Food Industry*, Wageningen 2011
- Garrec, D. A., Mills, T. B. & Norton, I. T. Is rheology of any use in understanding and controlling product/human interaction*?*, *IbeReo*, Lisbon 2011
- Garrec, D. A., Guthrie, B. & Norton, I. T. Fluid gel rheology, tribology and sensory perception as a function of volume fraction and particle stiffness. *Food Structures, Digestion and Health*, New Zealand, 2012.
- Garrec, D. A., Guthrie, B. & Norton, I. T. Gel particulate rheology and tribology as a function of volume fraction and particle stiffness. *6th International Symposium on Food Rheology and Structure*, Zurich, 2012

Chapter 2.

Literature Review

2.1. Introduction

The aim of this chapter is to provide a comprehensive review of relevant literature. This will include an overview of hydrocolloid solution behaviour, and chemical and physical properties of the major hydrocolloids employed throughout the thesis. Then, the mechanisms of gelation and literature on the formation and properties of fluid gels are discussed.

Particulate suspensions are then examined in terms of fundamental theories for hard-spheres, the production and properties of microgel suspensions and their mouth-feel perception of suspensions.

The fundamental theories on tribology are then reviewed as well as the rationale for studying tribology in food research. This then leads into literature on the development of tribometers with soft surfaces, their tribological properties and examples of where tribology, and other material properties, has correlated well with the perception of mouth-feel attributes. This section then discusses literature on the influence of hydrocolloid structures on friction. Finally, the Hofmeister series is introduced along with a discussion on the impact of salts on tribology.

2.2. Hydrocolloids

2.2.1. Structures and properties

Food hydrocolloids are a class of naturally occurring polysaccharides and proteins although the work presented in this thesis is mainly focused on polysaccharides. They originate from a range of sources including botanical sources (*e.g.* trees, plants and leguminous seeds), seaweeds, microbial growth and animals (*e.g.* collagen and milk proteins) (Phillips and Williams, 2009). Hydrocolloids are hygroscopic (Torres *et al.*, 2012) and of high molecular weights (~ $0.5 – 5 \times 10^6$ g mol^{-1}) and, as such, 'bind' large volumes of water to themselves thereby increasing the viscosity of water by disrupting its flow.

The contribution of a hydrocolloid solute to solution viscosity is given by its intrinsic viscosity [η] which is principally dictated by the polymer 'shape' and 'size' (Harding, 1997). This relationship is described in the Mark-Houwink equation (Eq. 2.1) where M is the polymer molecular weight, and K' and α (a constant and the Mark-Houwink exponent, respectively) are related to the polymer conformation in solution. The α values lie between 0 and ~1.8 where 0.5 - 0.8 gives the range for polysaccharides with a random coil solution conformation, and greater values indicate enhanced stiffness (reduced flexibility), up to 1.8, for rigid-rod structures (Tombs and Harding, 1998).

$$[\eta] = K'M^{\alpha} \qquad \textit{Eq. 2.1}$$

The viscosity of a polysaccharide solution is determined by the polymers' intrinsic viscosity, its concentration and chain interactions. Polysaccharide viscosities follow a power-law dependence on concentration until reaching a critical concentration (C^*), above which a pronounced increase in that dependence occurs (Morris *et al.*, 1981). This behaviour is attributed structurally as single entity polymer chains existing in dilute conditions below C^*,

and the combined hydrodynamic radii of the chains exceeding that of the sample volume at concentrations greater than *C** where physical chain interpenetration and entangled network formation occurs (this behaviour is shown schematically in Fig. 2.1).

The remainder of this section will review the chemical polymeric structures and physical properties of the most important polysaccharides for this thesis. Guar gum (GG) and locust bean gum (LBG) galactomannans are neutral branched polysaccharides sourced from albuminous or endospermic seeds (Phillips and Williams, 2009). The linear (1→4) β-d-mannose backbone has a varying range of (1→6) α-d-galactose branches. GG and LBG, derived from the guar plant and carob tree, respectively, differ in their ratios of mannose-to-galactose where GG typically has a ratio of 2:1; and LBG, 4:1 (these structures are shown in Fig. 2.2). GG is described as a random coil polymer with α = 0.723 (Robinson *et al.*, 1982)

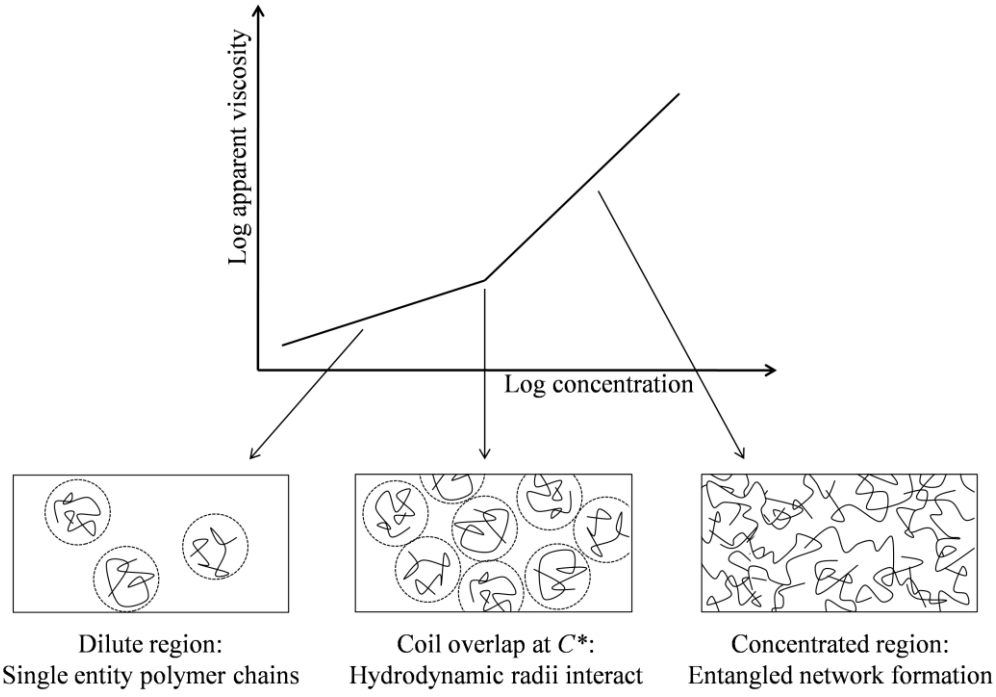

Fig. 2.1. Schematic representation of the dependence of viscosity on polysaccharide concentration showing C (critical concentration) behaviour. Image adapted from (Clegg, 1995).*

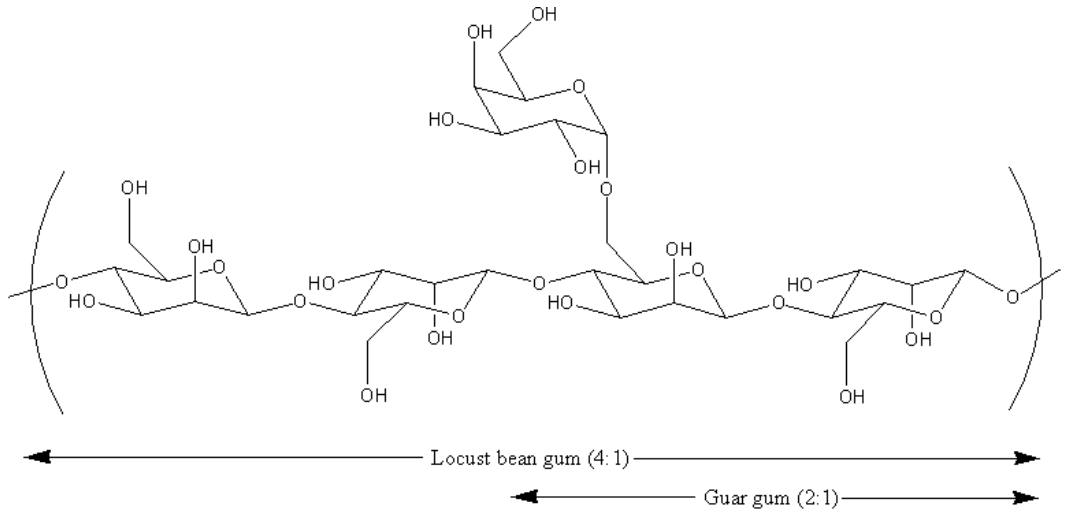

Fig. 2.2. Chemical structures of locust bean gum (LBG) and guar gum (GG) polymeric repeat units with their mannose:galactose ratios indicated. Image adapted from (Phillips and Williams, 2009).

and LBG behaves in a similar manner to GG, both possessing equal chain expansion properties (Launay *et al.*, 1997).

Scleroglucan (SCL), produced from *Sclerothinia* fungi, is a neutral (non-charged) polysaccharide consisting of a (1→3) β-D-glucose backbone with a (1→6) β-D-glucose branch for every third backbone residue (Fig. 2.3). Since the glucose units of SCL are chemically similar to the galactose and mannose of GG and LBG, they are all expected to have similar

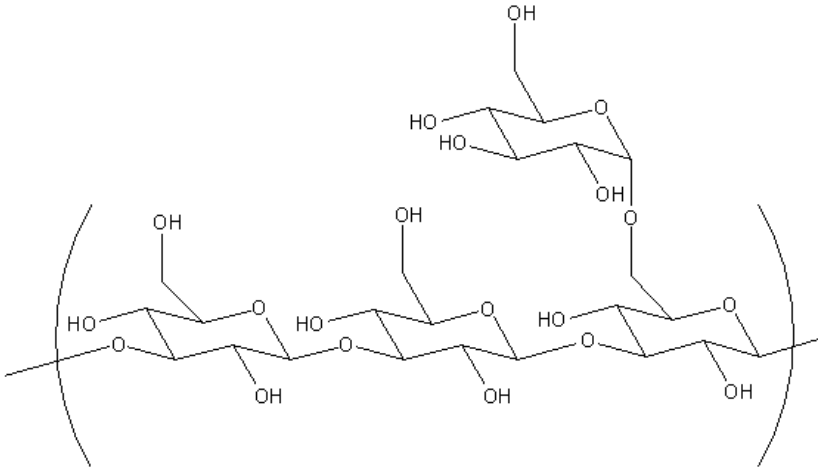

Fig. 2.3. Polymeric repeat unit of scleroglucan (SCL). Image adapted from (Cargill, 2012a).

chemical and electrostatic adsorption properties to the tribological surfaces used in this study (this will be discussed in more detail in Chapter 5). SCL adopts a triple helix structure held by intermolecular hydrogen bonds (Noīk and Lecourtier, 1993) and has the most extended and rigid structure of the polysaccharides (Yanaki and Norisuye, 1983) with $\alpha = 1.7$ (Gidley and Nishinari, 2009). Whilst SCL is a non-food grade polysaccharide, it is employed in this study for the purpose of maximising the extent of the conformation range investigated.

Carrageenans are derived from red seaweeds and are alternating repeat polyanionics. Kappa-carrageenan (κC) is a (1→3)-β-D-galactose-4-sulfate-(1→4)-3,6-anhydro-α-D-galactose copolymer (Fig. 2.4, left) (Rochas and Rinaudo, 1980). It has an extended flexible coil conformation where the chain expansion is owed to electrostatic interactions of the sulphated groups (Vreeman *et al.*, 2004). The Mark-Houwink coefficient indicates an extended, almost rigid structure (Harding *et al.*, 1997), with a chain expansion coefficient of $\alpha = 0.9$ in 0.028 M NaCl (which is expected to increase without NaCl) (Vreeman *et al.*, 2004). Lambda-carrageenan (λC) is a (1→3)-3,6-anhydro-α-d-galactose-(1→4)-α-d-galactose-2,6-disulfate copolymer (Fig. 2.4, right), and also has an extended flexible coil conformation (Rees, 1969) with a greater α value expected due to its additional charged sulphate group leading to greater intramolecular electrostatic repulsion.

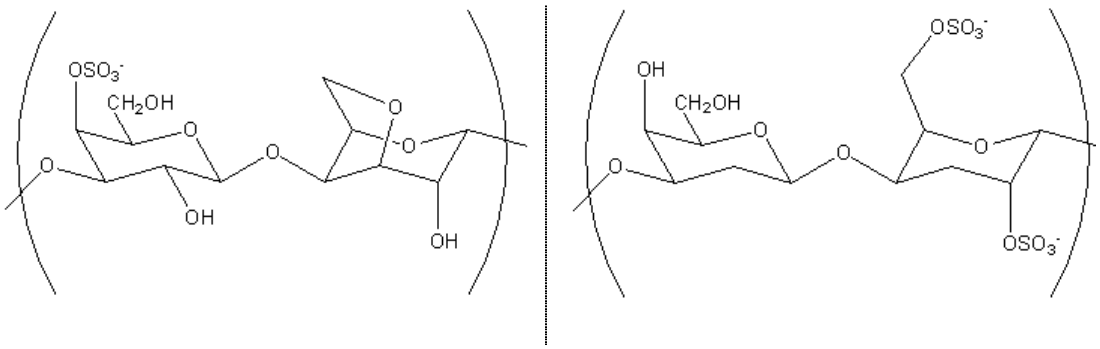

Fig. 2.4. Polymeric repeat units of kappa carrageen (left) and lambda carrageenan (right). Images adapted from (Phillips and Williams, 2009).

2.2.2. Gelation

κC may form aqueous gels through a molecular ordering process whereby the polymer chains adopt double helical conformations. The co-polymeric structure idealised in Fig. 2.4 (left) favours helix formation, however, κC polymers also have regions of deviation from that structure where the (1→4)-3,6-anhydro-α-D-galactose saccharide unit is replaced with that shown in Fig. 2.5 which causes an interruption of helix formation (Norton *et al.*, 1983a).

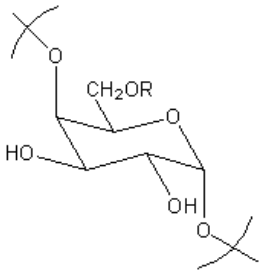

Fig. 2.5. The interrupting saccharide monomer of κC where R is H or SO_3^-. Image adapted from (Norton et al., 1983a).

Thus, κC chains have regions where helix formation is favoured, and these regions are separated by non-helix forming 'kinks'. These kinks are required for κC gelation as they allow for a single polymer chain to form helical domains with numerous neighbouring chains and thus allow formation of macroscopically cross-linked networks.

The mechanism of gelation has been described as a 'domain model' by Morris and co-workers (1980b) and is depicted schematically in Fig. 2.6 with KCl. The process begins with the reduction of chain expansion with salts (*e.g.* KCl) due to a screening effect of the charged sulphated groups (Goodall and Norton, 1987). The coil to helix transition then takes place on cooling (with or without gelling salts) where the ordered double helical 'domains' are in a metastable/transient state (specifically for the case of κC), which has been imaged by electron microscopy revealing a fine network structure (Hermansson, 1989), until aggregated side-by-side in the presence of gelling salts (which are: K^+, Na^+, Rb^+, Cs^+ and NH_4^+) forming densely

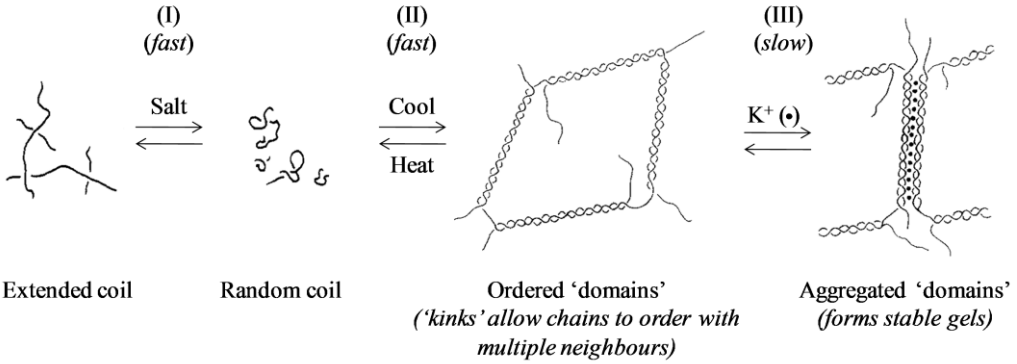

Fig. 2.6. The domain model for κC gelation with K^+. Images for this figure are from (Goodall and Norton, 1987) and (Morris et al., 1980b).

packed ordered superstrands and a thermodynamically stable state gel. The cation specificity for gelation is due to the ion radii being required to fit within the gaps created between neighbouring helices where K^+ provides a good fit and therefore stable aggregates and gel structures (Rochas and Rinaudo, 1980).

Kinetic studies reveal that the conformational disordering that occurs in step (I) (Fig. 2.6) takes place almost instantaneously (< 5 ms), the conformational ordering (II) of the coil-helix transition is fast, then the final aggregation step (III), which also includes annealing of the helices ('zipping-up') where imperfections initially form, takes place on a much slower timescale of minutes to days (Goodall and Norton, 1987).

Effect of K^+ concentration (Morris *et al.*, 1980b; Goodall and Norton, 1987):

- On increasing K^+ concentration, the (forward) rates of the ordering (II) and aggregation (III) steps are increased due to reduced electrostatic repulsion by a salt screening effect.
- Typical of an aggregated helix gelation mechanism, κC observes a gelling/melting temperature hysteresis where higher temperatures are required to provide enough energy to disrupt the stabilised aggregated structures on melting. This temperature hysteresis

increases with K^+ concentration due the aggregates becoming more stable (again, because of suppressed electrostatic repulsion).

- Since aggregated domains are promoted with K^+ concentration, so is the strength of the resultant gels.
- The transition midpoint temperature (T_m) represents the temperature where the number of moles in the ordered state equals that of the disordered state and where the rates of helix growth and decay are equal *i.e.* the forward rate of step (II) is zero at T_m. This temperature (as well as the gelling and melting temperatures) increase with K^+ concentration.

2.2.3. Sheared gelation: (fluid gel production)

Gelation of hydrocolloids under quiescent conditions results in the formation of an infinitely crosslinked network which, for κC, is provided by kinked regions allowing chains to associate with numerous other chains and through helix aggregation. By applying a shear force during gelation, however, fluid gels are formed which are suspensions of gelled particles dispersed in a non-gelled continuous medium (Cassin *et al.*, 2000). Fluid gels can be produced with food ingredients to prepare reduced calorie or enhanced satiety products

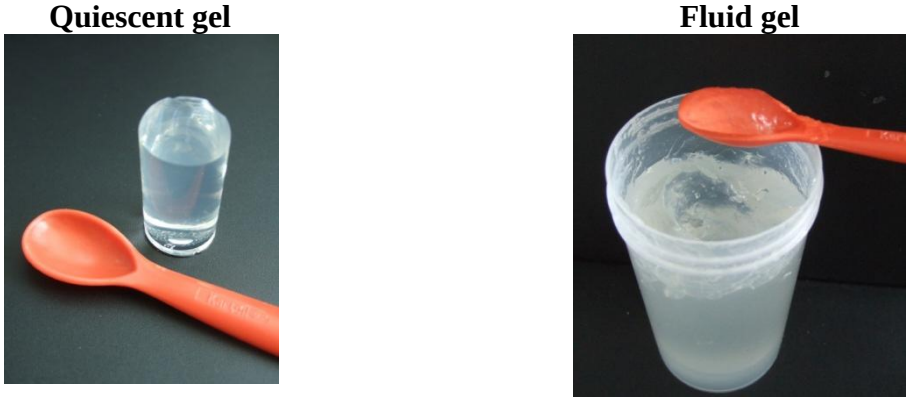

Fig. 2.7. Photographs of gels produced under quiescent (left) and sheared conditions (right). Both gels were produced from 1 wt.% kappa-carrageenan with 0.3 wt.% KCl using methods described in Chapter 3 Materials and Methodology.

(Brown *et al.*, 1996; Norton *et al.*, 2006) and have most notably been formed using gelling solutions of gelatin (Carvalho and Djabourov, 1997), gellan gum (Sworn *et al.*, 1995; Chalupa, 1997) and agarose (Norton *et al.*, 2000; Norton *et al.*, 1998). The fluid gel production process begins with the formation of gel nuclei that are segregated from one another by the shear forces which restrict the molecular ordering to within discrete particles. The resulting fluid gels have material properties vastly different to that of quiescently cooled gels where the former takes the shape of the vessel used to the contain the composition during gelation and can support its weight under gravity, whilst the latter is able to flow under stress (photographs to illustrate the influence of shear on gelation are shown in Fig. 2.7).

Gabriele *et al.* (2009) produced κC fluid gels within the cone-and-plate geometry of a rheometer conducting single shear viscometry tests on cooling. The tests were conducted at a range of shear rates and the authors concluded that smaller particles with lower bulk viscosities were produced on increasing shear rate. The results from that test are shown in Fig. 2.8 where it can also be seen that the viscosity rises on cooling which is due to the molecular ordering process reaching the helix aggregation stage. For the lowest shear rate tested (0.5 s^{-1}), the viscosity then decreases as the formed material starts to break down under the

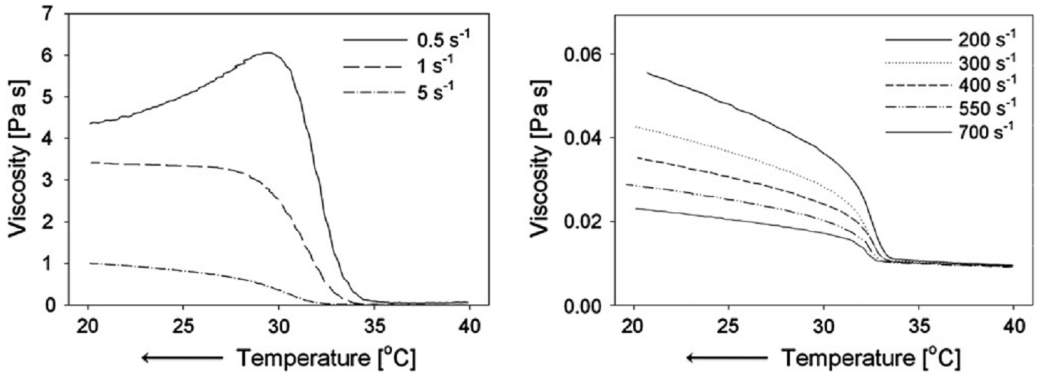

Fig. 2.8. Viscosity evolution of κC during gelation at 0.5 °C/min for a range of shear rates. The image for this figure is adapted from Gabriele et al. (2009).

continually applied shear force. The observed effect of reducing bulk viscosity on increasing shear rate (where smaller particles are formed, thus the surface area to volume ratio increases which would be expected to increase particle-particle interactions and therefore viscosity) has also been observed for fluid gels prepared with agarose (which is a neutral biopolymer – therefore, the behaviour seems unrelated to a particle repulsion effect) and is therefore ascribed as a reduction in particle volume fraction with increasing shear rate (Norton *et al.*, 1999). The study by Gabriele *et al.* (2009) then went on to discuss the oscillatory rheological properties of fluid gels shortly after their formation from a sheared cooling step. The sample storage modulus (*G'*) was shown to increase throughout a 2 h period due to 'ripening' which is likely to be due to helix annealing and further aggregation formation during the first two hours after production.

Fluid gels have also been prepared using a scraped surface heat exchanger to provide sheared cooling of agarose forming highly anisotropic gelled particles as shown in Fig. 2.9 (Norton *et al.*, 1999). The particles' anisotropy was shown to have a profound effect on the influence of particle volume fraction on rheology; this was the focus of a study by Frith *et al.*

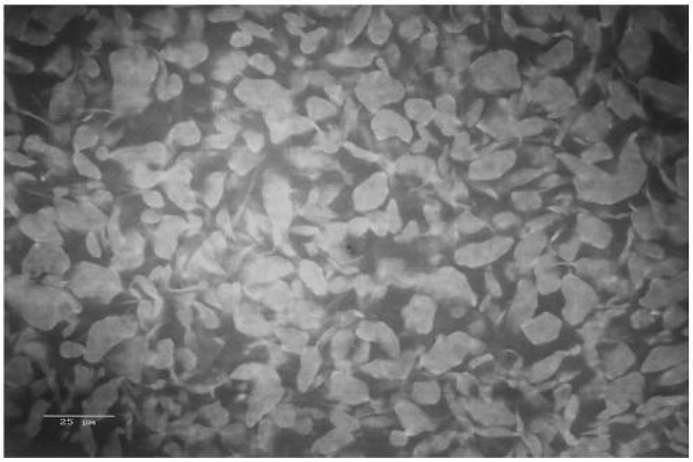

Fig. 2.9. Confocal micrograph of a 3 wt.% agarose fluid gel showing the highly anisotropic structures. The scale bar is 25 μm and the image is adapted from (Norton et al., 1999).

(2002). Frith compared the rheological properties of sheared agarose anisotropic fluid gels with those of spherical uniform agarose microgels that were formed *via* a water-in-oil emulsion route described by Adams *et al.* (2004). The spherical uniform particles were produced by first forming a water-in-oil emulsion where the aqueous phase contains agarose; this was then cooled under gentle agitation to allow the agarose droplets to gel into micro-beads which, finally, were separated from the continuous oil phase by successive steps of dilution with water and centrifugation.

This study by Frith *et al.* (2002) compared the volume fraction dependence of the storage modulus for the spherical uniform agarose microgels and the anisotropic sheared agarose fluid gels. This test was designed so that differences in behaviour could be ascribed to the shapes/structures of the particles since both systems are composed of the same material (agarose) and therefore are expected to have the same inter-particle interaction forces. The

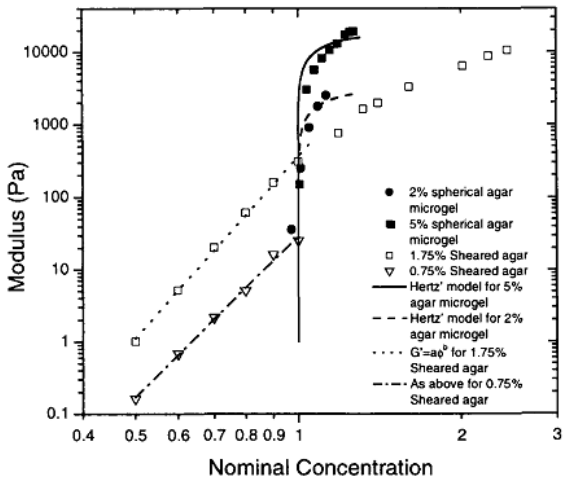

Fig. 2.10. Dependence of storage modulus on nominal concentration (volume fraction) for spherical agarose microgels (filled symbols) and sheared agarose fluid gels (empty symbols). For the fluid gels, the volume fraction of particles obtained after their production has a nominal concentration of 1. Fluid gel concentrations were increased by centrifugation to remove the continuous phase and were reduced by dilution with water. For the microgels, a nominal concentration of 1 represents the critical volume fraction (Φ_C) where random close packing occurs (observed from extrapolation of the data to the x-axis). The image for this figure is adapted from Frith et al. (2002).

results of this comparison are shown in Fig. 2.10. The most striking feature of this Figure is that the fluid gels displayed storage moduli over a broad range of fractions whilst the spherical uniform particles, as expected, did not have a modulus until the volume fraction exceeded a critical concentration. This critical volume fraction (Φ_c) is that required to form an interconnected network where the elastic response exceeds that of the viscous forces and gel-like properties prevail. For monodisperse spherical particles, Φ_c is just below the maximum packing fraction (Φ_m) which is ~ 0.64; anisotropic agarose fluid gel particles, however, 'extend through space' to a greater extent than spherical particles and, therefore, allow interactions and a percolated network to form at lower fractions than expected for spheres, hence the broad range of data observed for the fluid gels (Frith *et al.*, 2002). Thus, it has been shown that microgel rheology is influenced by the shape of the particles where spheres yield an elastic dominated response at $\Phi > \Phi_c$ and anisotropy enhances particle interactions thereby providing elastic properties over a broad range of dilutions.

A molecular model for fluid gel formation was described from a study on sheared agarose gelation (Norton *et al.*, 1999). From that study, a number of conclusions were made which will now be summarised. Firstly, it was stated that fluid gels can be formed from gelling biopolymers provided there is an aggregation step and that T_m is sufficiently greater than the storage temperature. Gelatin, therefore, cannot form stable fluid gels since it is close enough to its T_m (Eldridge and Ferry, 1954) that molecular rearrangements occur (at, *e.g.*, refrigeration temperature) resulting in a loss of the particulate structure. The model also described fluid gel particles as 'hairy' due to unordered chains existing at the particle surfaces until ordering completes. It was also discussed that fluid gels are not heat-stable because quiescent re-ordering events occur after application of heating-cooling steps thus forming bulk gels. Finally, the enthalpy of melting agarose gels (under quiescent, high shear and low

shear conditions) was shown to be independent of the applied shear *i.e.* shear did not influence the number of saccharide residues in helical domains.

2.3. Particulate Suspensions

2.3.1. Sensory perception of particulate suspensions

The previous section reviewed the structures and properties of hydrocolloids formulated as linear polymeric and particulate thickeners. These types of structures represent two principle classes of thickener that are often used to impart texture and stability to a wide range of food products. When prepared at comparable viscosities, their structural dissimilarities have been shown to influence the perception of taste, where scores are higher with particulate thickeners than polymeric thickeners (Mitchell, 2008). This was suggested to arise from differences in the efficiency with which they mix with saliva, where particulate thickeners allow for efficient mixing and, therefore, transfer of tastants to receptors on the tongue, whilst polymeric thickeners mix poorly with saliva (Ferry *et al.*, 2006) at concentrations exceeding C^* due to the entanglements of polymer chains. Additionally, reduced perceptions of aroma have been observed on increasing concentration of entangled polymers due to reduced in-mouth mixing efficiency and, therefore, reduced flavour replenishment at the surfaces (Baines and Morris, 1987).

Aqueous gelled particles have been used as fat replacements for phase separated semi-solid foods, *e.g.* mayonnaise or margarine (Chronakis and Kasapis, 1995), where they mimic the physical behaviour of the dispersed phase. An example is microparticulated whey protein concentrates that are formed by shearing proteins during a heating step to form aggregates of a size determined by the applied shear force (Singer *et al.*, 1988; Walkenstrom and Hermansson, 1998). Their sensory perception is dependent on protein aggregate size where watery/empty sensations are perceived below 0.1 μm, creaminess is perceived between 0.1 and 3 μm and powdery to gritty sensations are perceived on increasing size beyond 3 μm (Singer and Dunn, 1990). A similar effect of particle size on creaminess perception has been

observed with calcium carbonate and alumina-type particles (Kilcast and Clegg, 2002) thus highlighting the sensorial benefits of including particulates in food formulation, provided they are of appropriate dimensions.

2.3.2. Rheological models of particulate suspensions

The relative viscosity of hard-sphere particles suspended in a solvent was determined by Einstein (1906) to depend solely on the particle volume fraction (Φ) as in Eq. 2.2 (relative

$$\eta_{rel} = \frac{\eta_0}{\eta_s} = 1 + 2.5\phi \qquad \textit{Eq. 2.2}$$

viscosity (η_{rel}) is the ratio of the apparent viscosities of the suspension (η_0) and solvent (η_s)). This equation holds only for hard-spheres (where it is assumed that there is no particle deformation or inter-particle interactions) where the volume fraction is < 0.1. For systems where this model applies, the intrinsic viscosity is given by Eq. 2.3 where *c* is the particle

$$[\eta] = \frac{2.5\phi}{c} \qquad \textit{Eq. 2.3}$$

mass concentration in g/ml (Stokes, 2011). Thus, for those systems, the volume fraction of a suspension can be identified from the intrinsic viscosity and particle mass concentration.

To account for interactions between particles, Batchelor (1972) modified Einstein's equation to that in Eq. 2.4 (referred to as the Batchelor-Einstein equation) which holds true for

$$\eta_{rel} = \frac{\eta_0}{\eta_s} = 1 + 2.5\phi + 6.2\phi^2 \qquad \textit{Eq. 2.4}$$

hard-spheres up to $\Phi \sim 0.2$. For volume fractions greater than 0.2, suspension viscosities of hard spheres can be modelled by the Krieger-Dougherty equation (Krieger and Dougherty, 1959) given in Eq. 2.5. The Krieger-Dougherty model states that suspension viscosities

increase with volume fraction approaching infinity as the volume fraction reaches the maximum packing fraction (Φ_{max}) which, for hard spheres, is 0.64 and the intrinsic viscosity ($[\eta]$) is 2.5 dL g^{-1}.

$$\eta_{rel} = \frac{\eta_0}{\eta_s} = \left(1 - \frac{\phi}{\phi_m}\right)^{-[\eta]\phi_m} \qquad \textit{Eq. 2.5}$$

2.3.3. Microgels

Microgels are class of soft matter material composed of soft gel particles on the micron scale and are becoming increasingly important in applications of paint, enhanced oil recovery, surface coatings, pharmaceutical, home care and food products (Stokes, 2011). This section aims to discuss available methods for forming microgels, and their material properties which tend to lie between that of hard spheres and linear polymers depending on internal particle cross-link densities.

As discussed in section 2.2 (Hydrocolloids), microgels may be formed from hydrocolloids by sheared gelation (referred to herein as fluid gel formation) and quiescent gelation within aqueous droplets of a water-in-oil (w/o) emulsion where the formed microgel particles are separated from the oil by centrifugation (referred to herein as the w/o emulsion technique for uniform microgel formation). Hydrocolloid quiescent gels may be sheared to yield anisotropic broken-up gel particles with microgel properties (Ellis and Jacquier, 2009). Hydrocolloid microgels can also be formed from phase-separation in mixed gels, *e.g.* gelatin and maltodextrin (Kasapis *et al.*, 1993a), where the dispersed particle shapes are controlled by shear during gelation (Wolf *et al.*, 2001; Wolf *et al.*, 2000); and, furthermore, phase separated microgel particles can be produced from a microfluidic device using an oil continuous phase (Wassén *et al.*, 2012). In addition to using hydrocolloids, microgels may also be formed from

synthetic polymers *via* an emulsion polymerisation route (Saunders and Vincent, 1999). A typical emulsion polymerisation is conducted in an aqueous medium in the presence of a surfactant and monomer where the polymerization is carried out *via* a free radical pathway, often using a water soluble initiator (Smith and Ewart, 1948). Such synthetic microgels offer versatility through particle softness and swellability control by adjusting the relative concentration of a cross-linking monomer.

Rheological models can be used to describe the behaviour of microgels by replacing the apparent volume fraction (Φ) term with an effective volume fraction ($\Phi_{eff} = kc$), where k is the specific volume (mL/g) and c is the mass concentration (g/mL) of the particles. For hard-spheres $k = 1$; and, this value increases as the volume occupied by the particles increases as linear polymer behaviour becomes more prominent (*i.e.* as k increases the intrinsic viscosity increases above 2.5 dL g^{-1}). Using Φ_{eff}, however, requires the value of k to be independent of c which may not be the case if particle overlap or compression occur at high packing fractions (Stokes, 2011). For microgels where Φ_{eff} can be applied, relative viscosities can be described by the modified Batchelor-Einstein (BE) equation (Eq. 2.6) for low volume fractions and the modified Krieger-Dougherty (KD) equation for high fractions (Eq. 2.7). Thus, for a given mass concentration of particles, a samples' volume fraction can be determined from fits of rheological data at a range of dilutions to Eq. 2.6 and/or Eq. 2.7. Agarose microgels prepared *via* the w/o emulsion route and *via* shearing quiescent gels have been shown to follow the KD model where viscosities asymptote to infinity as Φ_m is approached (Ellis and Jacquier, 2009;

$$\eta_{rel} = \frac{\eta_0}{\eta_s} = 1 + 2.5(kc) + 6.2(kc)^2 \qquad \textit{Eq. 2.6}$$

$$\eta_{rel} = \frac{\eta_0}{\eta_s} = \left(1 - \frac{(kc)}{\phi_{max}}\right)^{-[\eta]\phi_{max}} \qquad \textit{Eq. 2.7}$$

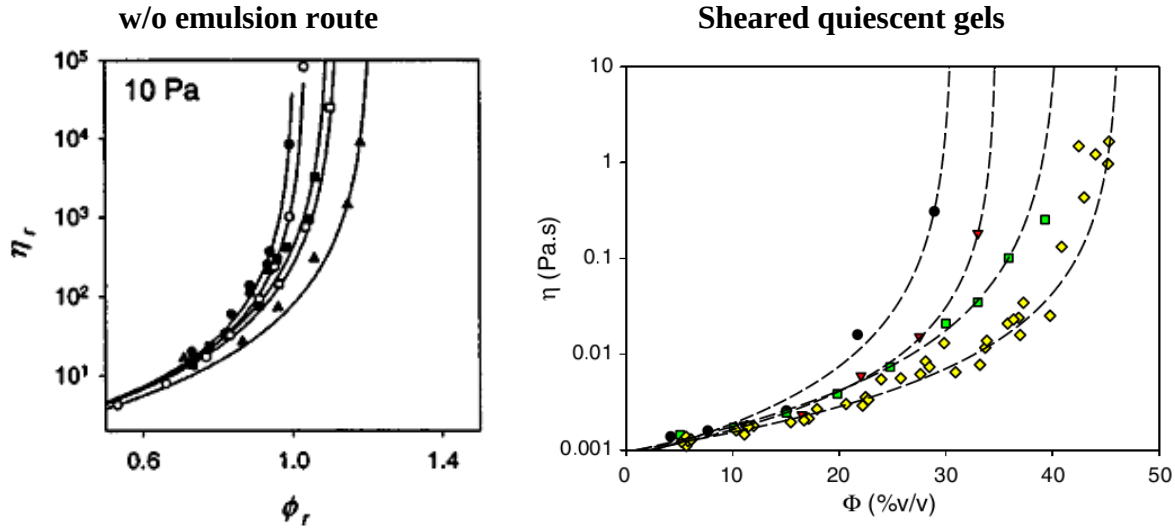

Fig. 2.11. Dependence of agarose microgel viscosity on effective volume fraction for microgels produced via the w/o emulsion route (left) and sheared quiescent gels (right). Both graphs show viscosities asymptoting to infinity as Φ_m is approached for a range of agarose concentrations. Solid lines (left) and dotted lines (right) represent fits to the KD equation. Images for this figure are adapted from Adams et al. 2004 (left) and Ellis et al. 2009 (right).

Adams *et al.*, 2004); the data from these studies is represented in Fig. 2.11. The maximum packing fraction attainable (Φ_m) for agarose microgels increases with particle compressibility as they become increasingly able to deform and fill the voids between the packed structures (Shewan and Stokes, 2012; Adams *et al.*, 2004). Whilst there is seemingly no graphical data in the literature for the viscosity dependence of fluid gels on volume fraction, it has been mentioned (Norton *et al.*, 1998) that agarose fluid gels fit the KD model; thus, the rheology of agarose microgels are described well by the KD model regardless of the formation method and therefore particle shapes.

For microgels formed *via* emulsion polymerisation of synthetic polymers, there are two notable publications on the influence of crosslink density on the rheology of poly(*N*-isopropylacrylamide) (PNIPAM) particles. Omari *et al.* (2006) showed the rheology

of PNIPAM particles with increasing crosslink density from 0-0.3% (shown in Fig. 2.12a) and Senff and Richtering (2000) showed the effect from 0.8-7% (shown in Fig. 2.12 b-c).

Fig. 2.12 (a) shows that the viscosity data diverges from the KD model and tends towards linear polymer behaviour as the crosslink density is reduced; specifically, the

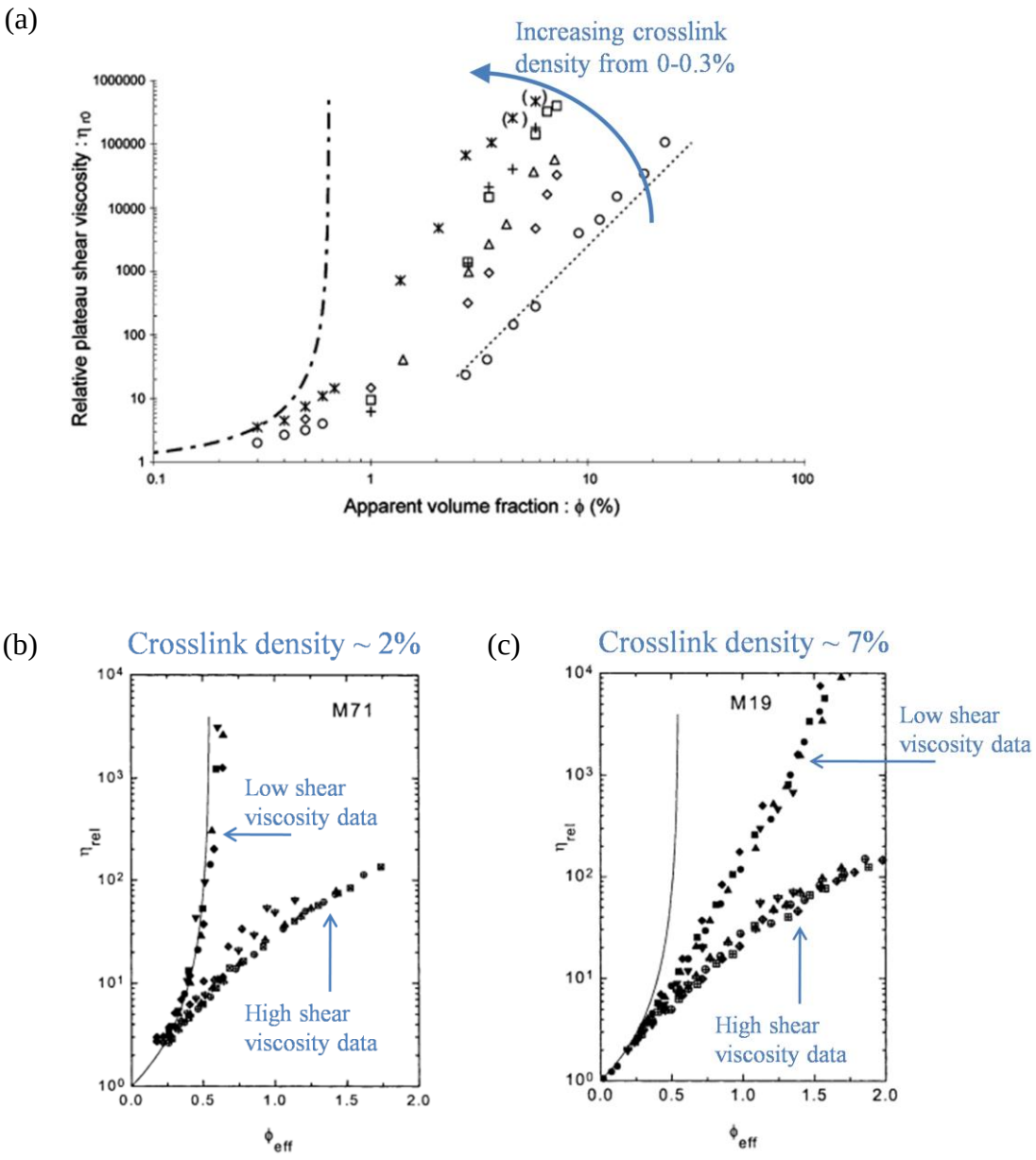

Fig. 2.12. Dependence of polyacrylamide viscosity on volume fraction as a function of crosslink concentration. Models are shown for KD (— · — ·) and linear polymer behaviour (·····) (a), hard-sphere behaviour is represented by the solid lines (b and c). The images are adapted from Omari et al. (2006) (a) and Senff and Richtering (2000) (b and c).

dependence of viscosity on volume fraction becomes weaker on decreasing crosslinker. In the absence of a crosslinking monomer (0%) the poly(*N*-isopropylacrylamide) forms linear polymeric chains without particulate structures and therefore can be modelled by a power law dependence with exponent ~ 3.4 ($\eta_{rel} \sim \Phi_{eff}^{3.4}$) which is expected for entangled polymer networks (Ferry, 1980; Morris *et al.*, 1981). Omari *et al.* (2006) described the weakly crosslinked particles as having a low viscosity dependence on volume fraction due to inter-particle penetration and particle compression occurring at packing fractions exceeding Φ_c.

Senff and Richtering (2000) showed that the polyacrylamide particles follow hard-sphere behaviour when the crosslink density is increased to ~ 2% (Fig. 2.12 b). The rheological properties of the microgels, however, deviated from hard-sphere behaviour when the crosslink density was increased further to 7% (Fig. 2.12 c). This was ascribed as the particles having a different structure to the hard-spheres formed with an intermediate crosslink density. This was expected to be because the crosslinker had a higher polymerisation rate than the *N*-isopropylacrylamide primary monomer; thus, at high relative concentrations the density of polymerised crosslinker is significantly higher in the centre of the particles than towards the surfaces. The result is the formation of particles with a highly crosslinked core and polymer chains at the surface allowing for inter-penetration and therefore a reduced viscosity dependence on volume fraction.

From the studies of Senff and Omari (2000, 2006, respectively), it can be concluded that microgel particles may possess reduced viscosity dependencies on volume fraction where the data does not asymptote to infinity or fit the KD model if the particle structures allow for inter-particle penetration or compression. This behaviour can be a result of particles whose crosslink density is low throughout (if formed with a low crosslink density) or just low towards the surface periphery (if formed with a very high crosslink density).

The characteristic architecture of hard and soft particles can be determined from an analysis of the volume fraction dependence of the elastic modulus (*G'*) (Koumakis *et al.*, 2012). Koumakis and co-workers prepared the following model particles for rheological analysis: hard spheres from poly-methylmethacrylate that were sterically stabilised with a layer of poly-hydro-stearic acid, hard-core/soft-shell particles composed of a polystyrene core and PNIPAM outer shell, and star-like micelles (ultra-soft particles) from PEP-PEO block copolymers (poly(ethylene propylene)-block-poly(ethylene oxide)). The resultant *G'* dependencies on Φ_{eff} are summarised for each particle type in Fig. 2.13 together with the scaling exponents for power-law fits. The power-law dependencies initiated at volume fractions required for close packing which increased with particle deformability. The value of the scaling exponents decreased with particle softness where they were 30 and 50 (below and above the glassy-state transition, respectively) for hard spheres; 7 for soft microgels; and, 2 for ultra-soft particles.

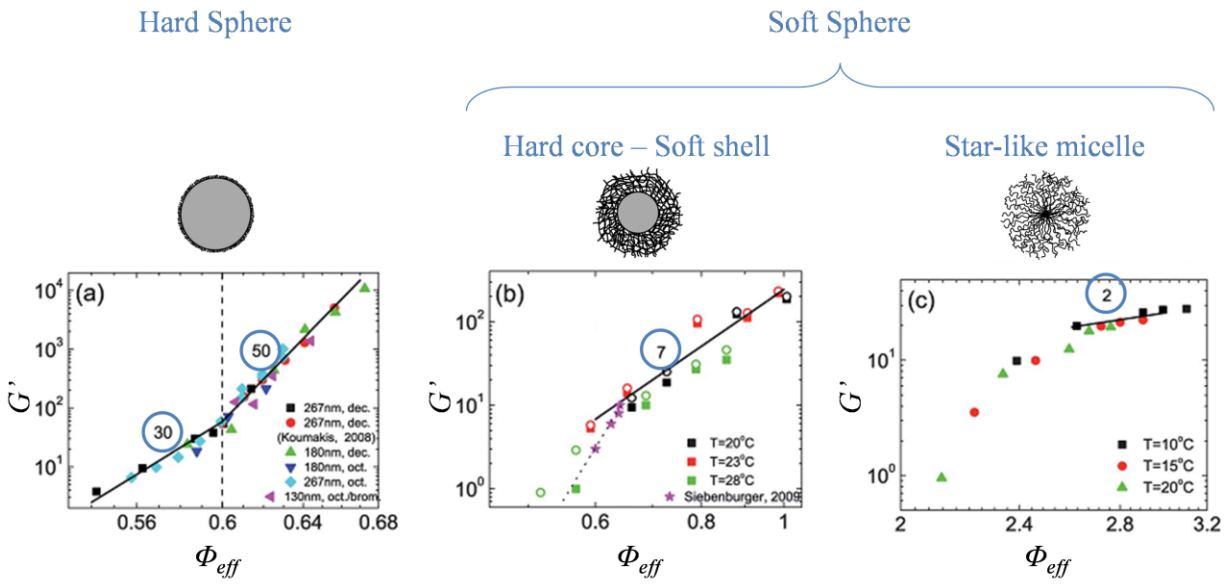

Fig. 2.13. The dependence of G' on Φ_{eff} for hard, soft (core-shell) and ultra-soft (star-like micelle) particles. Solid lines represent power-law fits with the scaling exponents given within the circles. The images for this figure are adapted from Koumakis et al. (2012).

The power-law dependencies of G' on Φ_{eff} displayed in Fig. 2.13 occur at volume fractions great enough to allow the particle surfaces to compress. On decreasing the volume fraction below this, the elastic response rapidly diminishes, which was also displayed by the agarose spherical microgels produced *via* the water-in-oil emulsion route (which was shown on Fig. 2.10, page 22).

2.4. Tribology

2.4.1. Introduction

Tribology is the science and technology of interacting surfaces in relative motion and encompasses the study of friction, wear, contact mechanics and lubrication. Tribology has long been studied for the purpose of optimising machine elements, *e.g.* bearings, gears and brakes, since their performance is determined by the behaviour of the contact between the rubbing surfaces in terms of, *e.g.*, resistance to wear, contact fatigue and friction generation (Bhushan and Hsu, 2001). Understanding the tribology of machine elements, therefore, can allow for the design of components/lubricants that have enhanced longevity or innovative properties.

The rationale for studying tribology in food research is that the tongue and hard-palate represent two contacting surfaces in relative motion that are lubricated by a film of food and saliva. Throughout oral processing, food is sheared and squeezed between the surfaces of the hard-palate, tongue and teeth where its deformation is determined by its bulk rheological and mechanical properties. Mechanical receptors within the oral mucosa detect the application and response of these forces which, in turn, are interpreted as the perception of textural attributes *e.g.* smooth, thick, slimy *etc* (Chen and Stokes, 2012). As the oral processing of food continues, the structure is continually broken down until only a thin-film is present. At this stage, the mechanical and rheological properties of the food are less important in determining texture and the tribology of the tongue-palate contact becomes increasingly relevant. It is agreed (de Wijk and Prinz, 2005; de Wijk *et al.*, 2003) that the lubrication by fat in foods is an important aspect in determining fat-related textural attributes. To that end, tribometry experiments have shown correlations with in-mouth sensory attributes (Dresselhuis *et al.*, 2007a; Malone *et al.*, 2003).

The most useful areas of tribology for the purpose of food research are friction, contact mechanics and lubrication. These topics will now be reviewed, in turn, to provide a background of the fundamentals and theories relevant for this thesis.

2.4.2. Friction

Friction is a force that resists motion and must be overcome to initiate or sustain motion. The two-term model of friction (Bowden and Tabor, 1964) states that, during the sliding of solid surfaces, friction forces can be considered to arise from breaking the adhesive forces at the interface and deformation at the sub-surface level. Thus, friction principally arises from two factors: adhesion and deformation, where their contribution to friction can be summarised as follows (Williams, 2005b):

- Adhesion – junctions formed between contacting asperities must be sheared before movement is allowed.
- Deformation – this can be plastic or elastic deformation and is a result of the movement and normal load.
- Hysteresis losses – this is relevant for significantly deformable surfaces, *e.g.* elastomeric surfaces, where there is a lag between applied stress and deformation response.

Friction forces are dissipated mostly as heat and noise (which constitute ~ 90% of the energy dissipation) and in wear (~ 10%). Friction is often represented as a dimensionless coefficient of friction (μ) given in Eq. 2.8 where F_t is the tangential friction force and N is the normal load, both in units of Newton's (N). During tribometry experiments, a load is applied (W)

$$\mu = \frac{F_t}{N} \qquad \textit{Eq. 2.8}$$

$$\mu = \frac{F_t}{W} \qquad \textit{Eq. 2.9}$$

normally; consequently, the friction coefficient will be represented from here on as that in Eq. 2.9.

Leonardo da Vinci and Guillaume Amonton were early pioneers in the study of tribology. They both independently theorised two important principles (although da Vinci's contribution was discovered much later) which are known today as Amonton's 1st and 2nd laws, these were published by Amonton (1699) and can be summarised as:

1. Friction force (F_t) is directly proportional to the applied load (W)
2. Friction force (F_t) is independent of the (apparent) area of contact (A_a)

The first law can be verified experimentally, a plot of F_t versus W gives a linear relationship for most surfaces. However, the explanation for this dependency came much later from Bowden and Tabor (1954) who described that the real area of contact (A_r) is actually less than the apparent area of contact (A_a) due to the roughness of 'real' surfaces only allowing contact at asperity junctions. F_t was described to be directly proportional to A_r (which is the sum of the asperity contact areas) through Eq. 2.10 where τ is the interfacial shear strength.

$$F_t = \tau A_r \qquad \text{Eq. 2.10}$$

Archard's law (1957) describes that the relation between A_r and W is linear if there is a load dependent number of contacting asperities *i.e.* increasing the applied load creates more contact sites. This was later verified experimentally and theoretically by Greenwood and Williamson (1966). Thus, to summarise, F_t is independent of the apparent area of contact

(Amonton's 2nd law), but directly proportional to the real area of contact (A_r) (Eq. 2.10) which is proportional to W (Archard's law); thus, explaining Amonton's 1st law that F_t is directly proportional to W.

2.4.3. Contact mechanics

The tribometry experiments carried out for this thesis were conducted on a tribometer consisting of a rotating ball and disc (images of which will be shown in Chapter 3 - Materials and Methodology) where the contact can be modelled as a sphere on a flat surface as depicted in Fig. 2.14. The geometry of such a contact is a circle with area $A = \pi a^2$, where a is the radius which is dependent on the applied load (W) according to Eq. 2.11 derived by Hertz (1881). R^*

$$a = \left(\frac{3WR^*}{4E^*}\right)^{1/3} \qquad \textit{Eq. 2.11}$$

$$\frac{1}{R^*} = \frac{1}{R_1} + \frac{1}{R_2} \qquad \textit{Eq. 2.12}$$

$$\frac{1}{E^*} = \left(\frac{1-\nu_1^2}{E_1} + \frac{1-\nu_2^2}{E_2}\right) \qquad \textit{Eq. 2.13}$$

and E^* are the reduced radius and reduced elastic modulus given by Eq. 2.12 and Eq. 2.13, respectively where the subscript numbers 1 and 2 denote the surfaces *e.g.* 1 = ball and 2 = disc. R_1 and R_2 are the radii of the contacting surfaces where for a flat surface, $R_2 = \infty$. E_1 and E_2 represent elastic moduli and ν_1 and ν_2 are the Poisson's ratios for the sphere and flat, respectively.

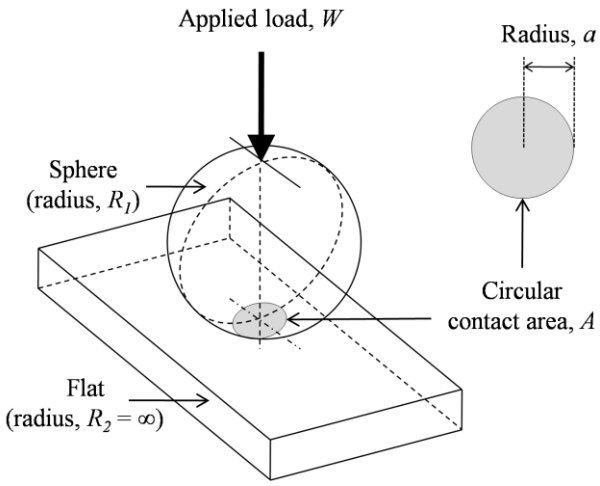

Fig. 2.14. Schematic representation of the circular contact area formed between a sphere and flat surface or, for tribometry, a ball and disc.

Hertzian contact theory assumes that the effects of surface roughness are negligible *i.e.* that the contact area (A) represents the real area of contact (A_r). The development of AFM (atomic force microscopy) has allowed the formation of truly single asperity contacts using silicon based surfaces or *e.g.* a carbon nanotube tip; this subject area has been reviewed by Szlufarska *et al.* (2008). AFMs have allowed Hertzian contact theory to be validated tribologically through a plot of F_t versus W yielding power-law curves with exponent 2/3. The experimentally observed F_t dependency on $W^{2/3}$ originates from Eq. 2.11 (Hertz) which states that $a \propto W^{1/3}$, and since $A_r = \pi a^2$, it follows that $A_r \propto W^{2/3}$. Given that $F_t \propto A_r$ (Eq. 2.10, Bowden and Tabor), F_t is then $\propto W^{2/3}$. Thus, for a truely single asperity contact, increasing the load causes the contact area to increase according to Hertz ($W^{1/3}$ dependency) which causes a $W^{2/3}$ dependency on friction. This behaviour has only been able to be experimentally confirmed in the advent of AFM; as previously discussed, 'real' contacts have significant surface roughness and therefore display a dependency of $Ft \propto W$ (Amonton's 1st law) due to Archard's principle of a load dependent number of contact sites.

2.4.4. Lubrication

Lubricants can separate surfaces thereby reducing friction and wear as well as dissipating heat, transferring debris and providing protection of surfaces from corrosion. In the application of tribology to food research, the lubricant is represented by saliva and a food or starter product to be investigated.

Analysis of the ball and disc contact reveals that the gap height between the ball and disc reaches a minimum at the centre of the circular contact area. As such, the contact may be termed a 'converging geometry' since the gap is initially high (towards the edges of the ball) and converges to a minimum at the centre. The result of this is that the lubricant pressure increases as it is dragged into the centre of the contact resulting in a lift of the ball from the disc. As the speed of the rotating ball and disc increase, so does the volume of lubricant dragged into the contact as well as the pressure and therefore surface separation. Monitoring friction coefficients (μ) as a function of entrainment speed (U) result in the formation of

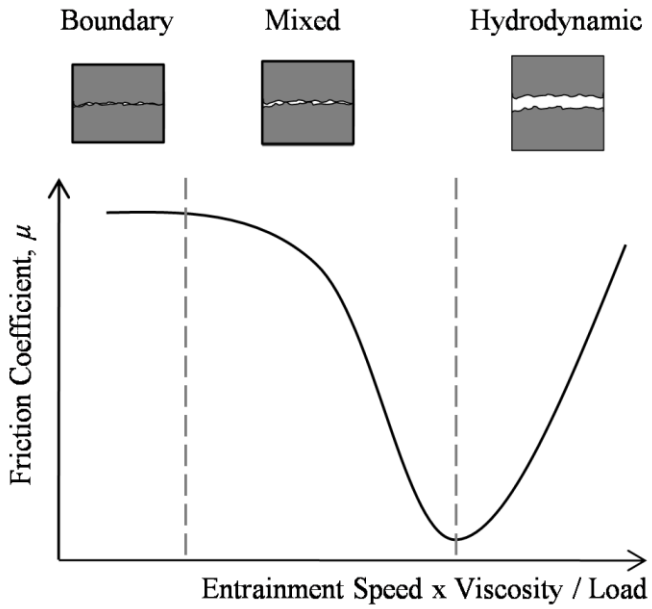

Fig. 2.15. Schematic of a complete Stribeck curve showing three principle regimes of lubrication: boundary, mixed and hydrodynamic where the ball and disc surfaces are in full contact, partial separation and full separation, respectively.

Stribeck curves (Stribeck, 1902) where friction initially decreases to a minimum, then increases, as the film thickness (or gap height) continually widens. Fig. 2.15 shows a schematic of an idealised Stribeck curve where three regimes of lubrication can be identified from the shape of the curve:

Boundary lubrication – This is observed from a horizontal start to a Stribeck curve where μ is independent of entrainment speed (U) and is observed at low speeds. In the boundary regime the surfaces are in full contact and the bulk lubricant is excluded from the contact. The applied normal load (W) is fully supported by the contact of the two surfaces. Whilst the bulk lubricant properties do not influence boundary conditions, surface adsorbed matter or low shear strength (τ) solid surfaces *e.g.* graphite or PTFE (polytetrafluoroethylene) may have a pronounced influence of reducing boundary lubrication which is particularly important during the start-up and shut-down of heavy machinery where rotation speeds are insufficient to create a lubricating film (Williams, 2005a).

Mixed regime of lubrication – this is observed from a reduction of friction with entrainment speed which occurs due to surface separation as a result of increased lubricant pressure. During this regime W is supported partially by asperity contact and partially by lubricant pressure. As a result, both the surface and lubricant properties influence friction. As the speed increases the asperity contact reduces until full separation occurs where μ reaches a minimum (Spikes, 1997).

Hydrodynamic lubrication (IEHL) – this is observed from an increase in friction with entrainment speed and occurs due to an increase in the film thickness requiring a greater volume of fluid to be sheared by the rotating surfaces. Friction in this regime is solely dependent on the lubricant rheology and is independent of the surface roughness or chemical

composition. Thus, hydrodynamic tribometry is essentially equivalent to bulk rheology. As a result, tribology in this thesis is primarily concerned with the boundary and mixed regimes whilst bulk rheology is studied using rheometers since the latter offers more precise control over gap heights, shear rates/stresses, temperatures and user defined testing profiles. When using deformable surfaces, the hydrodynamic regime may be referred to as elastohydrodynamic lubrication (EHL) (de Vicente *et al.*, 2005). This term, however, is also used to describe the lubrication at highly non-conformal (or counterformal) contacts, *e.g.* ball bearings or gears, which therefore have low contact areas causing high pressure, *i.e.* > 1 GPa, which results in elastic deformation of the surfaces and an increase in viscosity for piezoviscous oil lubricants (where the viscosity is a strong function of pressure) (Stachowiak and Batchelor, 2005). Such an increase in viscosity in the contact can result in an uneven pressure distribution and therefore uneven deformation of the surfaces. However, the soft and conformal surfaces (which provide large contact areas) and low normal loads used in the present study are not expected to influence the lubricant viscosity, thus the term iso-viscous elastohydrodynamic lubrication (IEHL) may be used.

It is worth mentioning at this stage that the contact mechanics theories discussed in the previous section (2.4.3) are only relevant in boundary conditions where the surfaces are in full contact *i.e.* they are not valid in mixed and hydrodynamic lubrication conditions.

2.4.5. Soft-surface tribometry

Tribology is a system property (rather than material property), strictly speaking, and as such, the surfaces used, as well as the lubricant, determine friction. Consequently, the properties of the surfaces are crucial in studying tribology for textural relevance. To that end,

tribological instrumentation involving pig's tongues, which are proposed to be similar to human tongues, has been conducted (Dresselhuis *et al.*, 2008) demonstrating the importance of tribological surface characteristics on food behaviour during testing. Dresselhuis and co-workers showed, during tribological testing of o/w emulsions between a tongue and glass surface (where confocal microscopy was used to visualise the emulsion structure at the contact), that shear induced droplet coalescence occurred due to entrapment of oil droplets within spaces created between tongue papillae. A PDMS/glass contact, however, did not show coalescence and thus may not be tribologically equivalent to oral behaviour (PDMS, polydimethyl siloxane, is a hydrophobic deformable rubber). On the other hand, there are issues with availability and reproducibility of animal surfaces since the properties of the surface used were shown to depend on tongue location, there is also variation from animal to animal and tissue degradation during experimentation. As a consequence, animal surfaces will not be considered in this work. PDMS surfaces can be formed with user defined roughness (by moulding onto *e.g.* sandblasted steel surfaces), elasticity (by controlling the base to crosslink ratio) and wetting characteristics (through oxygen plasma exposure) and therefore has been suggested to be a suitable material for 'soft-tribometry' (Dresselhuis *et al.*, 2008) where at least one of the two rubbing surfaces has a low Young's modulus.

Controlling the elasticity of the surfaces has shown that on increasing surface deformability there is an increased tendency for stick-slip behaviour and an unstable (erratic and unreproducible data) progression from boundary-mixed and mixed-hydrodynamic regimes (Krzeminski *et al.*, 2012). Thus, whilst the use of a soft-surface is useful in tribometry to mimic surface deformation and low contact pressures, there seems to be little control over Young's moduli without sacrificing the quality of the data.

Studies on the influence of PDMS surface roughness on friction have shown that increasing the surface roughness decreases friction coefficients and increases the speed required to make the transitions between lubrication regimes (Bongaerts *et al.*, 2007; Cassin *et al.*, 2001). These observed effects are because an increase in surface roughness reduces the real area of contact, and therefore friction (see equation Eq. 2.10), and because rougher surfaces require greater film thicknesses, and therefore faster entrainment speeds, to promote progression through the lubrication regimes.

The hydrophobic PDMS surfaces were temporarily rendered hydrophilic by Bongaerts *et al.* (2007) by oxygen plasma treatment to alter the surface chemistry by promoting reduction to anionic charges. In the presence of aqueous lubricants, the hydrophilicty was shown to reduce boundary and mixed regime friction coefficients due to enhanced entrainment to the contact. As expected, surface roughness and wettability did not influence friction in a hydrodynamic regime because friction is solely determined from lubricant bulk rheology in that regime.

An investigation into the influence of normal load on boundary regime friction force for PDMS surfaces revealed a $W^{2/3}$ dependency (Stokes *et al.*, 2011). This is despite the 328 nm root-mean square surface roughness which would not be expected to provide a single-asperity contact and was explained by the elastic conformity of the surfaces dominating the influence of load. Thus, the PDMS surfaces provide a F_t dependence on W that is analogous to single asperity contacts because the soft contact conforms and deforms elastically according to Hertzian theory.

To summarise the influence of load (W) on friction (F_t) for various contact types:

- Single asperity contacts (*e.g.* AFM setups) observe a fixed number of contact sites (one site) whose area increases with load according to Hertzian theory giving rise to $Ft \propto W^{2/3}$.

- ‘Real’ non conformal contacts (*e.g.* steel on steel contacts) observe Archard’s principle of a load dependent number of contact sites yielding $F_t \propto W$ which is Amonton’s 1st law.
- ‘Real’ highly conformal contacts (*e.g.* PDMS surfaces) display $Ft \propto W^{2/3}$ which is postulated to arise from a fixed number of contact sites (of which there could be one, or numerous, sites) whose (combined) area increases with load according to Hertzian theory due to elastic deformation of the conformable surfaces dominating the behaviour.

2.4.6. Influence of lubricant structure and properties on friction

A comprehensive understanding of the influence of food microstructure on boundary and mixed frictional response is lacking. The majority of research on the tribology of machine elements is focused on promoting hydrodynamic lubrication to minimise wear. There has been progress however, particularly on the influence of the viscosity of Newtonian fluids, surface adsorption of hydrocolloid boundary films, microgels and o/w emulsions; the results of which will now be discussed.

Bongaerts *et al.* (2007) showed that master Stribeck curves could be formed from plots of μ versus the product of the apparent viscosity (η) and entrainment speed (U) $U\eta$ for Newtonian fluids prepared at a range of viscosities. Fig. 2.16 shows such a master Stribeck curve for Newtonian fluids water, glycerol and corn syrup prepared at a range of viscosities. The low viscosity fluids form the boundary and mixed regimes and the high viscosity fluids form the mixed and hydrodynamic regimes where all the data superimpose onto one curve. This demonstrates that for the PDMS ball and disc contact used, and with non-adsorbing Newtonian fluids, that the friction coefficient is determined solely from $U\eta$.

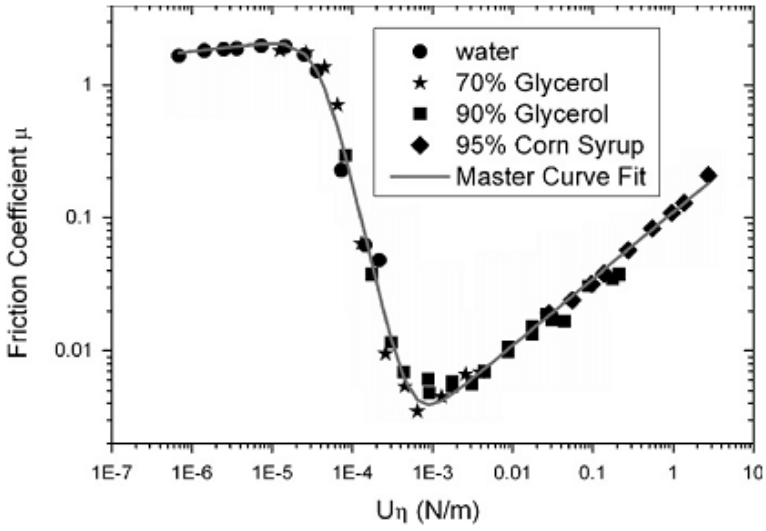

Fig. 2.16. Master Stribeck curve for a range of Newtonian fluids varying in viscosity measured on a PDMS-PDMS contact. The image is adapted from Bongaerts et al. (2007b).

Master Stribeck curves have also been attempted for non-Newtonian hydrocolloids guar gum (GG) and xanthan gum (XG) (de Vicente *et al.*, 2005; de Vicente *et al.*, 2006b). Since solutions of these hydrocolloids are shear thinning, and the shear rate in the ball-on-disc contact is unknown in boundary and mixed conditions, η values cannot be obtained. As a result, shift factor K values were used which, when used to provide curve superposition, were expected to represent effective viscosities *i.e.* the viscosity in the contact. However, this makes an assumption that the bulk fluid (which is measured rheologically) is entrained for lubrication during tribological testing. Additionally, the studies by de Vicente *et al.* (2005 and 2006b) suggested that the conformation of XG and GG had no influence on friction, except in controlling rheology, despite the small film thickness. This hypothesis, together with the significance of master Stribeck curves for non-Newtonian hydrocolloid fluids, will be discussed in Chapter 5 - Tribology of non-gelling hydrocolloid polymeric thickeners.

Adsorption of biopolymers to tribometer surfaces has been shown (Cassin *et al.*, 2001) to act as a boundary lubricant providing a significant reduction in boundary friction coefficient. This was shown from GG (which showed poor adsorption using evanescent wave spectroscopy) giving high friction coefficients whilst PGM (pig gastric mucin) (which strongly adsorbed) gave significantly lower boundary friction values. The lubrication was proposed to occur through steric or electrostatic repulsion from the PGM adsorbed surfaces. The properties of surface adsorbed hydrocolloid films were later probed by Stokes *et al.* (2011) who demonstrated, using QCM (quartz crystal microbalance) and SPR (surface plasmon resonance), that the wet and dry masses of the polymer film, viscoelasticity and film thickness were all important in determining friction coefficients. Furthermore, they showed that $U\eta$ values at the transition between mixed and hydrodynamic regimes were reduced on increasing wet mass and thickness of the adsorbed films. This was proposed to occur due to

the films reducing the surface roughness, increasing the wetting properties and providing a low shear strength boundary layer. Thus, hydrocolloids that adsorb to tribological contacts can provide boundary lubrication and promote the onset to the IEHL regime at lower speeds. LBG was shown to be a poor boundary lubricant due to having a low affinity to PDMS forming a thin rigid film whilst pectin showed strong adsorption forming a highly hydrated viscoelastic film and consequently was a more effective lubricant. Substantiating these 'macro-tribological' observations and proposed mechanisms, biopolymer 'nano-lubrication' has been demonstrated in an AFM setup where surface-adsorbed chitosan was suggested (Nordgren *et al.,* 2009) to form 'cushion-like' layers of trapped water resulting in markedly reduced friction.

Gabriele *et al.* (2010) conducted the first published tribological study on fluid gels. That investigation on agarose fluid gels used particles (~ 100 μm diameter) that were larger than the dimensions of the roughness of soft surfaces used. Consequently, the fluid gel particles were excluded from the contact at low speeds. This was identified from the Stribeck curves where the mixed regimes passed a maximum μ before the speeds were great enough to generate a film thickness to exceed that of the particle sizes and therefore allow bulk entrainment. This conceptual model for fluid gel tribology was shown schematically and is represented in Fig. 2.17 where three zones were envisaged. Zone A, at the lowest speeds, represents partial entrainment of the continuous phase in a mixed regime of lubrication; μ then increases with speed in Zone B as the particles begin to be entrained forming a monolayer; then Zone C is entered at high speeds where the bulk fluid is entrained and the mixed regime continues.

A similar ‘bump’ or increase in friction through the mixed regime was also observed (de Vicente *et al.*, 2006b) on Stribeck curves obtained for Carbopol microgel suspensions where, similarly to Gabriele *et al.* 2010, the particles were larger than the surface roughness dimensions (particle diameters ~ 2-4 μm; RMS ~ 10 and 800 nm for the ball and disc, respectively (RMS is the root mean square of the surface roughness)). The authors suggested that the upward slope of the ‘bump’ is similar to that observed in an IEHL regime because a micro-IEHL regime occurs for the continuous phase before the film thickness is large enough to allow for bulk entrainment. An alternative mechanism for the frictional increase is that the particles, being larger than the roughness dimensions, are excluded from entrainment and accumulate around the contact with increasing speed thus depriving the contact of lubricant.

Soft-tribology has also been conducted on much smaller microgels: starch granules (Zinoviadou *et al.*, 2008) and protein aggregates (Chojnicka *et al.*, 2008) have both shown reduced friction coefficients compared to water where each displayed typical Stribeck curves, that is, without a ‘bump’ in the mixed regimes. Despite the particulate structures of starch and protein aggregates, their small sizes prevented exclusion from the contacts. The starch

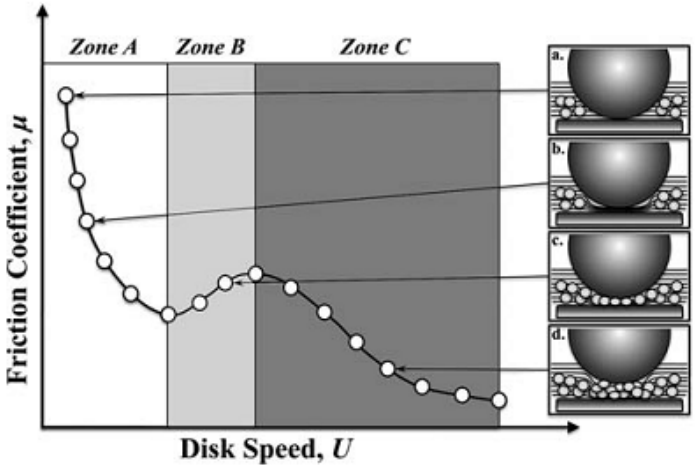

Fig. 2.17. Schematic for the conceptual model of fluid gel tribology where the particles are larger than the surface roughness dimensions. The Stribeck curves pass through a maximum in μ on increasing U through the mixed regime suggesting particle exclusion. This image is adapted from Gabriele et al. (2010).

granules were ~ 35 nm in diameter, presumably far smaller than the surface roughness's, and the whey protein isolate (WPI) globular protein aggregates (30-80 nm diameter) and ovalbumin fibrillar aggregates (30-700 nm length) were also much smaller than the roughness of the neoprene (RMS ~ 31 μm) and silicone (RMS ~ 9 μm) surfaces used. This study on protein aggregates by Chojnicka *et al.* (2008) also showed, through dilution with water to two concentrations, that boundary friction increased on dilution. Specifically, the number of particles was tested over a small range and showed a continued reduction in friction on increasing particle number. Furthermore, they showed that for a fixed number of particles, increasing aggregate size reduced boundary friction.

As briefly mentioned, there is also soft-tribological literature on the influence of food emulsion structures on friction. This is particularly on the effect of phase volume, the viscosity ratio of the two phases and particle coalescence. Since food emulsions are not tested in this thesis, this topic will be discussed now only to provide an overview of how tribological behaviour can be attributed to the properties and structures of the material entrained to the contact.

An important study by Malone *et al.* (2003) which related frictional data to sensory perceptions (which is discussed in the following section: Chapter 2.4.7) also showed the influence of the internal phase volume of a range of iso-viscous (obtained by adjusting the GG content of the aqueous phase) o/w emulsions on the obtained Stribeck curves. The results showed that in boundary and mixed regimes, the Stribeck curve from a 1% oil content emulsion superimposed onto the water curve, and the curves from above 20% oil superimposed onto the curve for pure oil. This suggests that for low oil content emulsions, the contact zone in boundary and mixed conditions is predominantly occupied by water and for high oil content emulsions it is mainly oil. At higher speeds, the hydrodynamic regimes were

observed to collapse onto the oil curve only for emulsions with more than 55% oil whilst the rest superimposed onto the water curve (it may be expected that for a range of iso-viscous emulsions that all hydrodynamic regimes would superimpose onto one curve). Data from the hydrodynamic regimes suggested that for emulsions of less than 55% oil, the bulk emulsion is entrained displacing the oil film present at low speeds; whilst for over 55%, oil remains the primary component in the contact.

This effect of the oil phase volume determining the phase entrained was later shown (de Vicente *et al.*, 2006a) to be a result of the ratio of the internal to continuous phase viscosity, p ($p = \eta_{oil\ phase}/\eta_{aqueous\ phase}$). This was suggested from equivalent Stribeck curves obtained for all samples within a range of o/w emulsions that varied in oil phase volume from 10-60% (plus pure oil and pure aqueous phase lubricants) where all samples were formulated to equal viscosity ratio, at $p = 1$, by using a glycerol (82.5 wt.%) solution for the aqueous phase to match the viscosity of the oil. The fact that all the Stribeck curves were similar, regardless of the oil content, strongly suggests that it is the viscosity ratio of the two phases that controls friction. Furthermore, they showed that for a range of o/w emulsions at 20% oil with varying concentrations of glycerol in the aqueous phase (*i.e.* a range of emulsions with varying viscosity ratio, p) that complete master Stribeck curve formation occurred when multiplying U by the viscosity (η) of the oil, for $p > 5$, and by the viscosity of the aqueous phase, for $p < \sim 1$. Considering that superposition of curves occurs when μ is plotted against $U\eta$ provided that η represents the viscosity of the entrained fluid, it was concluded that the more viscous phase of an emulsion is entrained for lubrication. The explanation proposed was that at high p values the oil droplets are rigid and so become confined in the contact where they coalesce and provide an oil lubricating film; conversely, for low p values the oil droplets deform preventing entrainment and cannot displace the more viscous aqueous phase in the

contact. Complementing this work, Dresselhuis *et al.* (2007b) showed that the coalescence of oil droplets in o/w emulsions reduced friction and enhanced fat-perception.

To summarise the literature on the influence of lubricant structures and properties on soft-tribometry: master Stribeck curves can be obtained for non-adsorbing Newtonian fluids where μ is solely determined by $U\eta$ regardless of the concentration of thickener. Surface adsorption of hydrated viscoelastic hydrocolloid films significantly reduces μ's and the speed required to enter an IEHL regime due to the formation of a low shear strength boundary layer and a smoothing of the surface roughness's. Particles of suspensions which are larger than the surface roughness dimensions are excluded from the tribological contact resulting in an increase in μ with U during the mixed regime whilst smaller particles are entrained at all speeds. Finally, the phase of an emulsion residing in the contact zone in boundary and mixed regimes of lubrication can be identified from Stribeck curves since they will superimpose onto either the curves for the aqueous or oil phase. Additionally, the more viscous phase tends to be entrained and, when this is the dispersed phase, coalescence occurs in the contact forming a lubricating film.

2.4.7. Relating the material and tribological properties of food with texture perception

A strong understanding of the influence of instrumental properties on perception can allow for the microstructural design of food products with predictable textural response and reduce the necessity for sensory analysis in food formulation and quality control. The benefit of reducing the dependency on sensory analysis is that it can be expensive, timely and occasionally unreliable. Examples from the literature on relating the material properties of

liquid and semi-solid foods on texture perception, and how soft-tribology is progressing this field of research, will now be discussed.

A particularly notable contribution is that by Shama and Sherman, in 1973, which showed a relation between rheologically determined viscosity and the perception of 'viscous'. Furthermore, they showed that the perception of 'viscous' did not occur during the same flow behaviour in the mouth for each product tested; rather, thick products were evaluated for viscosity at a fixed shear rate of 10 s^{-1} whilst for thin products the evaluation occurred at a fixed applied shear stress of 10 Pa. This suggests that thin products are orally evaluated for their deformation (flow) at a fixed applied pressure (stress) whilst for thick products the pressure required to obtain flow is assessed. This conclusion was made from a panel that assessed a range of commercially available liquid and semi-solid products in pairs that were asked to state which product of the pair was more viscous. Peanut butter, for instance, had a greater rheologically determined viscosity than chocolate spread below ~ 9 s^{-1}. However, the specific pseudoplasticity of the products meant that chocolate spread had a greater viscosity than peanut butter at greater shear rates. Since the panellist agreed that chocolate spread was more 'viscous', the flow conditions in the mouth could be determined to be above 9 s^{-1} for those types of product. Shama and Sherman assessed the perception of 'viscous', and rheological data from viscometry tests can also be related to the perceptions of 'thickness' and 'thinness' (Kokini, 1985; Richardson *et al.*, 1989). Furthermore, the perception of 'sliminess' has been related to the shear thinning behaviour for a range of hydrocolloids prepared at iso-viscosity (at low shear rate) (Szczesniak and Farkas, 1962). For solid food products, stress-strain curves from repeat compression tests are known to relate to sensory scores such as 'hardness', 'chewiness', 'elasticity' and 'cohesiveness' (Friedman *et al.*, 1963).

Whilst the above has shown that correlations can be made between rheology/texture analysis and texture perception, these mechanical testing techniques are perhaps rather limited considering the complicated and dynamic nature of food consumption. Foods go through numerous processes and structures during oral processing which has been considered to consist of three stages: ingestion/incisor biting, mastication then swallowing (Guinard and Mazzucchelli, 1996). During the mastication stage foods are broken down, heated/cooled to body temperature and lubricated by saliva where they are also exposed to α-amylase. To that end, rather than relating to a single material property, attributes which are more elusive to define may be related to the dynamic properties of foods which are said to undergo a decrease in structure and an increase in the degree of lubrication as a function of time during oral processing (Hutchings and Lillford, 1988). Until a mechanical instrument is devised which can mimic the entire behaviour of oral processing, a collection of data from numerous instruments which define a range of attributes that combine to form others is required. An example of this is 'creaminess' which has been shown to be strongly related to a function of the perceptions of thickness, smoothness and slipperiness (Kokini, 1987) as shown in Eq. 2.14. As discussed, thickness relates to viscometry data, smoothness relates to particle sizes within the dispersion (Guinard and Mazzucchelli, 1996) where in-mouth particle detection

$$Creaminess = thickness^{0.54} \,.\, smoothness^{1.56} \,.\, slipperiness^{0.32} \qquad Eq.\ 2.14$$

(inversely related to the perception of smoothness) depends on particle size, shape and hardness (Tyle, 1993), and slipperiness has been shown to relate to lubrication behaviour where friction is measured in a soft tribological contact (Malone *et al.*, 2003).

The notion that creaminess relates to slipperiness which is tribologically determined suggests that creaminess can be partly explained by tribology. To that end, values of friction

coefficients measured between surfaces lubricated by custards (de Wijk and Prinz, 2005) and milk (Chojnicka-Paszun *et al.*, 2012) have been shown to be inversely related to sensory perceptions of their creaminess. Thus, whilst rheological and mechanical properties of foods relate to textures perceived during the early stages of oral processing and tribology relates to later stages just before swallowing, they may also be combined to provide an insight into more complex attributes and those perceived at intermediate stages of oral processing (Chen and Stokes, 2012).

The study by Malone *et al.* (2003) showed that the perception of slipperiness is strongly correlated with friction coefficients and that this correlation is greatest in a mixed regime of lubrication. The same study highlighted the importance of tribology further by conducting a sensory test on a range of iso-viscous o/w emulsions that varied in oil phase volume (the influence of phase volume on the obtained Stribeck curves was discussed in the previous section, Chapter 2.4.7). Emulsions with similar tribological behaviour could not be discriminated by a tasting panel (testing for 'perceived fat content') whilst the samples which were tribologically dissimilar were also determined to be different by the sensory panel. The only exception to this rule was that 0% and 1% oil contents were not discriminated tribologically but were significantly different when tested sensorially. The explanation for these observations is that the panellists were measuring lubricity when assessing the fat content; however, panellists were able to detect 1% oil as a result of its taste and/or flavour.

Tribology has also been shown to be useful in determining the perception of astringency. The role of lubrication by saliva in the mouth plays an important role in mouth-feel and saliva has been shown to lubricate poorly after exposure to a known astringent compounds (Vardhanabhuti *et al.*, 2011). Furthermore, reduced perceptions of astringency were observed when panellists ingested lubricants after consumption of an astringent

compound alum, where more effective lubricants showed the greatest effect (Breslin *et al.*, 1993).

In summary, oral processing is a complicated and dynamic process where sensory attributes are continually being recognised. Currently available instruments are unable to mimic this behaviour entirely, requiring food researchers to obtain data from numerous instrumental devices which, when combined, can begin to provide correlations with many textural attributes. Whilst rheology measures bulk properties, tribology measures thin films and since these are both measured at different stages during consumption, they both provide correlations with sensory data and an insight into oral behaviour.

This section of the Literature Review has served to describe the importance of tribology for the sensory perception of textural attributes. As discussed in the Introduction, part of the objective of this thesis is to understand the influence of hydrocolloid structures on tribology. This objective is based on the fact that tribology is relevant in sensory perception and therefore consumer acceptance.

2.4.8. Tribology of salt solutions

This final section of the Literature Review discusses the tribology of aqueous solutions of salt. As briefly discussed in the Introduction, this thesis investigates the influence and mechanism of salt promoted lubrication in relation to salt properties that vary according

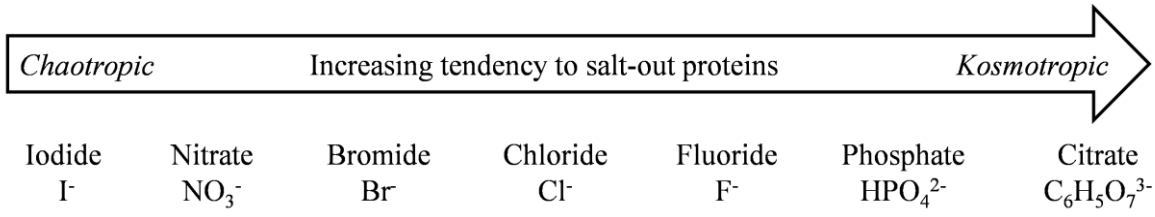

Fig. 2.18. Anions used in this thesis according to their position within the Hofmeister series of salts (Hofmeister, 1888).

to their position within the Hofmeister series. As such, this section aims to introduce the Hofmeister series of salts and provide a background into previous studies conducted on salt solution tribology.

The ability of ions to precipitate proteins can be ranked according to the Hofmeister series (Hofmeister, 1888) which, for anions, is summarised in Fig. 2.18. The work by Franz Hofmeister is available in English from a contribution by Kunz *et al.* (2004a). The physico-chemical rational behind this ordering has been intensely investigated and deliberated since it was first noted in 1888. Whilst there is seemingly no single factor explaining the Hofmeister series (Kunz *et al.*, 2004b), the greatest correlations are provided by ion polarizability (Conway and Ayranci, 1999), charge density (Nucci and Vanderkooi, 2008) and Gibbs free energy of hydration (Clarke and Lüpfert, 1999).

Solid surfaces modified with self-assembled monolayers (SAMs) have received significant interest due to their ability to provide ultralow fouling (Moro *et al.*, 2004; Li *et al.*, 2008; Holmlin *et al.*, 2001), and ultralow friction coefficients (Lee and Spencer, 2008; Chen *et al.*, 2009). In these systems, the highly solvated chains act as polymer brushes withstanding

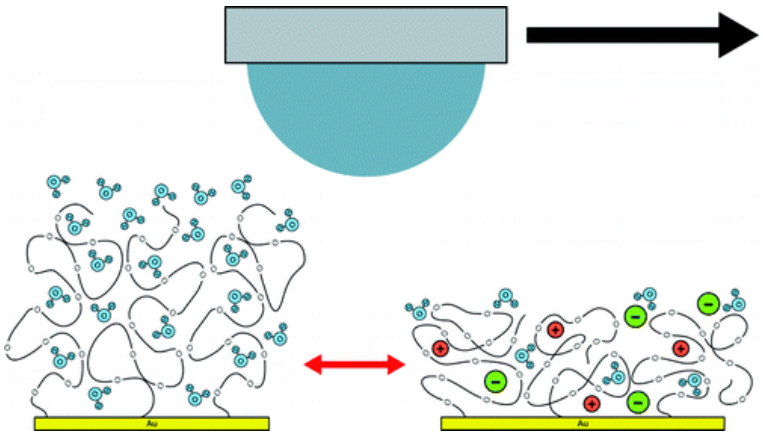

Fig. 2.19. Schematic representation of salt induced de-lubrication. Boundary lubrication is provided by SAMs due to steric repulsion of the polymer chains (left). Addition of salt reduces its lubrication effect as a result of adopting a more collapsed conformation (right). This image is adapted from Heeb et al. (2009).

compression forces due to steric repulsions. The repulsion in these systems minimises surface-surface contact, thereby providing high lubricity. The efficacy of this mechanism is dependent on the conformation that the SAMs adopt, which in turn is dependent on the solvent quality as shown in Fig. 2.19. To that end, friction forces have been shown (Nordgren and Rutland, 2009) to be influenced by chain conformation which can be controlled through pH and temperature which controls brush charge and polymer-solvent interactions, respectively. Salts have been shown to increase the friction of polymer brush contacts as they collapse the chain conformation by 'salting-out' effects (Heeb *et al.*, 2009). This later mechanism for the loss of lubrication with salts follows the Hofmeister series where strongly kosmotropic salts (those that have a tendency to "salt-out" proteins from solution) show a greater affect than chaotropic salts ("salt-in" tendencies) (He *et al.*, 2011).

In relation to polymer-free surfaces, the adhesion force between a silica particle and a mica sheet studied using AFM in an aqueous medium can be reduced using salts (Vakarelski *et al.*, 2000). In their study, Vakarelski *et al.* measured an increase in the minimum distance between surfaces in the presence of salts due to repulsion from surface bound hydrated ions, and found this effect to continue on increasing their concentration. They later showed (Donose *et al.*, 2005), using the friction force mode of an AFM, that this effect had a pronounced influence on aqueous lubrication. Studying monovalent cations (Li^+, Na^+ and

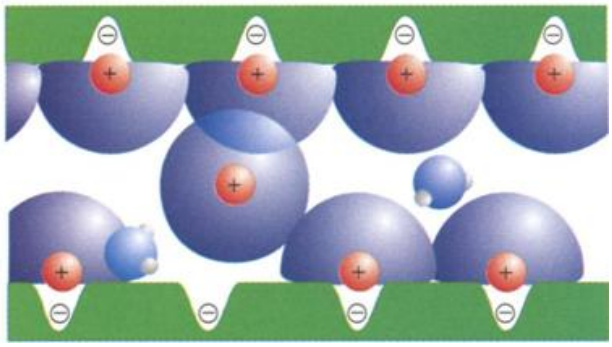

Fig. 2.20. Schematic representation of 'the fluidity of bound hydration layers' where hydrated ions that are bound to the surfaces provide boundary lubrication. The image is adapted from Raviv and Klein (2002).

Cs^+) they demonstrated that Li^+ solutions lubricate better than Cs^+ due to their greater enthalpy of hydration. Raviv and Klein (2002) have commented on the 'fluidity of bound hydration layers' between mica sheets in an aqueous media using a surface force balance (SFB). The ability of hydrated ions to provide lubrication for sliding surfaces, whilst being strongly bound to the surfaces was attributed to surface fluidity provided by the fast exchange of water molecules between neighbouring outer hydration shells (Fig. 2.20). Furthermore, they demonstrated that on compression the ions' repulsive hydration forces overcame surface van der Waals attractions at all separations, whereas water in the absence of salts was squeezed out of the confining surface contact.

In summary, salts have been shown to decrease lubrication when lubricity is provided by SAMs whilst they have also been shown to increase lubrication when hydrated and bound to the solid surfaces of an AFM. The influence of salt on SAMs has been shown to follow the Hofmeister series; however, the influence of lubrication by surface bound anions has not been related to the Hofmeister series, nor has it shown to be a relevant effect on macroscopic tribological setups with significant surface roughness.

Chapter 3.

Materials and Methodology

3.1. Introduction

This chapter provides detailed information on the materials used and the methods for sample formation and instrumental analysis. Additionally, a study into the formation of hydrophilic PDMS surfaces is presented in this chapter, as well as an investigation into the influence of the tribometer input parameters and surfaces on lubricant discrimination and data reproducibility. The results and discussion for these latter studies are given in this chapter, rather than a results chapter, because they relate to the development and understanding of the tribometer setup which determined the experimental procedures used for subsequent tests.

3.2. Materials

3.2.1. Hydrocolloids

Guar gum (GG) (4.18×10^6 g mol^{-1}, Sigma Aldrich), locust bean gum (LBG) (1.56×10^6 g mol^{-1}, Sigma Aldrich) and scleroglucan (SCL) (2.30×10^6 g mol^{-1}, Cargill) were used as supplied, but contained a small portion (~ 0.02 wt.%) of insoluble matter which was removed by centrifugation after aqueous hydration (this is discussed in section 3.3.1 on the sample formation of hydrocolloid solutions). Kappa carrageenan (κC) (5.10×10^5 g mol^{-1}) was a gift from Unilever supplied after being ion-exchanged with tetramethylammonium salt by ion exchange on Amberlite IR 120, thus preventing gelation and allowing linear polymeric behaviour. From this starting material, κC requires gelling salts to allow gelation. Lambda carrageenan (λC) (5.7×10^5 g mol^{-1}, Sigma Aldrich), xanthan gum (XG) (Sigma Aldrich) and κC were all used as supplied and solubilised fully. Single batches of each hydrocolloid were used throughout this work.

3.2.2. Salts

NaI (sodium iodide, Sigma Aldrich, purity ≥ 99.5%), $NaNO_3$ (sodium nitrate, Sigma Aldrich, purity ≥ 99.0%), NaBr (sodium bromide, Sigma Aldrich, purity ≥ 99.0%), NaCl (sodium chloride, Sigma Aldrich, purity ≥ 99.5%), NaF (sodium fluoride, Sigma Aldrich, purity ≥ 99.0%), Na_2HPO_4 (sodium phosphate, Sigma Aldrich, purity ≥ 99.0%) and $Na_3C_6H_5O_7$ (sodium citrate, Sigma Aldrich, purity ≥ 99.0%) were all purchased from Sigma Aldrich and used as supplied. Sodium azide (NaN_3, Sigma Aldrich, purity ≥ 99.5%) was used (where indicated) as a preservative without further purification.

3.2.3. Other materials

Corn syrup (Cargill) was used to represent Newtonian fluids and was not further purified.

3.2.4. Tribometer surfaces

Several surfaces were used in this study: elastomer discs, PDMS discs, PDMS balls and steel balls. The elastomer discs (4 mm White Silicone Sheet, Samco Silicone Products) were cut from large sheets and used as supplied after cleaning (the cleaning procedures are discussed in section 3.4.10.1). The steel balls were ¾ inch diameter AISI 400 stainless steel (PCS Instruments, London). The PDMS surfaces were made in-house following a procedure that will be discussed later using Sylgard, 184 (Dow Corning) with and without a siloxane surfactant poly [dimethylsiloxane-co-methyl (3-hydroxypropyl) siloxane]-graft-poly (ethylene glycol) methyl ether (Sigma Aldrich).

3.3. Sample formation

This section discusses the methods used to form the tested hydrocolloid systems. Hydrocolloid solutions were prepared which were then tested analytically or used to form gels.

3.3.1. Hydrocolloid solutions

All hydrocolloid solutions were prepared by first dispersing the polysaccharides in water, then heating to allow for hydration. Dispersion was achieved by slowly adding the required polysaccharide mass to cold (~5 °C) deionised water stirred using an overhead stirrer followed by continued stirring for ~30 min at room temperature. Whilst still stirring, samples were then hydrated by heating for ~1 h at 80 °C using a hot plate. Then, after allowing to cool to room temperature, deionised water was added to compensate losses to evaporation. For GG, LBG and SCL solutions, the insoluble matter (~ 0.02 wt.%) was removed by centrifugation at relative centrifugal force = 17,696×g for 30 min using a Beckman J2-21 centrifuge.

For all but the κC hydrocolloid solutions, sodium azide (0.02 wt.%) was added (to prevent bacterial growth) to the distilled water prior to the addition of hydrocolloids. Sodium azide was not used for κC samples to ensure that sodium cations were not influencing molecular ordering.

For the study on the influence of sodium salts on aqueous tribology (Chapter 5.3), salts were added to deionised water under agitation *via* an overhead stirrer and sonication using in a Branson 200 ultrasonic cleaner (Branson Ultrasonics corporation). The salt solutions were then diluted with water, or a combination of water and a 1 wt.% GG stock

solution to obtain required volumes for the desired concentrations. The GG stock solution was prepared following a dispersion and hydration process as described above.

3.3.2. Fluid gels

Fluid gels were made using both a rheometer and a pin-stirrer. A rheometer was used to accurately control and monitor the fluid gel formation process through the following parameters: shear rate, shear stress, temperature and time (cooling rate). A continuous process pin-stirrer was also used to probe the influence of the processing conditions and to produce large volumes of fluid gels to conduct detailed material testing using a range of techniques. For both fluid gel formation methods, the hydrocolloid solutions were prepared as above but with the required mass of KCl added to the deionised water prior to the addition of κC. After dispersion and hydration, as described above, the κC solutions were transferred to screw-top jars on a hot-plate (~ 80 °C) under agitation from a magnetic stirrer. Screw-top jars were used to prevent evaporation whilst the κC solutions were heated above their gelation temperatures. The solutions were then either transferred to the rheometer or pin-stirrer as described in the following sections.

3.3.2.1. Fluid gel formation within a rheometer

A TA Instruments AR-G2 stress controlled rheometer with a 60 mm 2° steel cone was used to produce fluid gels where the cooling rate and shear rate were controlled. Solutions of κC and KCl were transferred *via* pipette to the rheometer peltier plate set to 60 °C. The sample temperature was allowed to reach equilibrium (2 min) after the geometry was lowered and excess material removed. The shear cooling profiles were then conducted at 200 s^{-1},

which has been demonstrated to be roughly the average shear rate that particles are exposed to within the pin-stirrer experimental setup (Gabriele, 2011), whilst cooling at a rate of 3 °C/min, which is suitable for forming κC fluid gels with KCl (Gabriele *et al.*, 2009). By conducting these sheared cooling profiles to κC solutions, fluid gels are formed and their viscosities during formation can be probed.

3.3.2.2. Fluid gel production within a jacketed pin-stirrer

A continuous process jacketed pin-stirrer was used to produce fluid gels on a larger scale than capable *via* the rheometry method. The pin-stirrer consists of a shaft with 16 pins

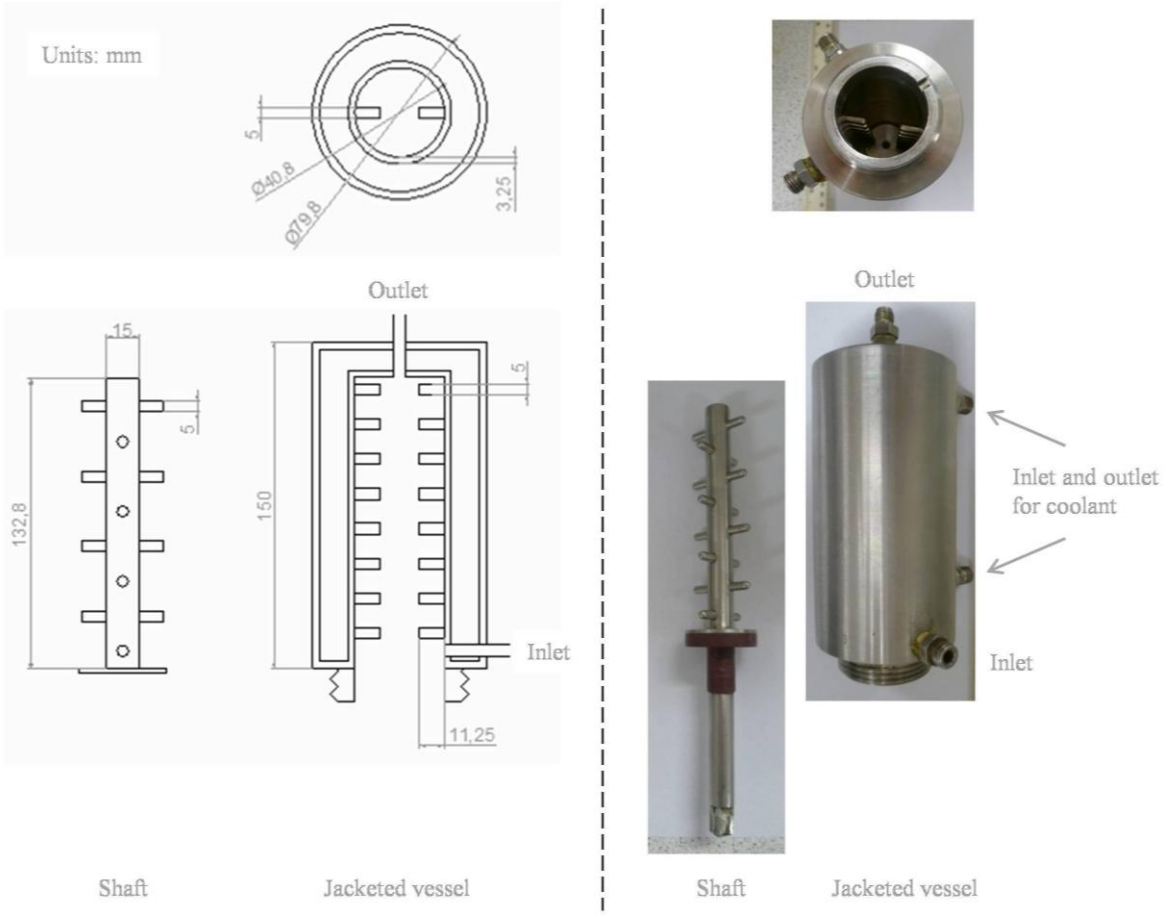

Fig. 3.1. Drawings (left) and photographs (right) of the pin-stirrer shaft and jacketed vessel (once dissembled).

evenly distributed along its length, which is inserted into a jacketed vessel with 16 stators running up the inside wall as illustrated in Fig. 3.1. The arrangement is such that the shaft pins are positioned between those of the vessel.

Heated κC solutions were fed from the jar on the stirred hot-plate (using a specially adapted jar-lid to prevent water evaporation) into a non-sheared temperature-controlled vessel (set to 53 °C) before entering the pin-stirrer. The temperature of the fluid entering (T_{in}) and exiting (T_{exit}) the pin-stirrer were recorded using thermocouples, and were controlled *via* recirculating water baths running through the annulus (jacket) of the vessels. Silicone tubing was used to connect all of the units within the process, and material flow was induced *via* a peristaltic pump. The pin-stirrer internal volume (with shaft inserted) is 150 mL and was used at maximum shaft rotation speed (~1438 rpm) with the flow rate maintained at 10 mL/min. Samples were collected in a beaker submerged in an ice bath where they were cooled to 5 °C; the cooling in this step was quiescent as no shear force was applied. Samples were then refrigerated (3 °C) and stored for at least 24 hours, before testing, to allow post processing ripening effects to fully take place (Gabriele *et al.*, 2009). A range of fluid gel volume fractions was prepared by diluting the fluid gels with deionised water and gently shearing with an overhead stirrer for ~ 3 min. A schematic of the pin-stirrer fluid gel production setup is given in Fig. 3.2.

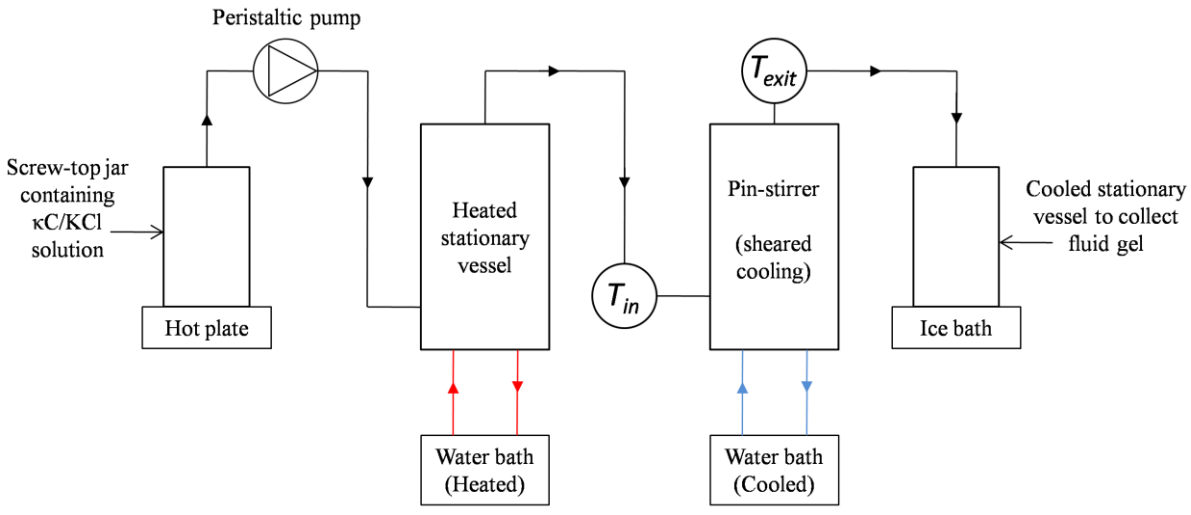

Fig. 3.2. Schematic representation of the pin-stirrer setup for fluid gel production.

3.4. Analytical methods

3.4.1. Texture analyser

Compression tests were conducted on quiescently cooled bulk gels using a TA.XT plus Texture Analyser (Stable Micro Systems Ltd., UK). Aliquots of the κC/KCl heated solutions were reserved for quiescent gelation into cylindrical tubes forming gels (21.43 mm diameter) that were cut into 10 mm length pieces. Mechanical properties were analysed in compression from a 40 mm diameter aluminium probe at a rate of 1 mm s^{-1}. True stress and true strain values were calculated from the measured force/distance data using equations described by Norton *et al.* (2011).

3.4.2. Goniometer

In order to characterise the hydrophilicity of the surfaces used in the tribometry tests, and to probe changes in the surface adsorption of GG, the wettability of tribo-surfaces under various conditions was analysed. To do this, water contact angle measurements were made with a Krüss Easy Drop FM40 goniometer using deionised water. Angles were measured from the images of 20 μL sessile drops using tools available in the provided software. The values reported herein are the average of 3 measurements taken from 3 surfaces *i.e.* 9 measurements in total, and error bars show ± one standard deviation of error. The surfaces were cleaned (as described later in Chapter 3.4.10.1), dried under compressed air, then tested immediately afterwards, or after subject to soaking in a GG solution to allow for GG surface adsorption. In the latter case, surfaces were immersed into 0.2 wt.% GG solutions with various salt contents, for 20 mins. The surfaces were then rinsed in de-ionsied water to remove bulk residue and non surface bound matter before drying under compressed air.

3.4.3. Polarimeter

An Anton Paar Gyromat automatic Polarimeter was used to measure optical rotations at 405 nm. The temperature was controlled *via* a recirulating water bath flowing around the cell annulus. Temperatures were measured using a thermocouple situated in the sample fluid. The cell path length used was 5 cm.

3.4.4. D.S.C

A Seteram μDSC3 evo Dynamic Scanning Calorimeter (DSC) was used to measure enthalpies and temperatures of thermal transitions. Screw-top 'closed batch cells' were used where sample cells were filled (~75%) with 0.86 ± 0.05 g of a fluid gel, and the reference cell with an equal mass of deionised water. The reference cell was used with water so as to cancel out the temperature dependence of the specific heat capacity, thus providing 'non-sloping' baselines. Fluid gels were tested by isothermally holding at 10 °C for 30 mins, then commencing the procedure as follows: heating to 70 °C, cooling to 10 °C, heating to 70 °C, and then finally cooling to 10 °C; all at 0.35 °C/min. 10 min isothermal holds were applied between each step. Enthalpies of transitions were calculated from the average of five repeats.

3.4.5. Optical microscope

An optical microscope (Brunel Microscopes Ltd SP-300F) was used with a 100x objective lens. Fluid gel samples were prepared by diluting with deionised water (1:3), shearing at 1000 s^{-1} for 5 mins using a rheometer with a cone and plate geometry, then pipetting one drop onto a microscope slide (VWR) covered with a cover slip (VWR thickness no.1). One drop of immersion oil (Panscan Xtra) was placed on the cover slip making contact

with the objective lens. Images were taken then processed on ImageJ software, by first converting the images to a 32-bit greyscale, then enhancing the contrast to more clearly identify particle edges. Particle diameters were then measured (over 1,500) from numerous images and converted from lengths in pixels to μm by undertaking the same process on a known length graticule slide.

3.4.6. STEM

STEM (scanning transmission electron microscopy) images of individual fluid gel particles were obtained to probe their internal structures. Samples were prepared by diluting (1:40) in deionised water, shearing, and then drying onto a sample stage under vacuum. Imaging of the dried samples was conducted on a JSM-7000F Scanning Electron Microscope (SEM) (JEOL USA) in STEM mode at 30 kV.

3.4.7. Interferometer

To characterise the roughness of the tribo-surfaces, interferometry was used. The instrument used was a MicroXAM interferometer (Scantron, UK). Using a 20x objective lens, the images were taken of areas: 432.3 × 321.5 μm. This procedure was repeated 9 times on 3 surfaces, *i.e.* 27 areas were scanned for each surface. Scanning Image Processor software (Image Metrology, Denmark) was used to analyse the images to provide the roughness data.

3.4.8. Centrifugation

A Sigma 3K30 centrifuge (Sigma Laborzentrifugen) was used at a range of centrifugal forces to sediment the fluid gel particles from the continuous aqueous phase. The relative centrifugal force (RCF) is calculated from Eq. 3.1 where *r* is the radius (8.4 cm) and *n* is the speed in rpm (revolutions per minute).

$$RCF = 11.18\left(\frac{n}{1000}\right)^2 r \qquad \textit{Eq. 3.1}$$

3.4.9. Rheometer

Two rheometers were used throughout this study. A Bohlin Gemini HR nano stress-controlled rheometer (Malvern Instruments) was used for testing non-gelled hydrocolloid solutions. A TA Instruments AR-G2 stress controlled rheometer was used for the fluid gel studies and $[\eta]$ determination. This latter rheometer was used because it had sandblasted geometries to minimise wall-slip for the suspension samples and a concentric cylinder geometry suitable for testing low viscosity samples which are required for calculating $[\eta]$s.

3.4.9.1. Viscometry of hydrocolloid solutions

To investigate the influence of shear on coil overlap behaviour, flow curves were obtained for a range of hydrocolloid concentrations. From that, *C** was identified at low and high shear rates. A parallel plate geometry with a small gap height (50 μm) is known (Connelly and Greener, 1985) to provide viscosity measurements up to high shear rates and so an acrylic (60 mm diameter) disc was used with a 50 μm gap for these studies. The resulting data fitted well to the Ellis model (Eq. 3.2) (Ratcliffe *et al.*, 2005) where zero shear viscosities

$$\frac{\eta - \eta_\infty}{\eta_0 - \eta_\infty} = \frac{1}{1 + (K\sigma)^n} \qquad \textit{Eq. 3.2}$$

(η_0) were identified (η = apparent viscosity, η_∞ = infinite shear viscosity, σ = shear stress, K = arbitrary constant and n = power law exponent). Tests were conducted at 37 °C (body temperature) and were repeated 3 times. Viscometry values at low and high shear were calculated from the mean of these repeats.

3.4.9.2. Viscometry for intrinsic viscosity determination

An aluminium double concentric cylinder geometry was used for identifying low shear viscosities of very dilute hydrocolloid solutions (< ~ 0.05 wt.%); this geometry had the following dimensions: rotor immersed depth, inner and outer diameters were 59.5, 20.38 and 21.96 mm respectively; stator inner diameter, 20 mm; approximate sample volume, 6.48 mL. Solutions for testing were pre-sheared at 100 s^{-1} for 60 s before being held stationary for 3 min to equilibrate. Steady state flow tests were taken by ramping from 0.01 to 10 Pa with a 1 min steady state period for each data point collected. η_0 values were taken from the fits of flow curves to the Ellis model (Eq. 3.2). Intrinsic viscosities were then determined from relative viscosities ($\eta_{rel} = \eta_{0\ solution}/\eta_{0\ solvent}$) and specific viscosities ($\eta_{sp} = \eta_{rel}$ -1) using the Huggins and Kraemer equations as discussed in the results chapters.

3.4.9.3. Viscometry of fluid gels

A 40 mm diameter sandblasted steel parallel plate geometry was used with a sandblasted bottom plate. A parallel geometry was used to take advantage of roughened surfaces for minimising wall-slip – a feature unavailable for the cone geometry. 10 min prior to rheological testing, fluid gels were subjected to a pre-shear of 10 s^{-1} for 10 s to alleviate

inconsistencies in the loading of samples on the rheometer. Tests were conducted with controlled stress at 10 °C with a 1 mm gap height and were repeated three times to ensure reproducibility. The observed viscosity trends were confirmed by repeating tests using a cone and plate geometry, switching to controlled rate experiments and using data from ramped-down as well as ramped-up shear profiles.

3.4.9.4. Thixotropy tests

Thixotropy tests were conducted by shearing from rest to 100 s^{-1} (in 1 min), holding for 2 min at 100 s^{-1}, then ramping down (in 1 min) constituting one sweep; after a 10 min rest period the experiment was then repeated (second sweep).

3.4.9.5. Creep tests for yield stress determination

Creep experiments were used to obtain yield stress data and were observed to be more reproducible than other tested methods including stress ramps and oscillatory experiments. Creep tests were conducted with a fixed shear stress (σ) applied for 20 s whilst the deformation (strain, γ) was monitored, followed by a 30 s rest period. This process was then repeated with the applied stress increased successively in intervals of 2 Pa. When the applied stress is below a material's yield stress, it behaves as an elastic solid where the measured strain (or compliance, γ/σ) is small and constant with time after an instantaneous response. The material then recovers instantaneously when the stress is removed. Upon application of a stress exceeding the yield stress, the material strains *i.e.* flows, thus allowing the yield stress to be identified from the lowest stress required to induce flow (Tharwat, 2004). An example to illustrate this behaviour is shown in Fig. 3.3, where 200 Pa is the lowest stress inducing flow, and so would be taken as the yield stress. Creep tests were initially conducted with 10 Pa

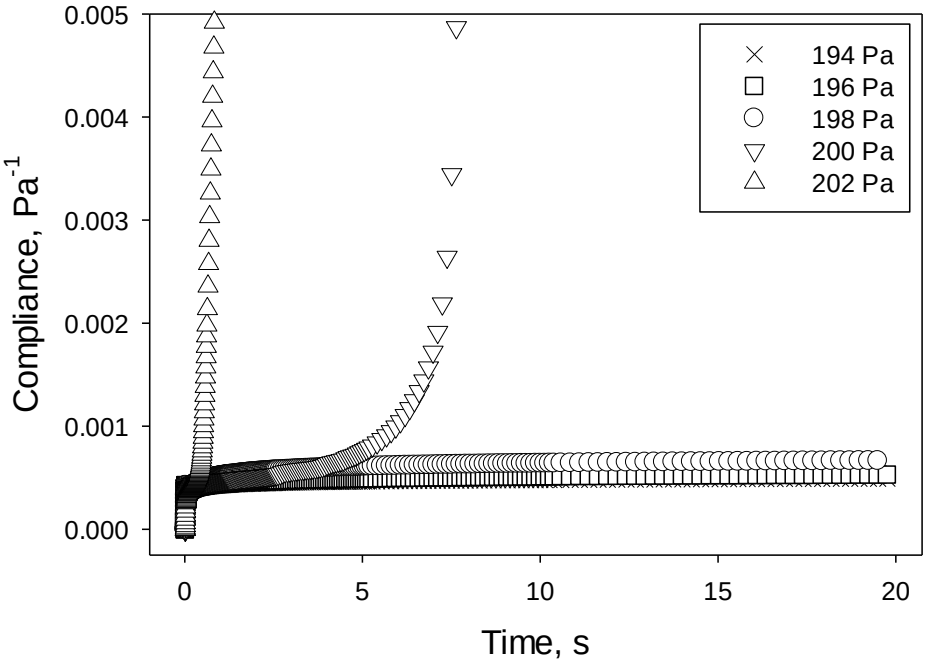

Fig. 3.3. Example of creep test data where the compliance (γ/σ) is measured in time as material is subjected to a fixed stress (σ). Successive stresses were applied (with 30 s rest intervals) and the yield stress is taken as the lowest stress required to initiate flow i.e. 200 Pa for the data above (2% κC fluid gel with 0.3 wt.% KCl).

intervals to identify the approximate yield value. All creep tests were conducted at 10 °C and the yield stress data reported are the average of five repeats.

3.4.9.6. Oscillatory rheometry

Oscillatory and creep tests were conducted with a sandblasted 40 mm parallel plate and sandblasted bottom plate with a 1 mm gap. Frequency sweeps were conducted in controlled stress mode with the stress set to be within the linear viscoelastic region for all samples tested (< 1% strain); stress sweeps were conducted at 1 Hz.

3.4.10. Tribometer

An MTM2 (Mini Traction Machine) tribometer (PCS Instruments, London) was used to measure the frictional properties of lubricated and unlubricated contacts. This instrument provides fully automated traction mapping of lubricants under boundary, mixed and hydrodynamic environments. In the setup, which is shown in Fig. 3.4, a ball is loaded against the face of a flat disc where the ball and disc are independently driven to form a test contact of user defined entrainment speed (*U*) and slide-roll ratio (*SRR*). *U* is the mean of the ball and disc speeds (U_{ball} and U_{disc}, respectively) and the *SRR* (Eq. 3.3) defines the ratio of sliding to rolling speeds at the contact.

$$SRR = \frac{U_{disc} - U_{ball}}{U} \qquad Eq.\ 3.3$$

At the start of a test, the ball is loaded against the disc at a user defined normal load (*W*). The ball and disc rotate whilst the frictional force at the contact is measured by force transducers. During a Stribeck test the friction coefficient (μ) is measured at a range of speeds *e.g.* from $U = 1$ to 1000 mm s^{-1}. At each *U* tested the ball and disc will be travelling at different speeds according the *SRR*. As an example, to obtain $U = 100$ mm s^{-1}, for a test

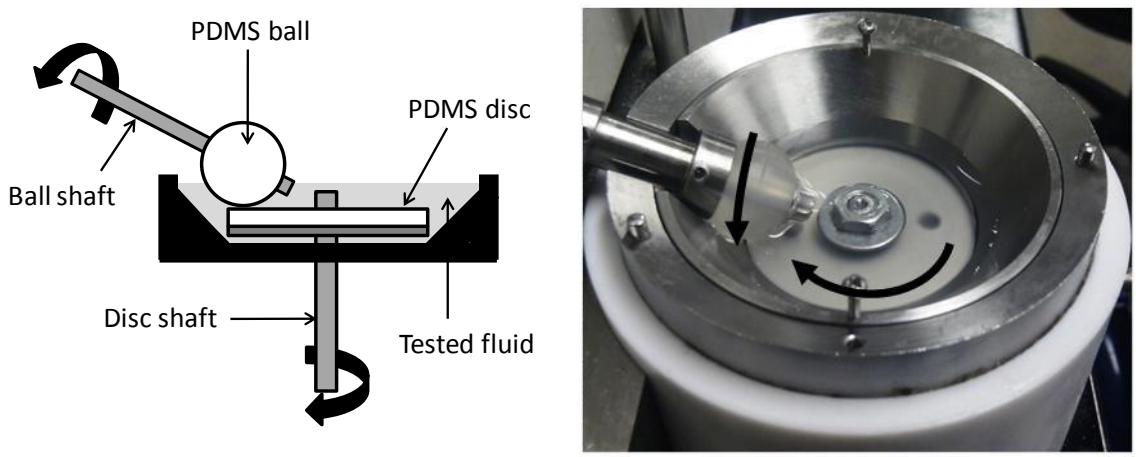

Fig. 3.4. Schematic (left) and photograph (right) of the tribometer setup with PDMS ball and disc. Thick arrows indicate the directions of the ball and disc rotation.

conducted at *SRR* = 50%, the ball and disc speeds will be 75 and 125 mm s^{-1}, respectively. The MTM2 instrument then conducts a test with the speeds of the ball and disc switched *i.e.* 125 and 75 mm s^{-1}, respectively. The μ value recorded is then the average of these two tests. It is important to note that the ball and disc always rotate in the same direction; it is just their relative speeds that alternate during Stribeck tests.

3.4.10.1. Tribopair preparation

As discussed in the materials section (3.2.4), several surfaces were used in this study: elastomer discs, PDMS discs, PDMS balls and steel balls. The elastomer-steel tribopair (pair of tribometer surfaces *i.e.* ball and disc) was used since it has previously been shown to provide data with correlations to 'slipperiness' sensory scores (Malone *et al.*, 2003). Additionally, a PDMS tribopair (ball and disc both made from PDMS) was used since it has been suggested to be useful for tribometry in food research because the deformability and roughness can be controlled (Dresselhuis *et al.*, 2008).

The elastomer discs were cut out from the supplied sheets and were cleaned by rubbing with washing-up liquid, sonicating in ethanol (5 min) and then sonicating in deionised water (5 min) and were not reused. The stainless steel balls were cleaned in the same way but were sonicated in acetone rather than ethanol and were reused ~ 30 times. The PDMS surfaces were prepared by first mixing the supplied base and curing agent (relative ratio 10:1) using an overhead stirrer then removing the air bubbles by vacuum at room temperature. This blend was then poured into spherical and flat moulds before being heated (~ 70 °C) overnight under vacuum. The spherical moulds served to form ¾ inch diameter balls and the flat moulds formed sheets which were used to cut the discs from (using a

specifically designed cutter/stamp). The PDMS surfaces were cleaned using the same procedure as for the elastomer discs and were used for 3 tests each.

3.4.10.2. Influence of tribometer input parameters

The *SRR* and *W* can be controlled which can enable the design of tests that mimic oral behaviour. In the mouth, tongue-palate forces have been recorded that vary between 0.01 and 90 N (Miller and Watkin, 1996), however, during the consumption of liquid and semi-solid foods the forces are expected to be of the order 1 N. The *SRR* parameter is useful because the tongue rolls over the hard-palate in addition to sliding, thus a mixed sliding/rolling contact is more relevant to oral movements than pure sliding. With this being said, the tribometer setup is not expected to fully resemble oral behaviour and so the choice of the input parameters *W* and *SRR* were based on the quality of data rather than maximising the resemblance to oral behaviour. To that end, the reproducibility of Stribeck tests (from U = 1 to 1000 mm s^{-1}) was investigated for a range of *W*s and *SRR*s for two tribopair contacts lubricated with a hydrocolloid solution: 1 wt.% κC, at 37 °C. Runs ramping up were performed from U = 1 to 1000 mm s^{-1} followed by ramping down; this was continued until 6 runs were completed which constituted 1 test. The standard deviation of the friction coefficients was calculated for each speed, expressed as a percentage of the average friction value, and averaged over the speed range to provide the 'average error' for each test.

Average errors for each test are given in Table 3.1. This data shows, firstly, that when testing at SRR = 50%, the lowest errors were obtained with a normal load W = 2 N; and secondly, that at W = 2 N, the slide-roll ratio with the lowest errors was SRR = 50%. As a result of this test, subsequent Stribeck curves were conducted at W = 2 N and SRR = 50%.

Table 3.1
Average error margins for Stribeck curves obtained for a range of Ws, SRRs and tribopairs.

Load (*W*), [N]	***SRR* [%]**	**Tribopair**	**Average error [%]**
1	50	Elastomer-steel	4.87
2			3.88
3			7.22
4			4.88
1	50	PDMS-PDMS	19.80
2			13.90
3			14.14
4			14.03
2	25	Elastomer-steel	6.68
	50		3.88
	75		5.01
	100		5.39
	125		5.32
	150		7.09
	175		5.95
	200		11.17

3.4.10.3. Development of hydrophilic PDMS surfaces

This section discusses the influence of saliva on tribology and methods to mimic its influence on PDMS surfaces.

Saliva plays an important role in providing lubrication to oral surfaces through a mucous layer coating. A tribological study on pig tongues, with and without human whole saliva coatings, demonstrated that saliva significantly reduces the sliding friction coefficient and changes the wetting properties of mucosa surfaces from hydrophobic (when dry) to hydrophilic (Ranc *et al.*, 2006). Thus, it may be beneficial to coat tribometry surfaces with saliva to enhance the resemblance to oral surfaces. However, saliva is a complicated viscoelastic solution that is difficult to replicate synthetically. Using saliva collected from humans can also be problematic since saliva's composition and properties are different from

person to person and are influenced by factors such as diet and food/drink intake prior to sampling (van Aken *et al.*, 2007). To that end, greater friction coefficients of an animal mucosa contact have been recorded for stimulated human saliva compared to unstimulated saliva (Prinz *et al.*, 2007) demonstrating that inconsistencies may occur for tribological testing with human saliva.

An alternative option to saliva (synthetic or natural) is to modify the surface chemistry of the PDMS to make it more hydrophilic thus influencing the wetting properties and forming a hydrated film at the surface, similarly to a saliva coated surface. PDMS surfaces may be rendered hydrophilic using an oxygen plasma cleaner (Bongaerts *et al.*, 2007) although the change in wetting behaviour is not permanent and so friction coefficients may be susceptible to change throughout testing. A hydrated boundary lubrication film can be formed on PDMS surfaces after soaking in aqueous solutions of poly(ethylene oxide)-poly(propylene oxide)-poly(ethylene oxide) (PEO-PPO-PEO) which forms regions of PPO adsorption, through the hydrophobic effect, which anchors the polymer whilst the hydrophilic PEO chains occupy the aqueous solution (Lee *et al.*, 2004). This method of surface modification is unsuitable for the work in the present study because the PEO-PPO-PEO is unlikely to remain adsorbed after a cleaning procedure to remove the excess polymer. A more permanent surface modification can be achieved by chemically grafting chitosan and hyaluronic acid onto PDMS in a multi-step layer-by-layer dip-coating procedure (Bongaerts *et al.*, 2009). This multi-step process, however, is time consuming and not appropriate for producing large quantities of ball and disc surfaces.

In an effort to produce permanently modified PDMS surfaces using a single-step process, a siloxane surfactant was added to the base and curing agent during preparation which has previously been shown to enhance wettability (Kim *et al.*, 2010). To the author's

knowledge, this technique has not been described for the purpose of tribometry and will now be discussed in detail.

The procedure used for preparing the modified hydrophilic (HL) surfaces was the same as that described earlier for standard PDMS except that the siloxane surfactant (poly [dimethylsiloxane-co-methyl (3-hydroxypropyl) siloxane]-graft-poly (ethylene glycol) methyl ether) was included in the ratio 100:10:1 for the base, curing agent and siloxane surfactant, respectively. The structures of PDMS and the siloxane surfactant (Fig. 3.5) suggest that the backbone of the latter will physically entangle with the PDMS whilst the poly(ethylene glycol) (PEG) side chains towards the surface of the bulk material will preferentially reside in contact with the steel moulds during the curing stage. The polar PEG chains were expected to increase the PDMS hydrophilicity whilst being strongly physically bound within the cured (cross-linked) PDMS network and thus withstanding the typical cleaning procedure for PDMS surfaces. To test this, PDMS surfaces (with and without the siloxane surfactant) were prepared into sheets and were tested for their water contact angles after application of the cleaning procedure (as described previously, Chapter 3.4.10.1). The results of this test, averaged over 5 repeats, are given in Fig. 3.6 as a function of time.

The results show that the contact angle of the modified PDMS is significantly lower than standard PDMS, particularly after ~ 1 min. This demonstrates that the addition of the surfactant, which contains polar side chains, makes the PDMS surfaces substantially more

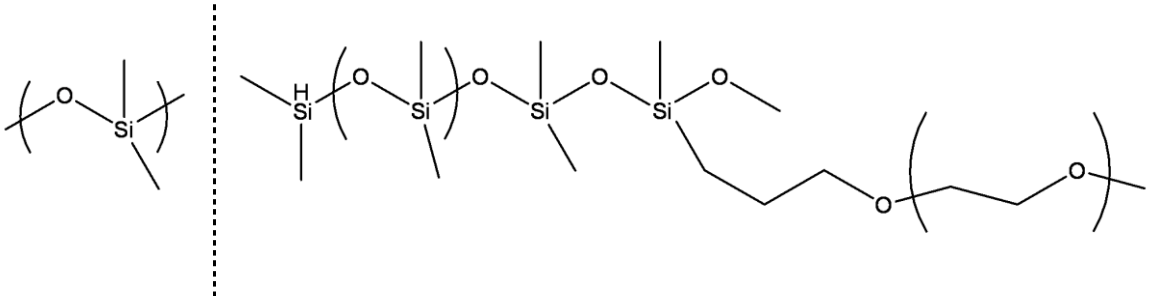

Fig. 3.5. Chemical structures of the polydimethyl siloxane (PDMS) monomer (left) and the siloxane surfactant poly [dimethylsiloxane-co-methyl (3-hydroxypropyl) siloxane]-graft-poly (ethylene glycol) methyl ether (right)

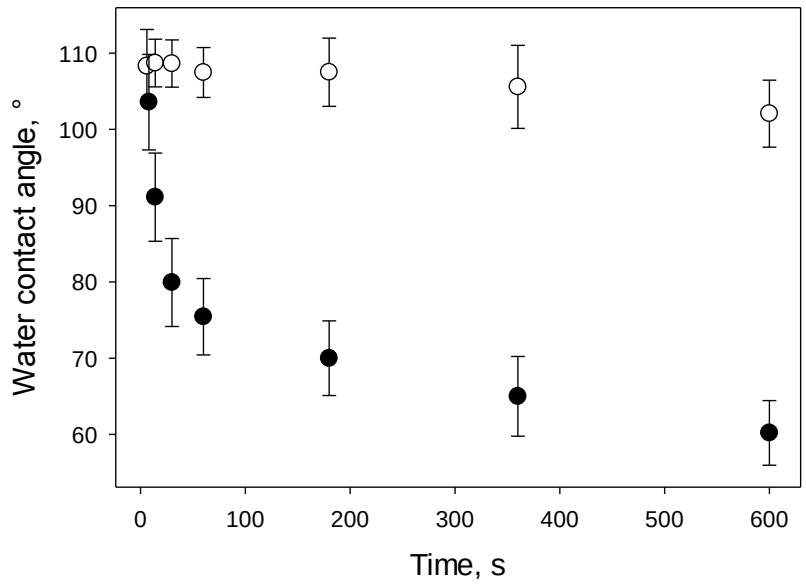

Fig. 3.6. Water contact angles as a function of time for standard PDMS (○) and silioxane surfactant incorporated modified HL-PDMS (●).

hydrophilic.

To analyse the surfaces further, the effect of adding water to a dry contact of both standard and HL- PDMS tribopairs was tested and compared with the results obtained by Vardhanabhuti *et al.* (2011) who investigated the effect of adding saliva to a standard PDMS contact. The latter test, by Vardhanabhuti *et al.* (2011), recorded friction coefficients at a fixed entrainment speed as a function of time. After obtaining a steady state with a dry contact, 100 μL of saliva was transferred *via* pipette to the disc such that it entrained the contact zone. The saliva significantly reduced the friction coefficient and after reaching a steady state, astringent solutions (and a water control), 50 mL, were then added. Their test was designed so that the friction measured at a steady state with saliva represented a baseline from which the effect of adding astringent compounds could be explored. The results are provided in Fig. 3.7 (a) and showed that the addition of astringent solutions increased friction

(a)

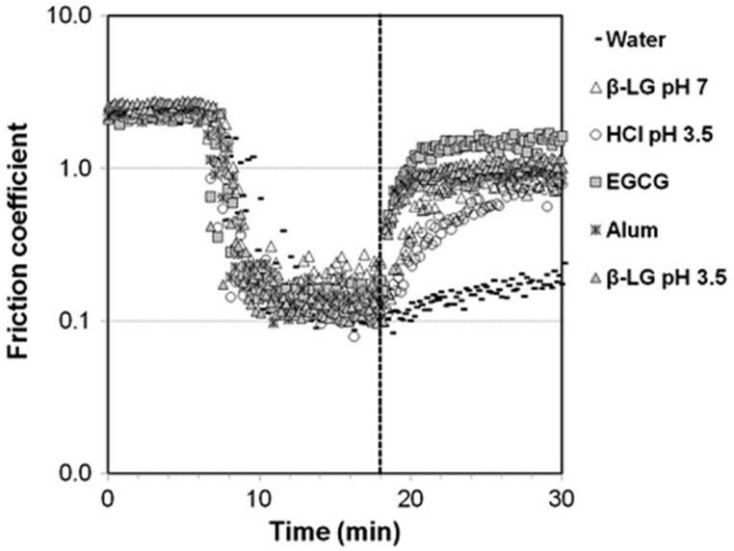

(b)

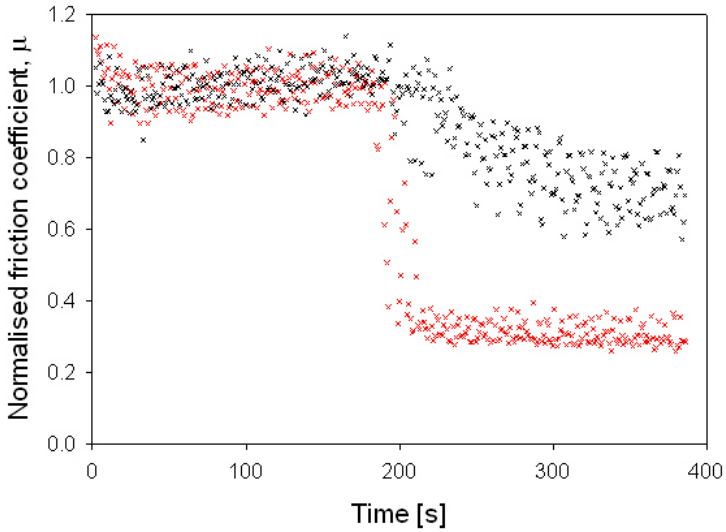

Fig. 3.7. Top: the effect of adding 100 μL of saliva to a standard PDMS-PDMS contact at ~ 8 min, followed by the addition of 50 mL of water or astringent compound solutions at ~ 19 min (a). Bottom: the effect of adding 100 μL of water to a fixed speed sliding/rolling contact of standard PDMS (black) and the modified hydrophilic PDMS (red) at ~ 200 s (b). The top figure (a) is adapted from Vardhanabhuti et al. (2011).

from the saliva baseline to a value greater than obtained from the addition of water; this was proposed to be a result of saliva induced protein precipitation.

Fig. 3.7 (b) shows the results from a timed test at $U = 15$ mm s^{-1}, $W = 2$ N and $SRR = 50\%$ where 100 μL of deionised water was added to the ball and disc contact after ~ 200 s for both the modified and standard PDMS tribopairs. The data shows that compared to the standard PDMS, the addition of water to the modified surfaces gives a more significant reduction in the friction coefficient over a shorter period of time. The results observed from adding water to the modified HL-PDMS tribopair (Fig. 3.7 b) is similar to the behaviour observed from the addition of saliva to standard PDMS (Fig. 3.7 a).

To further test the lubrication properties of the modified surfaces, Newtonian master Stribeck curves were obtained from a range of corn syrup solutions using three tribopairs: PDMS, HL-PDMS and for comparison, elastomer-steel (Fig. 3.8). The master Stribeck curves show that PDMS and HL-PDMS tribopairs have greater boundary and mixed friction

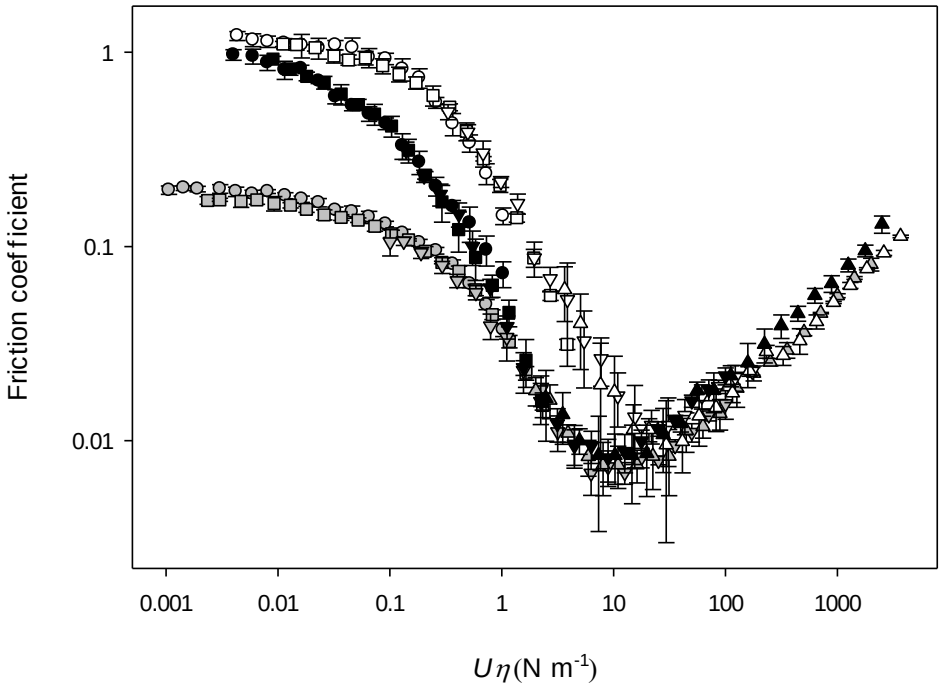

Fig. 3.8. Newtonian master Stribeck curves obtained using corn syrup 5% (○), 30 % (□), 85% (▽) and 100% (Δ). Data is shown for three tribopair surfaces: standard PDMS (white filled symbols), HL-PDMS (black) and elasomter/steel (grey).

coefficients than the elastomer-steel tribopair which is due to increased surface deformation and hysteresis loses caused by the greater deformability of the PDMS based tribopairs. It can also be seen that the HL-PDMS has lower boundary and mixed regime friction coefficients when compared to PDMS. This is because water has a greater affinity to the more polar HL-PDMS surfaces and so can begin to entrain in to the contact at lower speeds providing more effective lubrication. The hydrodynamic regimes are similar for all the tribopairs because their surface characteristics do not influence friction when surface-surface separation occurs.

The results presented in this section suggest that a one-step modification to the preparation procedure of PDMS can be used to prepare a PDMS tribopair that has enhanced wettability compared to standard PDMS. This change in hydrophilicity enhances the entrainment of water for lubrication and allows water to form a lubricating film analogous to saliva on a standard PDMS surface. However, it should be noted that the modified surfaces are not expected to interact with astringent compounds in the same way as saliva.

3.4.10.4. Influence of tribopair

Two tribopairs were utilised throughout the work presented in the results Chapters of this thesis: elastomer-steel, since it is known to provide friction coefficients that correlate with sensory attributes, specifically, the perception of slipperiness during consumption of guar gum solutions (Malone, Appelqvist, & Norton, 2003); and HL-PDMS-HL-PDMS, because it can be formed to user defined properties and has previously been studied as a tribopair to understand the effect of surface elasticity (Krzeminski, Wohlhüter, Heyer, Utz, & Hinrichs, 2012), wettability (Bongaerts, Fourtouni, & Stokes, 2007) and surface roughness (Cassin, Heinrich, & Spikes, 2001). Whilst the HL-PDMS tribopair is more deformable and

hydrophilic than the elastomer-steel tribopair, and therefore more similar to oral mucosa, the choice of tribopair for each tribological study conducted in this thesis was based on the tribopair that gave the highest quality data. Data quality was considered in terms of reproducibility of the Stribeck curves obtained for the same lubricant, and discrimination between Stribeck curves obtained for different lubricants. This test was conducted for the two types of lubricant tested in this thesis: hydrocolloid solutions and fluid gels, both using κC. To create a range of lubricants for each type, they were prepared at a range of κC concentrations: 0.5, 1 and 2 wt.%. The results of this test are shown in Fig. 3.9 where the average error values are given from the repeat of 3 tests (*i.e.* 18 runs) for each lubricant. Normalised friction coefficients (μ_{norm}) were used in Fig. 3.9 to allow direct comparisons of the influence of tribopair on the reproducible discrimination of lubricants. Absolute friction coefficient values (μ) were not compared between tribopairs because their values (for the same lubricant) were very different. On comparison of the two tribopairs tested here, greater absolute friction values were observed with HL-PDMS are expected to arise from greater adhesive forces and deformation under load; this effect dominates the fact that the HL-PDMS tribopair has a greater surface roughness and therefore lower real area of contact than elastomer-steel.

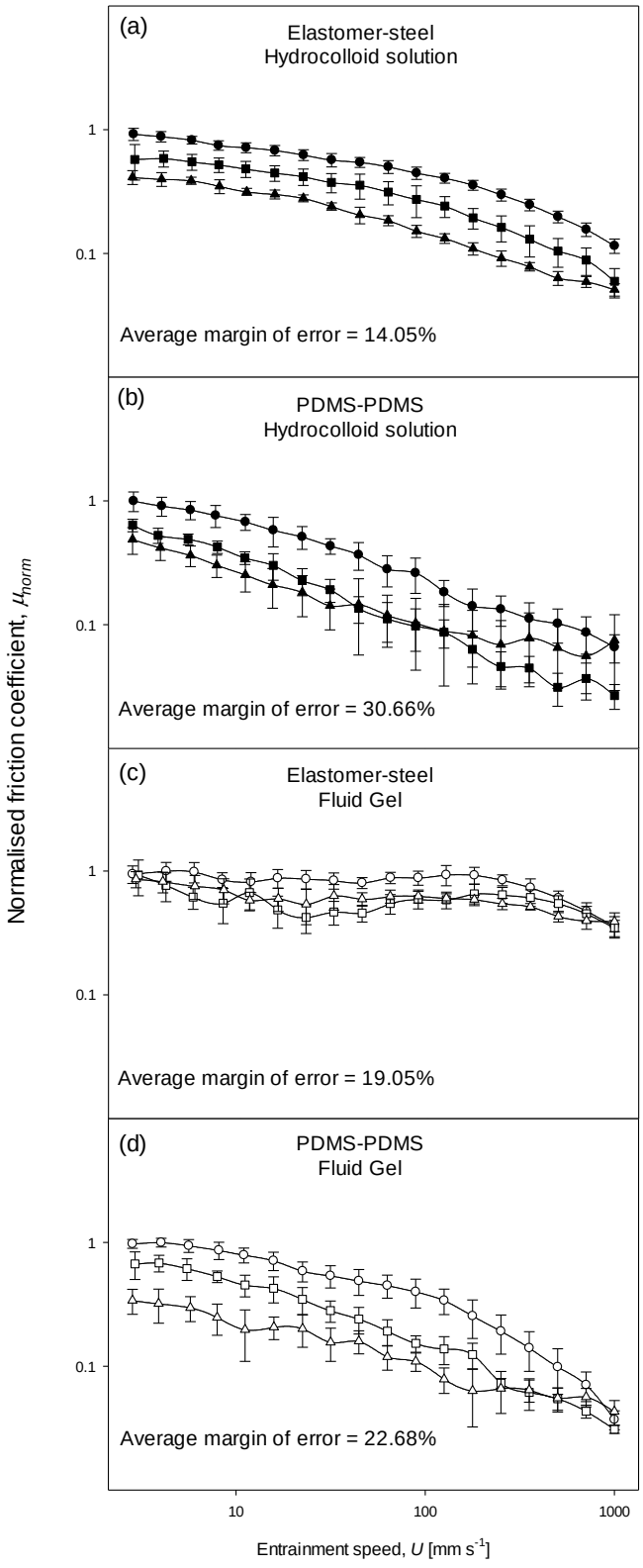

Fig. 3.9. Comparison of Stribeck curves obtained for Elastomer-steel and PDMS-PDMS (modified hydrophilic) tribopairs lubricated by κC at three concentrations (0.5 ●○, 1 ■□ and 2 wt.% ▲Δ) for κC as a hydrocolloid solution (without KCl) (filled symbols) and fluid gels (sheared gelation of κC with 0.3 wt.% KCl) (empty symbols) structures. Data is normalised for each graph (against the greatest friction coefficient value) to allow for comparisons between tribopairs.

For the hydrocolloid solutions (Fig. 3.9 a and b), the greatest reproducibility (lowest margins of error) and discrimination between varying concentrations is provided by the elastomer-steel tribopair. For the fluid gel lubricants (Fig. 3.9 c and d), the margins of error are similar for both tribopairs but HL-PDMS shows greater discrimination between differing fluid gel concentrations. Consequently, the elastomer-steel tribopair was selected for further analysis on hydrocolloid solutions; and HL-PDMS for the fluid gels (the influence of concentration on the tribology of hydrocolloid solutions and fluid gels will be discussed in Chapters 5 and 6, respectively).

The reason for such poor discrimination between κC concentrations of fluid gels with the elastomer-steel tribopair may result from the low surface roughness's of the tribopair preventing entrainment of the fluid gel particles to the contact, thereby eliminating the effect of the differing particle stiffness's with concentration. The influence of particle size and surface roughness on the lubrication mechanism of fluid gels will be discussed in detail in Chapter 6. This discussion will refer to the surface roughness properties of the elastomer-steel and HL-PDMS tribopairs which were obtained by interferometry and are reported in Table 3.2 and Fig. 3.10, where interferometry surface profiles are shown for the elastomer disc (a), stainless steel ball (b), HL-PDMS disc (c) and HL-PDMS ball (d).

Table 3.2
Roughness characteristics of surfaces used in this study

Surface	Surface Roughness (nm)			
	Centre Line Average (R_a)	R_a Standard deviation	Root Mean Square (R_q)	R_q Standard deviation
Elastomer Disc (Samco Silicone Products)	572	54	801	103
Stainless steel ball (PCS Instruments)	19	26	41	46
PDMS Disc (Dow Corning)	272	34	324	36
PDMS Ball (Dow Corning)	650	241	894	383

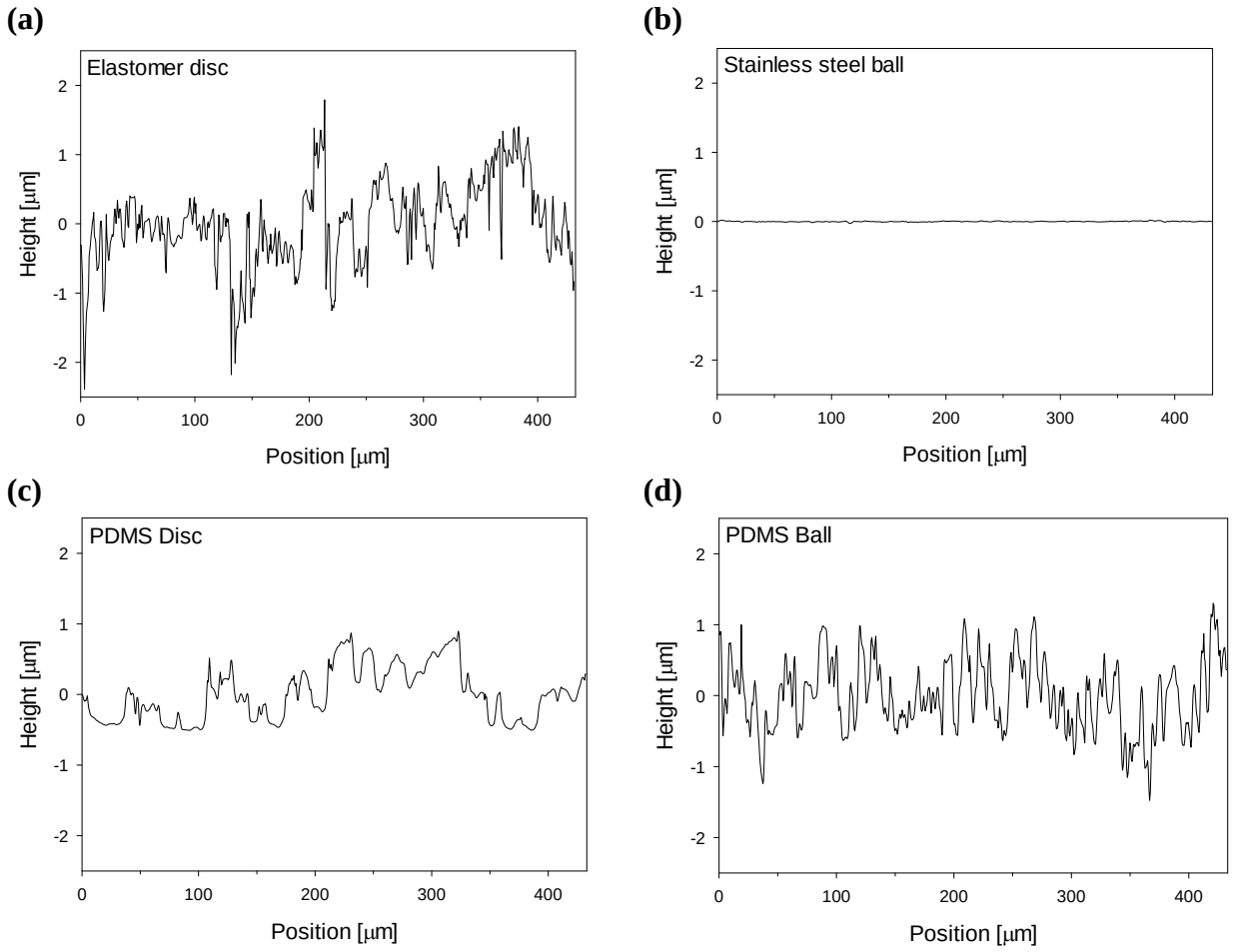

Fig. 3.10. Interferometry surface profiles for the elastomer disc (a), stainless steel ball (b), HL-PDMS disc (c) and HL-PDMS ball (d) used in the tribological measurements.

3.4.10.5. Conclusions on the tribometer setup

This section has investigated the influence of input parameters on data reproducibility, the influence of the tribopair on data reproducibility and lubricant discrimination and the formation of hydrophilic PDMS surfaces. As a result of these tests, a procedure was developed for optimising data quality and the resemblance to oral properties/behaviour where possible; this procedure will now be summarised.

Stribeck curves were conducted from speeds spanning U = 1 to 1000 mm s^{-1} at a normal load of W = 2 N and SRR = 50% (which were shown to minimise error margins). The

speeds were ramped up, then down until 6 runs were completed (1 test). 3 tests were completed for each lubricant tested using cleaned or new surfaces. The data shown herein is the average of the 3 tests *i.e.* 18 runs, and error bars show ± 1 standard deviation of error. Prior to testing, after lowering the ball to the disc, the test procedure was set to rotate the surfaces at 1000 mm s^{-1} for 5 mins at a normal load of 0 N, *i.e.* without surface contact. This pre-experiment step was set to allow the lubricant to mix well and for the surfaces to fully wet before commencing Stribeck tests. Based on minimising error margins and maximising discrimination between lubricants, the elastomer-steel tribopair was used for testing the tribology of hydrocolloid solutions and the HL-PDMS tribopair was used for fluid gels.

Chapter 4.

Formation and characterisation of fluid gels

4.1. Introduction

The aim of this chapter was to advance the understanding of fluid gels from that discussed in the literature review on their formation and properties. To do this, fluid and quiescently formed gels were analysed using a range of techniques to characterise their structural properties and material behaviour. Fluid gel formation was then probed by controlling the shear profile while cooling so that shearing was stopped partway through gelation. This allowed control over the ratio of sheared to quiescent molecular ordering thereby allowing the influence of processing conditions to be explored. Finally, a method for determining fluid gel particle volume fractions is described.

4.2. The coil-helix transition

The coil-helix transition of κC was required to be explored in order to identify molecular ordering events taking place during a cooling profile and to determine the process conditions required for sheared gelation (such as T_{in} and T_{exit}). To do this, fluid gels were initially formed using a rheometer at a range of κC and KCl concentrations.

Viscosity profiles on cooling from 60 °C at 200 s^{-1} and 3 °C/min are shown in Fig. 4.1 as a function of the concentration of KCl (a) and κC (b). The profiles are similar to those obtained by Gabriele *et al.* (2009) where, on cooling, the viscosity sharply rises due to the initial stages of molecular ordering forming gel nuclei. On continued cooling the nuclei grow to a size permitted by the shear and at this point a fluid gel is considered to have been formed; in some instances the viscosity reaches a maximum before breaking down due to the shear. Fig. 4.1 (a) shows that the temperature at which the viscosity rise initiates, is strongly dependent on KCl concentration. This is expected since the coil-helix transition of κC is facilitated by K^+ which suppresses the electrostatic repulsion of the κC anionic groups and

(a)

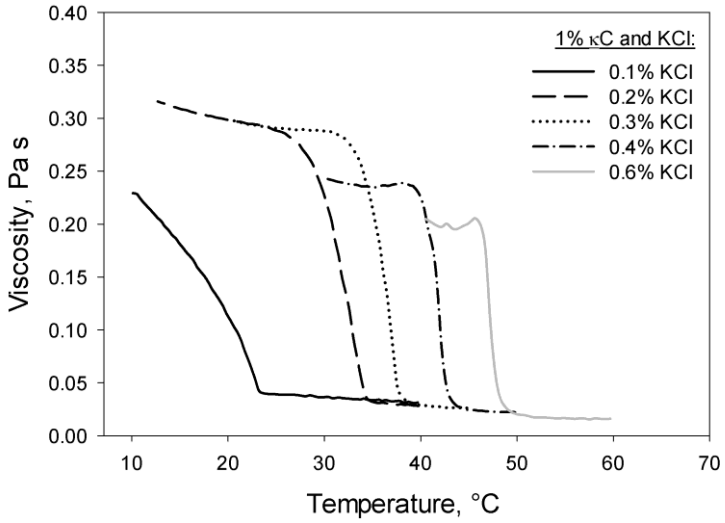

(b)

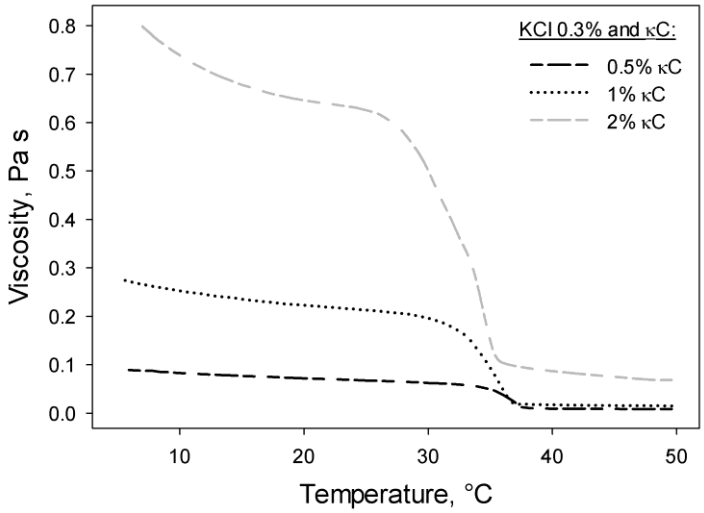

Fig. 4.1. Fluid gel production: viscosity profiles during the sheared cooling of κC/KCl solutions at 3 °C/min and 200 s^{-1}. Data is shown as a function of KCl concentration (a) and κC concentration (b).

forms specific polymer-cation interactions which are required for dimer formation (Norton *et al.*, 1983b). At 0.3 wt.% KCl, the fluid gel viscosities increase with κC concentration (Fig. 4.1 b) due to the production of less deformable particles (Norton *et al.*, 1999).

On visual inspection, the properties and stability of fluid gels was determined to be dependent on KCl concentration, where ≥ 0.4 wt.% yielded in-homogenous samples containing large, ~ 1 mm, particulates (0.3 wt.% KCl yields ~ 1 μm particles and will be

discussed in section 4.3); and after 24 hours storage at 5 °C, samples with ≤ 0.1 wt.% KCl reverted to materials resembling quiescently cooled gels.

The observed production of large particles with high KCl contents can be explained by understanding the factors that affect their size. Fluid gel particle sizes are controlled *via* three processes: the growth, breakup, and coalescence of gel nuclei (Carvalho and Djabourov, 1997). The growth process occurs *via* enrichment from the non-gelled continuous phase and is dictated by the rate of the coil-helix transition (k_{CH}) and the heat transfer coefficient (h). Heat transfer can be manipulated *via* the experimental process, for example, scraped surface heat exchangers provide large temperature gradients and therefore produce large particulates; h can also be controlled *via* the product flow rate and coolant properties, *e.g*., temperature, specific heat capacity and the rate and direction of flow. k_{CH} is different for all biopolymers, and for κC it is increased with K^+ concentration (Norton *et al.*, 1983a); thus, it is expected that the large particulates that formed with high salt contents are due to increased rates of molecular ordering and therefore particle growth. The process of growth, however, is restricted by the applied shear forces that also dictate the rates of nuclei breakup and coalescence. Thus, it seems the KCl content is required to be below 0.4 wt.% in order to prevent the growth of large particulates (this conclusion is made for sheared cooling conditions of 200 s^{-1} at 3 °C/min which mimics the sheared cooling expected within the pin-stirrer continuous process setup).

The instability of low salt content fluid gels during storage requires the salt dependent coil to helix transition to be explored. At the transition midpoint temperature (T_m) the ratio of disaccharide mole fractions in the coil or helix state is one, *i.e.* there is an equal proportion of both structures (Goodall and Norton, 1987). T_m increases with KCl content (Morris *et al.*, 1980b) thus, when stored at 5 °C, samples prepared with low KCl concentrations will be close

to their T_m. Therefore, it seems that samples with ≤ 0.1 wt.% KCl are close enough to T_m at 5 °C that there are sufficient chains in the coil state such that within 24 hours there is a considerable amount of structural rearrangement occurring quiescently, which results in the loss of the particulate structure; hence their resemblance to quiescently cooled gels on storage.

In summary, fluid gels with small particles and stable structures are only formed with a suitable KCl concentration. At conditions mimicking the continuous process pin-stirrer, this concentration was identified to be between 0.1 and 0.4 wt.%. Lower KCl concentrations cause quiescent reordering which leads to structural instability and greater concentrations increase k_{CH} and thus form large particulates. A KCl concentration of 0.3 wt.% was used to produce the fluid gels that are discussed throughout the remainder of this thesis.

Molecular ordering events were investigated as a function of temperature using polarimetry. The optical rotation of ultraviolet light has previously been demonstrated to show a temperature dependence in accordance with the conformational order/disorder of κ-

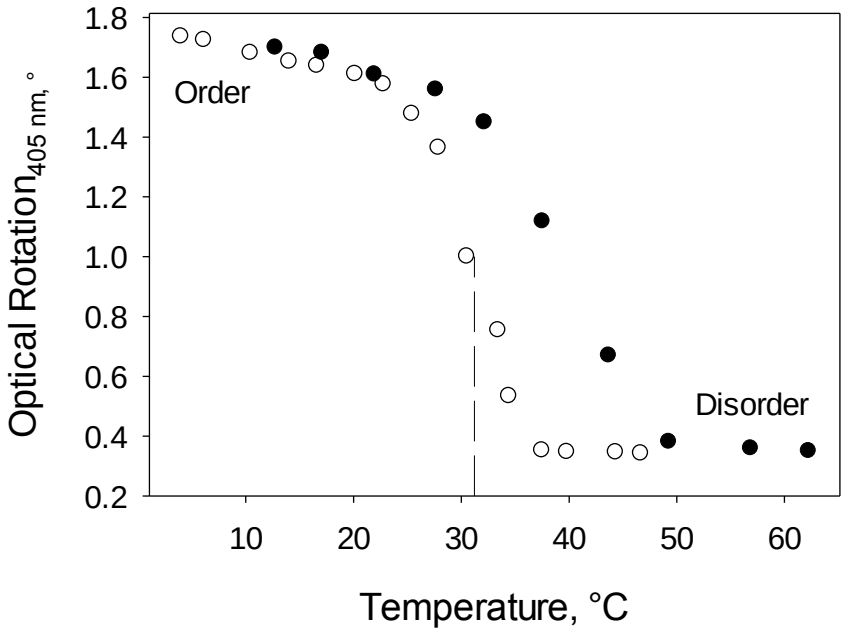

Fig. 4.2. Optical rotation during a quiescent cooling (open symbols) and heating (closed) cycle of 0.5% κC with 0.3% KCl. The dotted line indicates the midpoint temperature, T_m, at 31.2 °C.

carrageenan (Rees, 1970; Liang *et al.*, 1979). Fig. 4.2 shows the optical rotation temperature course for κC (0.5 wt.%) with KCl (0.3 wt.%) under quiescent conditions. On cooling, the optical rotation increases (at ~ 35 °C) due to the coil-helix transition taking place involving the dimerization of two chains into a double helix (Goodall and Norton, 1987). Lateral helix aggregation then occurs where the K^+ ions screen the electrostatic repulsion between chains and bridge neighbouring helices at the sites of their specific chain interactions (Morris *et al.*, 1980b). On heating, the aggregated regions must be disassembled before the helix-coil transition can occur, hence the observed temperature hysteresis. The dotted line on Fig. 4.2 indicates the midpoint temperature (T_m) for the coil to helix transition, identified as the midpoint between the two linear regions corresponding to disordered and ordered polymer conformations; for this system, T_m = 31.2 °C.

Optical rotation tests could not be conducted accurately with κC concentrations greater than 0.5 wt.% as the samples became too opaque, although it is expected that T_m will not be strongly dependent on κC concentration (Morris *et al.*, 1980a). Fluid gels samples could also not be tested as they too were opaque, at all concentrations, due to their particulate structure.

4.3. Fluid gel characterisation

This section characterises the properties of bulk (and particle) fluid gel properties that were formed by sheared gelation within the continuous process pin-stirrer. The processing conditions used were: rotation at maximum speed (1438 rpm) to minimise particle diameters and T_{in} and T_{exit} at ~50 and ~5 °C, respectively, to ensure gelation under shear (T_m = 31.2 °C). The ingredients used were 0.3 wt.% KCl (as discussed in section 4.2, this forms small particles that are stable on storage) and a range of κC concentrations (0.5, 1 and 2 wt.%) to investigate the influence of κC concentration on material properties.

4.3.1. Rheology – Frequency sweeps

Small amplitude oscillatory frequency sweeps were carried out to test the material response of fluid gels. This technique is commonly used to characterise biopolymer systems where 'entangled solutions', 'weak gels' and 'strong gels' can be identified (Ross-Murphy, 1995). The mechanical spectra in Fig. 4.3 show storage moduli (*G'*), loss moduli (*G"*) and phase angles (δ) for 1 wt.% guar gum (a) and xanthan gum (b), and 0.5 wt.% kappa carrageenan cooled under quiescent and sheared conditions (c and d, respectively) with 0.3 wt.% KCl.

The spectra for guar gum, xanthan gum and quiescently cooled κC are shown for comparison of the fluid gels with characteristic spectra. The guar gum used at 1 wt.% is a concentrated solution where coil overlap occurs (Morris *et al.*, 1981) and is referred to as an 'entangled solution'. This has a characteristic spectra where $G" > G'$ at low frequencies, indicating a viscous liquid, however, at higher frequencies the entanglements provide an elastic response hence *G'* and *G"* cross over.

Xanthan has the ability to form 'weak gels' at rest, a property of which is utilised in products that demand high zero shear viscosities for stability, but can flow under shear when required for application *e.g.* salad dressings (Barbara, 1998). During small deformation rheological tests the continuous xanthan network, provided by weakly associated single helices (Norton *et al.*, 1984), is not destroyed thus *G'* is greater than *G"* at all frequencies. The xanthan helices will, however, dissemble under shear thus allowing the material to flow.

The κC gel cooled under quiescent conditions provides a 'strong gel' spectra where, in contrast to xanthan, the storage and loss moduli are less dependent on frequency, and the phase angles (δ) ($\tan \delta = G"/G'$) are lower because *G'* is considerably greater than *G"*. On comparison, the κC fluid gel displayed characteristics somewhere between a 'weak gel' and a

'strong gel' in terms of the dependence of *G'* and *G''* on frequency, and the δ values. The 'weak gel' behaviour of fluid gels can be ascribed structurally: closely packed particle interactions allow an elastic network to form at rest, similarly to associated xanthan helices. The 'strong gel' component arises from the strong elasticity of the gel particles. The 'weak' and 'strong' gel tendencies are therefore expected to be a function of particle stiffness and their packing fraction.

(a)

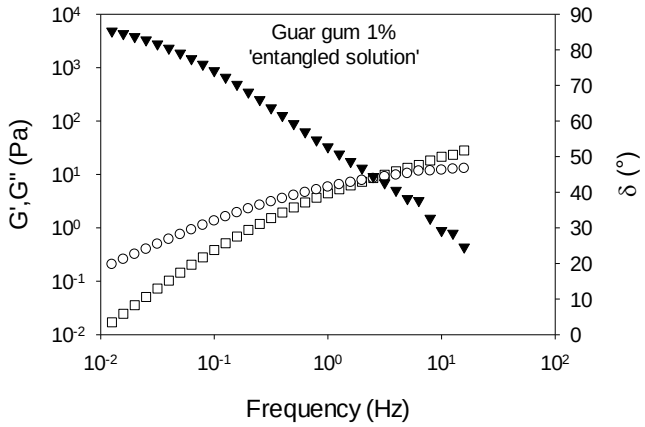

(b)

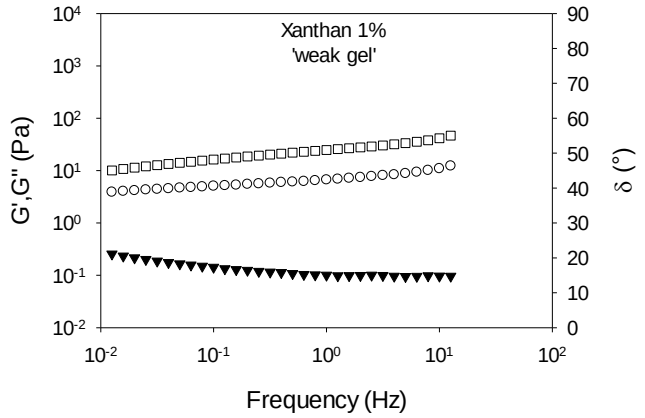

(c)

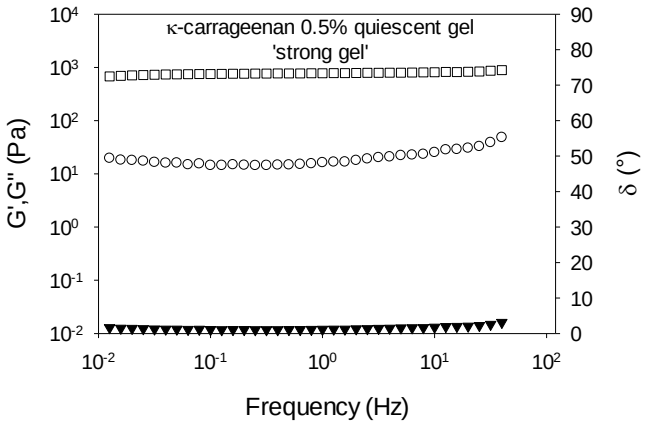

(d)

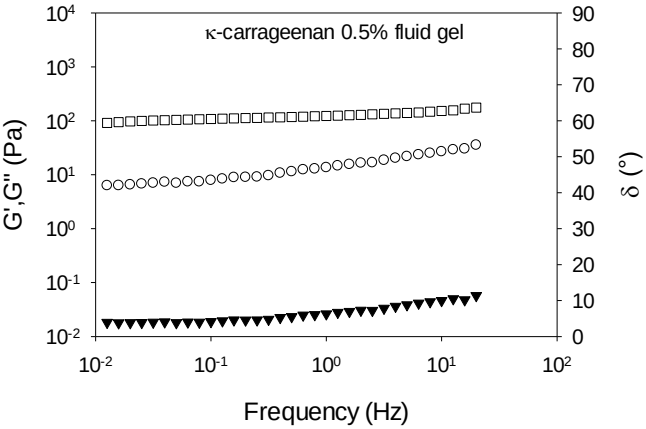

Fig. 4.3. Linear viscoelastic frequency sweeps displaying characteristic mechanical spectra of an entangled solution (a), weak gel (b), strong gel (c). Fluid gels (d) have a spectra lying between that of a strong and weak gel. Phase angles, δ, (▼), G' (□) and G" (○) are shown as a function of frequency.

4.3.2. Calorimetry

DSC was used to identify the enthalpy of the coil-helix transition on both heating and cooling. The experimental procedure used allowed a direct comparison of fluid and quiescently formed gels to be made. This was achieved by running four successive scans on a material that was initially a fluid gel. The thermal scans were conducted as follows: heating, cooling, heating then cooling (as depicted in Fig. 4.4). The first scan investigated the thermal transition of melting a fluid gel. Next the cooling scan formed a quiescently cooled gel within the cell (no external shear force was applied during the DSC testing). This was then melted during the third scan thereby probing the thermal transition of melting a quiescent gel. This was then cooled again to gauge the accuracy of the data, since the second and fourth scans (both cooling) should be similar. The first and third scans (both heating) were used to directly compare the melting profiles of fluid and quiescent gels.

Fig. 4.5 shows curves of a representative individual procedure for heating (a) and cooling (b) scans for 0.5 wt.% κC fluid gel (with 0.3 wt.% KCl, produced *via* the pin-stirrer). From the average of 5 repeated procedures, the enthalpy of melting fluid gels ($\Delta H_{m\,FG}$ = 0.174 ± 0.003 J/g) was observed to be 9.4% lower than that of quiescent gels ($\Delta H_{m\,QG}$ = 0.186 ±

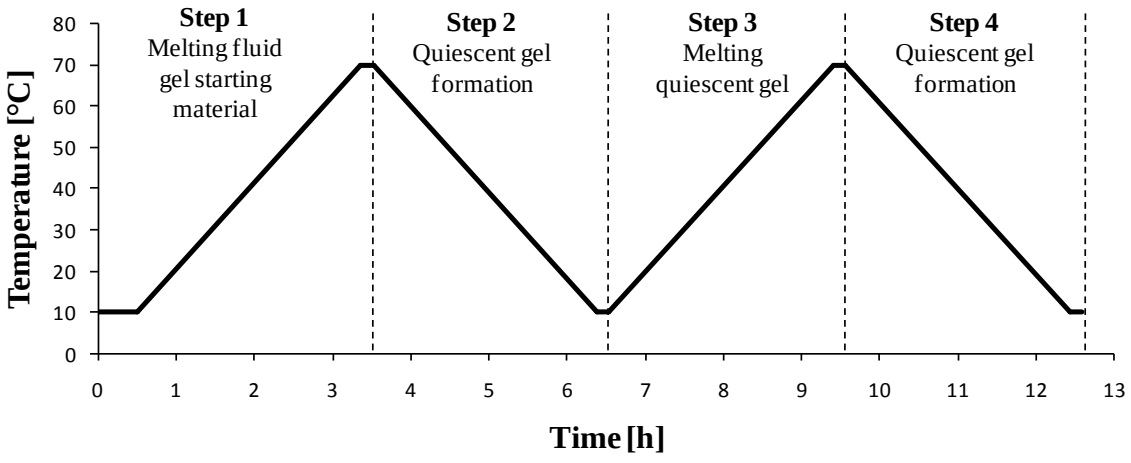

Fig. 4.4. Schematic of the DSC temperature profile used. Temperature ramps were conducted at 0.35 °C/min, for more information on the procedure see section 3.4.4.

0.002J/g); and the fluid gel melting peaks (47.87 ± 0.08 °C) were lower than for quiescent gels (48.98 ± 0.02 °C). The close similarity of the two cooling peaks (Fig. 4.5b), where gels are formed quiescently, indicates a strong accuracy of the data, thus differences observed between the heating scans can confidently be related to differences between gels formed under sheared and quiescent conditions. The fact that $\Delta H_{m\,FG} < \Delta H_{m\,QG}$, suggests that the total

(a)

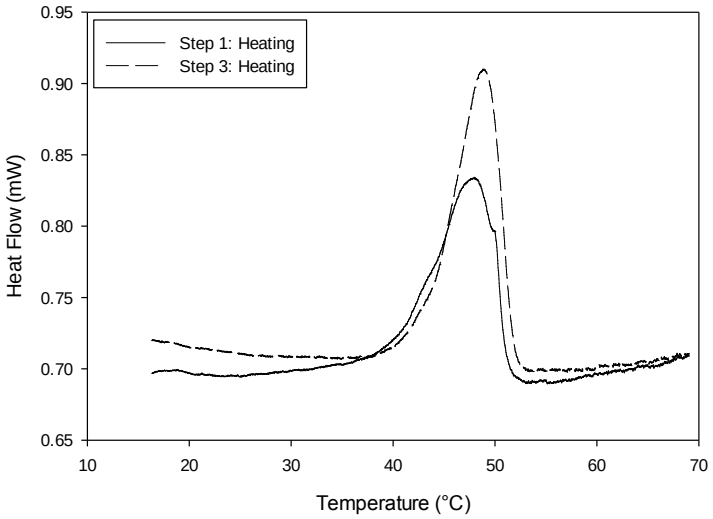

(b)

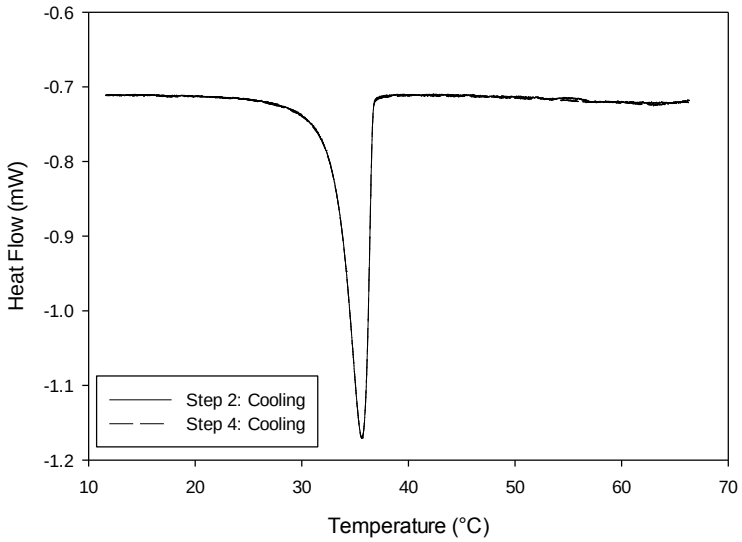

Fig. 4.5. DSC heating (a) and cooling (b) profiles for a product that was initially a fluid gel prepared from 0.5 wt.% κC and 0.3 wt.% KCl. The first heating scan (Step 1) shows melting of a fluid gel; the second (Step 3), quiescent gel.

number of helical domains is fewer in the fluid gels. Additionally, the lower melting point of fluid gels indicates smaller aggregates of helices. Therefore, fewer helical residues, and smaller aggregates of helices are present, probably towards the surfaces of the particles, where the applied shear disrupts helix formation and restricts the extent of their growth. This raises an important issue because DSC studies on agarose fluid gels determined that the enthalpies of melting fluid and quiescent gels were equal (Norton *et al.*, 1999). It therefore seems that the κC gels formed in the present study are more influenced by the applied shear than the agarose gels prepared by Norton *et al.* (1999). This is likely to be a result of a slower ordering process for κC due to the inherently lower rate of the coil to helix transition (the rate constant for κC helix nucleation is 2-3 orders of magnitude lower than for agarose (Norton *et al.*, 1986)) and a lower heat transfer from the pin-stirrer experimental setup (Norton *et al.* (1999) used a scraped surface heat exchanger). Additionally, the κC particles (which are ~ 1 μm, as discussed further in section 4.3.4) are smaller than the agarose particles (100 μm) and therefore have a higher surface area/volume ratio which may increase the influence of the shear on the particles.

It has been suggested that the fluid gel internal particle polymeric network, and therefore the stiffness of individual particles, is equivalent to that of their quiescently cooled counterparts (Frith *et al.*, 2002; Caggioni *et al.*, 2007). This can therefore only be used as an approximation for κC fluid gels as the DSC data in this study suggests fewer saccharide residues in helical structures. This will have an effect of lowering fluid gel particle stiffness's compared to the bulk quiescent gels, albeit only a small difference (~9%) and perhaps only towards the particle surfaces.

4.3.3. Fluid gel particle properties – texture analysis

To assess an approximation of the stiffness of the fluid gel particles, compression tests were conducted on quiescently cooled bulk gels. As discussed in the previous section, the absolute Young's moduli (*E*) values are not expected to represent that of the fluid gel particles since the applied shear interferes with the particles' polymer network during their formation. However, compression tests were conducted in this study to give an indication of the particle material properties and provide a trend for *E* with polymer concentration. True stress/true strain curves for the quiescently formed gels are shown in Fig. 4.6 for quiescent gels prepared with κC concentrations of 0.5, 1 and 2 wt.%. The curves shown are representative of the data obtained and the Young's moduli (*E*) values quoted in the figure (obtained from gradients below 0.05 strain) are the mean average of 5 repeated experiments. The Young's moduli increase with polymer concentration providing a range of stiffness's which is expected for the fluid gel particles.

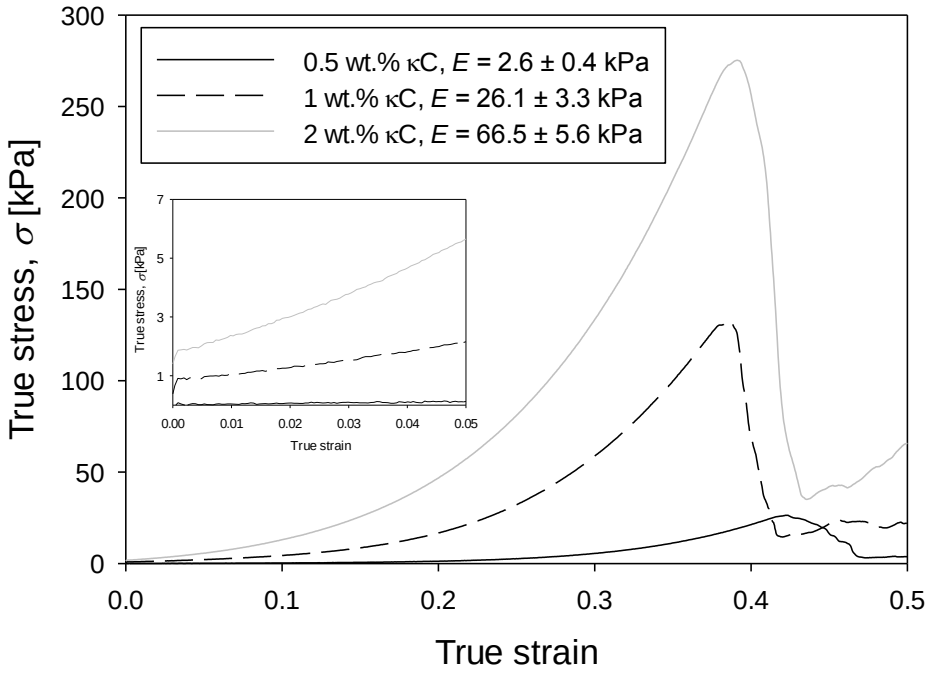

Fig. 4.6. True stress/true strain curves for quiescently formed gels. Young's moduli (E) were identified from gradients below 0.05 strain and are shown on the figure.

4.3.4. Microscopy and particle sizing

Microscopy was used to probe the shape and size of the fluid gel particles (light scattering techniques were ineffective due to the similarity of the refractive index of the aqueous particles and continuous phase). Optical micrographs of fluid gels are shown in Fig. 4.7 after being sheared and diluted with water. Over 1,500 particle diameters were measured from numerous images taken for each κC concentration: 0.5, 1 and 2 wt.%. The particle shapes are roughly spherical for each concentration, and their particle size distributions are shown in Fig. 4.8. Mean average particle diameters were calculated to be 1.36 ± 0.045 μm, 1.27 ± 0.035 μm and 0.97 ± 0.045 μm for κC concentrations 0.5, 1 and 2%, respectively. On increasing polymer concentration, the fluid viscosity increases; thus for the fixed pin-stirrer rotation speed used, 1438 rpm (fixed shear rate), the shear stress acting on the particles increases, hence the observed decrease in particle diameter. The particle diameters and stiffness were such that they were not detected as particles during oral consumption, rather, the fluid gel samples were perceived as 'smooth'.

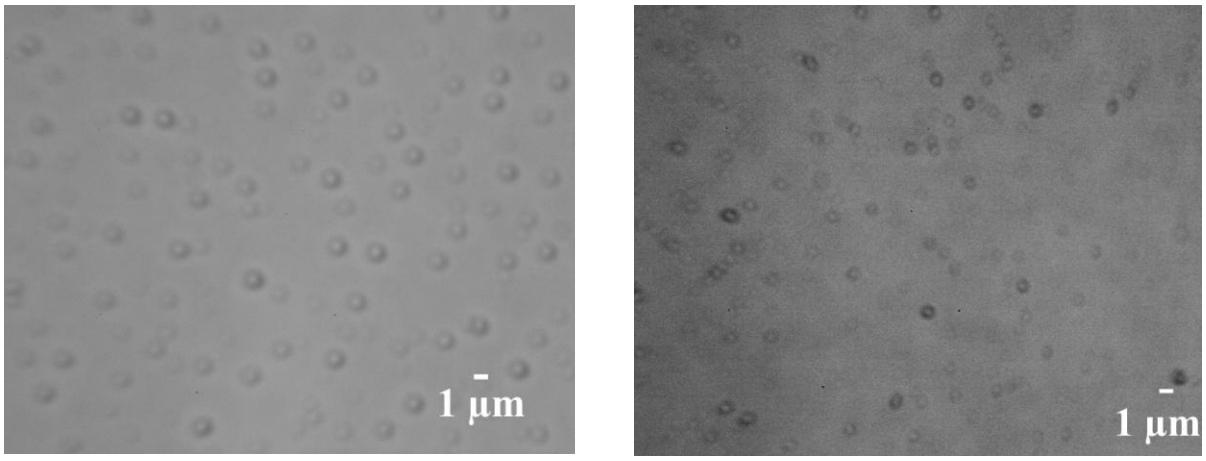

Fig. 4.7. Optical micrograph of a diluted (1:3) fluid gel prepared from 0.5 wt.% (left) and 2 wt.% (right) κC with 0.3% KCl. Scale bar shows 1 μm.

The small (~ 1 μm) and spherical particles produced here are in contrast to that previously reported for fluid gels produced with agarose which were large (~ 100 μm) (Gabriele *et al.*, 2010) and anisotropic (Norton *et al.*, 1999) (a confocal micrograph image of agarose fluid gels was shown in Fig. 2.9, page 21). This difference in size and shape is likely to result from the differences in their rates of gelation. As discussed in section 4.3.2, the rate of agarose gelation is faster than that for κC. The fast gelation of agarose will kinetically trap the gelled regions into shapes dictated by the processing unit. In contrast, the slower gelation of κC allows for the formation of thermodynamically driven spherical shapes where the surface energy is minimised. The size of the particles is also related to the rates of molecular ordering since the faster gelation for agarose rate will allow for growth to larger sizes.

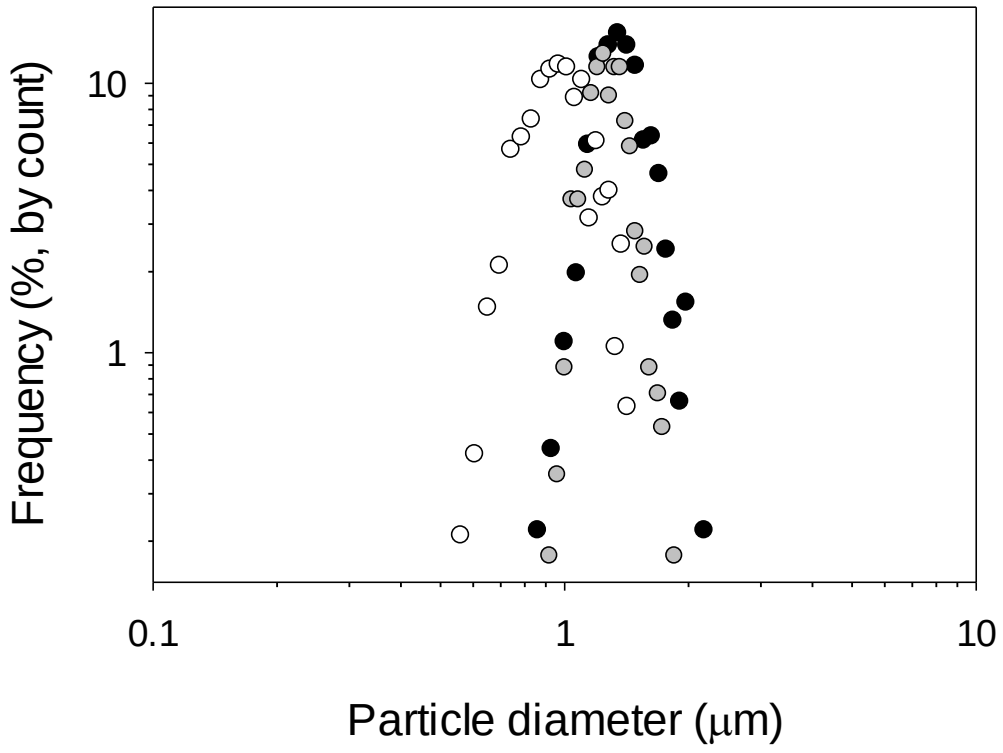

Fig. 4.8. Particle size distributions for fluid gels prepared from 0.5 (black), 1 (grey) and 2 wt.% (white) κC.

To probe the internal structure of the fluid gel particles, Scanning Transmission Electron Microscopy (STEM) was conducted. Fig. 4.9 shows STEM images of dried fluid gel particles. Since the samples were dried before imaging, shapes of the internal network and surfaces cannot be elucidated, but it seems that there is a polymer density gradient through the particles which is greatest in their centre.

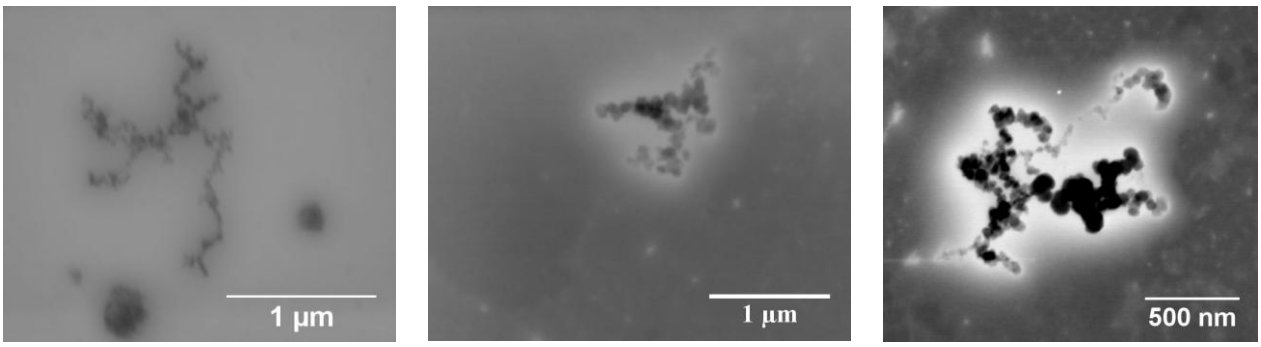

Fig. 4.9. STEM images of individual fluid gel particles (dried).

In summary of the characterisation conducted on κC fluid gels thus far: rheologically the fluid gels behave similarly to both 'weak' and 'strong' gels due to the strong particles forming weak associations at rest. The molecular ordering rate for κC is suitably slow to produce spherical fluid gel particles with small diameters (~ 1 μm) that are not detected during oral processing. This slow gelation rate causes the applied shear to interrupt helix growth thereby reducing the number of helical residues and the sizes of the helix lengths and aggregates. This causes a weakening of the gelled networks thus increasing deformability and this effect is expected to increase towards the particle surfaces. This results in internal structures where the polymer network density is greatest in the centre.

4.4. Identifying fluid gel particle volume fractions

The volume fraction of particulate systems plays a significant role in determining their rheological behaviour. Thus, identifying fluid gel particle volume fractions is important for characterising them and understanding their formation process. Whilst the volume fraction of fluid gels has been suggested to increase with biopolymer concentration from NMR relaxation studies (Norton *et al.*, 1998), there is not currently a suitable method for accurately probing their values when there is 'hairiness' and therefore poor distinction between particles and the continuous phase. The rheological data of fluid gels on dilution was unable to fit to available models where volume fractions can typically be identified (this will be discussed in detail in Chapter 6.2), furthermore, the aforementioned NMR relaxation technique is not expected to be appropriate for κC given the 'hairiness' and therefore numerous aqueous environments; thus, a centrifugation method was explored and will now be discussed in detail.

Fluid gels were centrifuged at a range of centrifugal forces to sediment the fluid gel particles from the continuous aqueous phase. The fluid gel solid phase volume (φ_{FG}) was then determined by identifying the mass of the solid component ($M_{FG.s}$) in relation to the original pre-centrifugation total mass ($M_{FG.0}$) (assuming the density is unity for the particles and continuous phase) according to Eq. 4.1.

$$\varphi_{FG} = \frac{M_{FG.s}}{M_{FG.0}} \qquad \textit{Eq. 4.1}$$

Upon application of a centrifugal force, the gel particles themselves release fluid due to compression. It has previously been determined (Lopez-Sanchez *et al.*, 2011), for plant cell dispersions, that the centrifugation of dispersions alone cannot discriminate particle packing from particle deformability. Thus, the supernatant of a centrifuged fluid gel will consist of the true continuous phase volume present at ambient conditions and fluid expelled from within

the particles due to the centrifugation process. Measuring the particle volume fraction (Φ_{FG}), therefore, requires the expelled fluid (particle compressibility) to be calculated. This was estimated by centrifuging quiescently cooled bulk gels on the assumption that the fraction of fluid released after their centrifugation is equal to the fraction released from within the fluid gel particles, for a given centrifugal force, time and polymer concentration. The validity of this assumption is discussed later in this section.

The quiescently cooled bulk gel solid phase volume (φ_{QG}) was calculated from the ratio of the mass of the solid component after centrifugation ($M_{QG.s}$) to the total original mass ($M_{QG.0}$), Eq. 4.2. The supernatant phase volume from centrifuged quiescent gels (equivalent to that released from fluid gel particles on centrifugation), is therefore given by (1-φ_{QG}). The fraction of fluid released from the gels due to syneresis (φ_{syn}, liquid expulsion on gel storage) must also be considered since this process is expected to take place to fluid gel particles and therefore contribute to the continuous phase. To calculate this, the fluid gel syneresis was assumed to occur to the same extent as for quiescently cooled bulk gels, thus φ_{syn} is calculated by dividing the mass of the fluid released from a quiescent gel after 72 h (at 5 °C with no centrifugation force), by the original total mass.

$$\varphi_{QG} = \frac{M_{QG.s}}{M_{QG.0}} \qquad \textit{Eq. 4.2}$$

$$\Phi_{FG} = \varphi_{FG} + [(1 - \varphi_{QG}) - \varphi_{syn}] \qquad \textit{Eq. 4.3}$$

Eq. 4.3 shows that the fluid gel particle volume fraction (Φ_{FG}), for a given centrifugation force can be given by the fluid gel solid phase volume (φ_{FG}), plus the fraction of fluid released from within the particles as a result of centrifugation (1- φ_{QG}), whilst also accounting for the portion of that owed to syneresis occurring at ambient conditions (φ_{syn}). The workings of this equation are summarised schematically in Fig. 4.10.

Fig. 4.11 (a) shows the dependence of phase volume on relative centrifugal force. Data is shown for the solid material phase volume of fluid gels (φ_{FG}) and quiescently formed gels (φ_{QG}), which together were used to calculate fluid gel particle volume fractions (Φ_{FG}) using Eq. 4.3. By fitting the φ_{QG} data to a linear fit, and extrapolating to 1 g, the value of syneresis can be identified (φ_{syn}) which agreed well with the values obtained from analysis of quiescent gels after 72 h without centrifugation. Fig. 4.11 (a) shows that the fluid released from the quiescent gels is dependent on the centrifugal force, although the majority of the fluid is

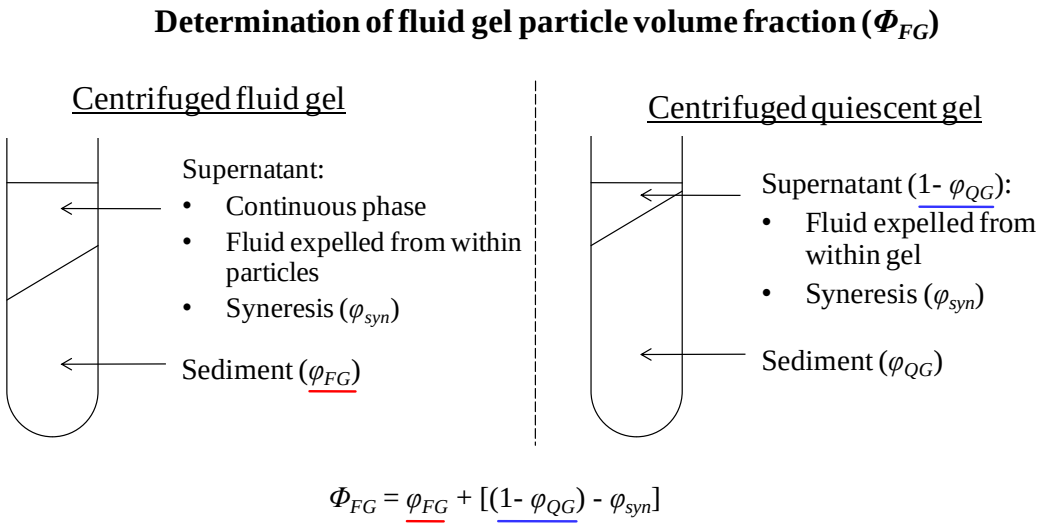

Fig. 4.10. Schematic representation of the centrifugation method used to determine fluid gel particle volume fractions.

released without centrifugation and is therefore attributed to syneresis. The fluid gel solid phase volume data (φ_{FG}) also shows an RCF (relative centrifugal force) dependence, although at the highest forces attainable (41,415 g, which was 21,000 rpm), the dependence is similar to that for the quiescent gels (φ_{QG}). This similarity in force dependence implies that further increases in force would act to remove the same additional fraction of liquid from both fluid

(a)

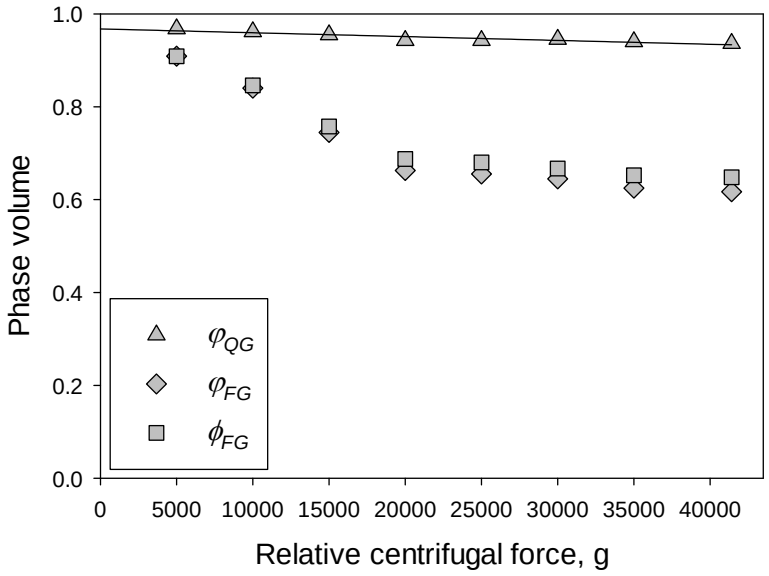

(b)

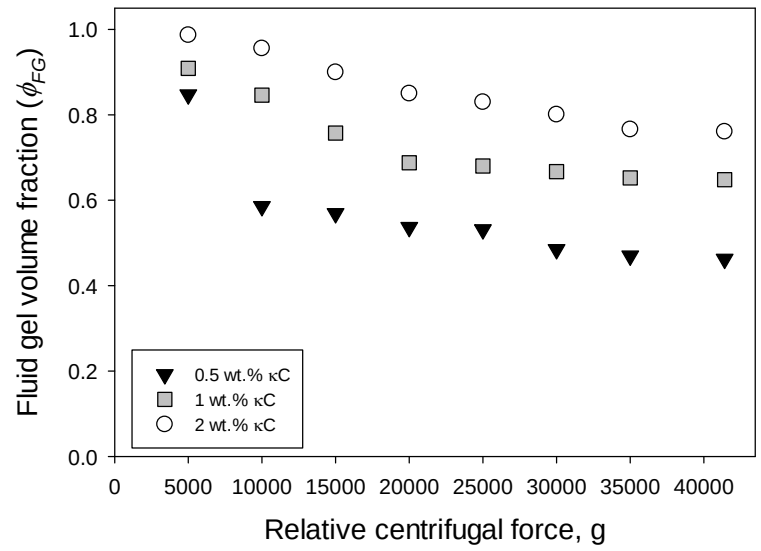

Fig. 4.11. Effect of relative centrifugal force (RCF) on relative phase volumes. Quiescent gel and fluid gel solid phase volumes (φ_{QG} and φ_{FG}), and fluid gel volume fractions (Φ_{FG}) are shown (a) for samples prepared with 1 wt.% κC. The line represents a linear fit extrapolated to 1 g identifying the fraction of syneresis (φ_{syn}). Fluid gel volume fractions (Φ_{FG}) for 0.5, 1 and 2 wt.% κC show their dependence on κC concentration (b).

Table 4.1
Summary of the properties of the fluid gels produced in this study

Concentration of kC used for fluid gel formation [wt.%]	Fluid gel particle volume fraction after production (Φ_{FG})	Particle diameter, $D_{1,0}$ [μm]	Approximate particle Young's Modulus[1], E [kPa]
0.5	0.46	1.36 ± 0.045	2.6 ± 0.4
1	0.65	1.27 ± 0.035	26.1 ± 3.3
2	0.76	0.97 ± 0.045	66.5 ± 5.5

[1] *Based on that of quiescently cooled bulk gels for the same κC and KCl concentrations*

and quiescent gels suggesting the particles have fully sedimented, deformed and packed to become similar to a quiescent gel. The result of this is that the fluid gel particle volume fraction, Φ_{FG}, shows little dependence on RCF at high forces. Values of Φ_{FG}, for three κC concentrations (0.5, 1 and 2 wt.%) versus RCF are shown in Fig. 4.11 b. Volume fractions of the fluid gels were taken from the maximum attainable centrifugal force and are shown in Table 4.1 together with particle diameters and approximate Young's moduli (the latter were discussed earlier in sections 4.3.4 and 4.3.3, respectively).

The volume fractions are shown to be dependent on κC concentration; specifically, greater concentrations yield greater volume fractions. Given that particle diameters decrease through the concentration range it seems that the increase in volume fraction with concentration is due to a greater number of particles produced. This would be expected with more rapid gelation occurring with increasing κC concentration.

The validity of the assumption made that fluid gel particles will release an equivalent fraction of fluid as quiescently cooled bulk gels under centrifugation will now be considered. As discussed in section 4.3.2, the κC fluid gel particles are composed of fewer helices with smaller aggregated regions than their quiescently formed counterparts, which, is expected to reduce their stiffness. Thus, (1 - φ_{QG}) represents an approximation of fluid gel particle compressibility and so too, Φ_{FG} can only be an approximation of the fluid gel particle volume fraction.

4.5. The influence of exit temperature on gel material properties

In this section, results are discussed on fluid gels that were produced at a range of exit temperatures (T_{exit}) to control the ratio of sheared to quiescent cooling. The inlet temperature to the pin-stirrer (T_{in}) was maintained at ~ 50 °C throughout to ensure that molecular ordering did not occur before entering the sheared regime. T_{exit} was varied from 5 to 40 °C, and upon exiting the sheared environment all samples were collected in a stationary vessel held at 5 °C, thus, all samples were cooled to 5 °C, but their shear profile on cooling was varied (the experimental setup was shown in Fig. 3.2, page 66). As previously discussed, the κC samples used here with 0.3 wt.% KCl initiate their molecular ordering process on cooling at ~ 35 °C. Therefore, when T_{exit} = 40 °C, none of the molecular ordering takes place within the pin-stirrer, instead it takes place within the stationary vessel thus producing a quiescently cooled gel. However, as discussed in the previous two sections (4.3 and 4.4) on fluid gel characterisation, when T_{exit} = 5 °C, the molecular ordering takes place under shear, thus forming a fluid gel. Therefore, by varying the T_{exit} temperature between 5 and 40 °C, it was anticipated that a range of material properties will emerge varying from that of a fluid to a quiescently formed gel. This test will now be discussed in detail where the aim is to advance the understanding of the fluid gel production process and to investigate methods of controlling their material response.

The area under the DSC cooling curve (Fig. 4.5 b, page 99) can be used to represent 100% of the coil-helix transition. By expressing the area under the curve, up to a particular temperature (*e.g.* T_{exit}) as a fraction of the total area, allows an indication of the amount of (un)ordered chains at that temperature to be estimated.

Gels produced at $35 \leq T_{exit} \leq 40$ °C (which represents between 56 and 0% of the molecular ordering process – region (d) on Fig. 4.12) yield products resembling quiescently

cooled gels. This indicates that the matrix surrounding the gel nuclei that form under shear through this temperature range still have a considerable degree of unordered coils (56%) that once ordered quiescently, form a strong gel equivalent to the quiescently formed gels.

When $25 \leq T_{exit} \leq 35$ °C (between 3.3 and 56% unordered coils remain - region (c) on Fig. 4.12) heterogeneous gelled 'lumps' on the cm scale were produced that were unstable against sedimentation leaving a pool of non-gelled liquid at the surface. In this instance, the amount of unordered coils that cool quiescently is enough to bridge many nuclei together forming the large gelled regions, but not enough to cross-link (or gel) the entire volume of the system and so 'broken quiescent gel' products are formed.

Materials produced at $20 \leq T_{exit} \leq 25$ °C (between 1.6 and 3.3% unordered coils remain - region (b) on Fig. 4.12) were stable against sedimentation but were not homogenous. Some large particulates (~1 mm) resided within the fluid gels that were detectable on touch, and visible to the naked eye.

$T_{exit} \leq 20$ °C (region (a) on Fig. 4.12) resulted in fluid gels stable against sedimentation, and with all particles ~ 1 μm which were perceived as 'smooth' and 'without

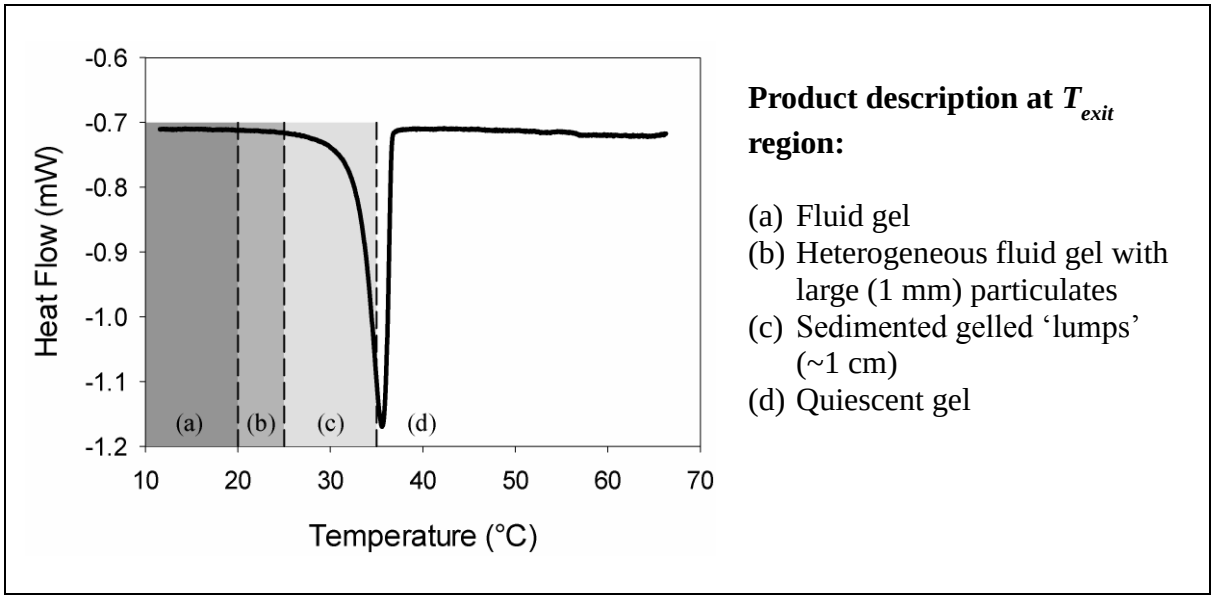

Fig. 4.12. Schematic representation of the influence of T_{exit} on gel properties

particulates' on oral consumption. On cooling to 20 °C, 1.6% of the κC remained unordered, thus the vast majority of the coil-helix transition (98.4%) must take place under shear in order to produce homogenous κC fluid gels with this setup.

Thus, $T_{exit} \leq 20$ °C (region (a) on Fig. 4.12) represents a range of temperatures where T_{exit} can be varied whilst still producing stable (against sedimentation) and homogeneous fluid gels. The rheological properties of fluid gels produced within this temperature range were explored and will now be discussed.

Fig. 4.13 shows storage modulus data from frequency sweeps of fluid gels produced at a range of kC concentrations and T_{exit}'s ≤ 20 °C. On increasing κC concentration the storage moduli are observed to increase, for each T_{exit}; this behaviour is a result of the particle

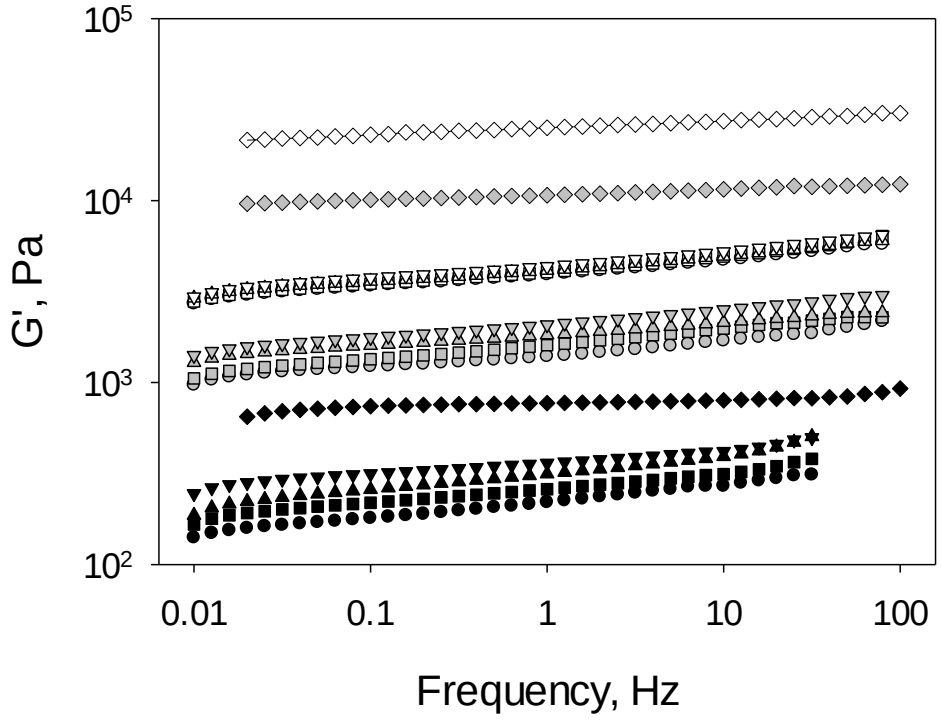

Fig. 4.13. Storage modulus of fluid gels as a function of frequency, κC concentration and exit temperature. κC concentrations are 0.5 (black), 1 (grey) and 2 wt.% (white). T_{exit}'s are 5 (○), 10 (□), 15 (Δ) and 20 °C (▽). For comparison, data for quiescently cooled gels are shown too (◇).

Young's moduli (section 4.3.3) and volume fractions (section 4.4) increasing with κC concentration. The storage moduli increase with T_{exit} although this effect is only apparent for the lower concentration fluid gels. This behaviour indicates a strengthening of the product as the degree of quiescent cooling increases, perhaps due to inter-particle molecular ordering forming bridges between neighbouring particles. Since this effect is not conclusive for all concentrations, their yield stresses were also measured as inter-particle connections will have to be overcome before the particles can move past one another *i.e.* yield. Yield stresses were determined from creep tests (described in the Methods section 3.4.9.5) and are shown in Fig. 4.14 as a function of κC concentration and T_{exit}.

By considering the non-sheared (white symbols) data first, it can be seen that the yield

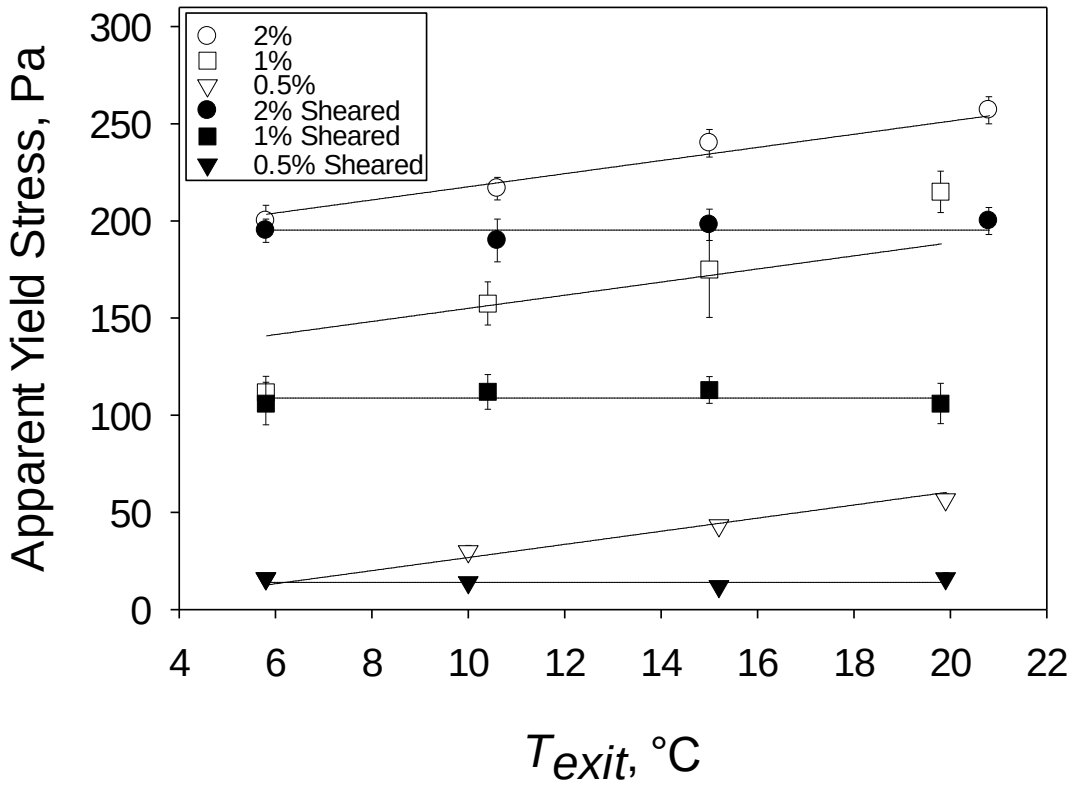

Fig. 4.14. Apparent yield stress dependence on pin-stirrer exit temperature (T_{exit}) for fluid gels prepared with 0.5 (▽), 1 (□) and 2 wt.% κ-carrageenan (○). Samples were tested as produced (white symbols) and by 24 h after shearing (black symbols). Linear fits are shown with equal gradients for each series (gradient values are 3.4 for non-sheared; 0, sheared).

stresses increase with κC concentration and T_{exit}. As mentioned, polymer concentration controls fluid gel particle stiffness and volume fraction; these parameters influence the material yield stress in agreement with the behaviour observed for uniform microgels (Adams *et al.*, 2004). The yield stress dependence on T_{exit} compliments the frequency sweep data that indicated greater *G'* values as the extent of quiescent cooling increased. This product strengthening with greater amounts of quiescent cooling is likely to be partly due to the remaining 1.6% of the molecular ordering being able to take place between particles, and therefore bridge them together. However, since the cooling peak, and therefore the coil-helix transition, was observed to have completed at 14.4 ± 0.2 °C (average of 10 repeats), this cannot explain all of the observed data. For this, the dynamic nature of the coil-helix equilibrium must be considered. As mentioned previously, T_m represents the temperature at which the number of moles of saccharide residues in the disordered and ordered state are equal; more specifically, the events of helix growth ('zipping-up') and decay ('un-zipping') are occurring at equal rates (Goodall and Norton, 1987). The coil-helix transition has been described as a dynamic equilibrium where the rate constant at T_m is zero, and on decreasing temperature the likelihood of growth events is increased relative to those of decay (Norton *et al.*, 1983a). Thus, molecular rearrangements to both quiescent and fluid gels, *via* decay and growth mechanisms, are reduced on decreasing temperature below T_m. Consequently, the closer the gel is to its midpoint temperature, the greater the amount of disorder and order events that take place. Thus on increasing T_{exit}, the number of disorder-order events that take place quiescently is increased. In the absence of shear, the re-ordering can take place between fluid gel particles (as well as within particles) thus the products require a greater stress to allow the particles to move past one another (greater yield stress) and store more energy under oscillation (greater *G'*).

The same range of fluid gels was also sheared to break the interparticle connections before being rheologically tested for their yield stress. The shear was conducted at 5 °C using the rheometer with a vane geometry to shear at 3000 s^{-1} for 30 mins. The samples were tested 24 hours later (stored at 3 °C) so as to prevent the measurement of time dependent effects. The yield stress of the sheared samples (Fig. 4.14, black symbols) is dependent on κC concentration, but not T_{exit}. This suggests that the inter-particle connections, formed *via* partial quiescent cooling, can be irreversibly broken with shear. The particle diameters were also measured at each T_{exit}. They too were independent of T_{exit} below 20 °C (measurements of over 500 particles at three T_{exit}'s showed no statistical difference in mean diameter, at each concentration), indicating that the structural difference between samples produced within this range lies only in the interparticle connectivity, and that the particles themselves are essentially equivalent. Thus, controlling quiescent cooling, once 98.4% of the molecular ordering has taken place under shear, can be used to tailor inter-particle connections to control their mechanical behaviour, and these can be irreversibly broken by shear.

4.6. Concluding remarks

With the potential use of fluid gels in reduced calorie or satiety enhanced foods, this chapter focused on their formation and properties. Fluid gel formation was explored by producing gels at a range of κC and KCl concentrations and a range of temperatures to vary the ratio of sheared to quiescent cooling. This allowed conclusions to be drawn on the formation of fluid gels and the dependence of ingredients and processing conditions on their material response; both of which are required for the effective incorporation of fluid gels into food products. Additionally, the knowledge on fluid gel properties was enhanced by conducting microscopy, calorimetry and centrifugation techniques.

The KCl concentration influences k_{CH} and T_m which was shown to determine fluid gel properties. More specifically, high KCl contents produce large particulates due to faster gelation and low salt contents are unstable against molecular reordering. Thus, for small diameter and stable particles, the KCl concentrations should lie within a specific range which is dependent on the cooling and shear rates

Fluid gels formed with κC were demonstrated to have fewer helical residues and smaller regions of aggregated helices than quiescently cooled gels due to the disruption of helix formation caused by the applied shear during their production. This is in contrast to agarose fluid gels whose number of helical residues is equal to that formed in quiescent gels. This contrasting behaviour is hypothesised to be a result of κC having a lower rate of molecular ordering to agarose (by 2-3 orders of magnitude (Norton *et al.* 1986)) which makes it more susceptible to disruption by the applied shear during gelation. Compared to the large (100 μm) and anisotropic agarose fluid gels, the low gelation rate of κC also allows for the production of small (1 μm) and spherical particles.

More than 98% of the molecular ordering process is required to take place under shear in order to form κC fluid gels without large particulates. With this criterion met, the temperature that fluid gels exit the sheared environment can be used to control their rheological properties. This is partly because the remaining disordered chains can then order quiescently, but also because fluid gels produced at greater temperatures will experience a greater amount of quiescent re-ordering as a result of being closer to their T_m where the likelihood of disorder-order events is increased. Both of these effects act to bridge particles together which increase fluid gel storage moduli and yield stresses. Shearing fluid gels once formed, however, breaks these inter-particle bridges so as to eliminate the influence of the exit temperature on their properties. At this stage, they behave as a particulate gel system displaying 'weak' and 'strong' gel characteristics as a result of the particles being associated through weak interactions whilst being composed of strong gel networks.

Fluid gel particle volume fractions can be determined by identifying their solid contents and stress-induced particle compression. Through the course of the chapter, it was shown that increasing κC concentration increases particle elasticity and volume fraction whilst reducing particle diameters.

Chapter 5.

Tribology of non-gelling hydrocolloid polymeric thickeners

5.1. Introduction

The aim of this chapter was to understand the influence of hydrocolloid chain conformation and coil overlap effects, that is, hydrocolloid structure, on tribology. Secondly, the influence of salts on hydrocolloid tribology was investigated since salts are often incorporated into food matrices for taste, preservation or to allow for hydrocolloid gelation and can influence polymer solubility and therefore chain conformation.

The influence of hydrocolloid chain conformation on lubrication was investigated using a rheological and tribological study of five polysaccharides that vary in chain expansion from random coil to extended chain and rigid-rod. To conduct the study, a range of concentrations of each polysaccharide was prepared that varied from dilute to entangled conditions. Aqueous salt solutions without hydrocolloids were also investigated tribologically as a function of position within the Hofmeister series to probe their influence on the tribo surface properties. Guar gum was then used to investigate the influence of salt on hydrocolloid lubrication.

5.2. The influence of hydrocolloid hydrodynamics on lubrication

The dependence of lubrication on hydrocolloid polymer conformation and concentration was investigated in this study using guar gum (GG), locust bean gum (LBG), lambda carrageenan (λC), kappa carrageenan (κC) and scleroglucan (SCL). GG and LBG (both galactomannans) were employed because of their widespread use in the food industry and random coil secondary structures. λC is also commonly used in foods; it has an expanded coil secondary structure and, similarly to the galactomannans, it does not form gels. κC also has an expanded coil secondary structure but it allows for gelation with appropriate cations (*e.g.* K^+); however, in the salt form used here (tetramethylammonium), gel formation is not

favoured, thereby allowing linear polymeric solution behaviour. In addition to different secondary structures (random coil versus expanded chain), carrageenans and galactomannans also have different primary structures (which are displayed in Chapter 2.2.1) which may influence tribological behaviour through chemical or physical adsorption to the tribopair surfaces. Because of this, SCL, which has a similar primary structure to galactomannans (and is therefore expected to have similar adsorption properties) but a rigid-rod secondary structure, is used in this study to substantiate arguments based on secondary structures, despite being a non food-grade polysaccharide.

*5.2.1. Rheology: effect of shear on coil overlap concentration, C**

In order to understand the influence of polysaccharide conformation and concentration on tribological behaviour, their influence on rheological properties was first characterised. This was achieved by identifying the onset of chain overlap by calculating *C** for each polysaccharide tested. *C** values were determined by first identifying zero-shear viscosities (η_0) for a range of concentrations from viscosity/shear rate plots (such as that shown in Fig.

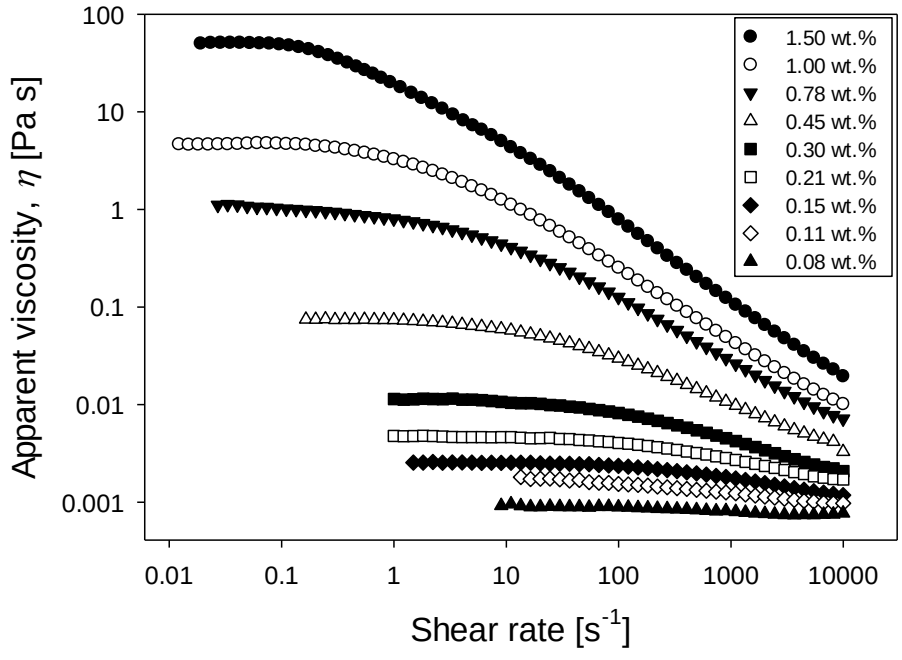

Fig. 5.1. Flow curves for GG at a range of concentrations.

5.1 for GG) by extrapolation, of low-shear Newtonian plateaus, to zero-shear. From these, *C** values were found from the intercept of straight lines formed on double logarithmic zero-shear viscosity versus concentration plots, the results of which are shown in Fig. 5.2 (a). The concentration at which the intercept lies marks *C** and the transition from single entity

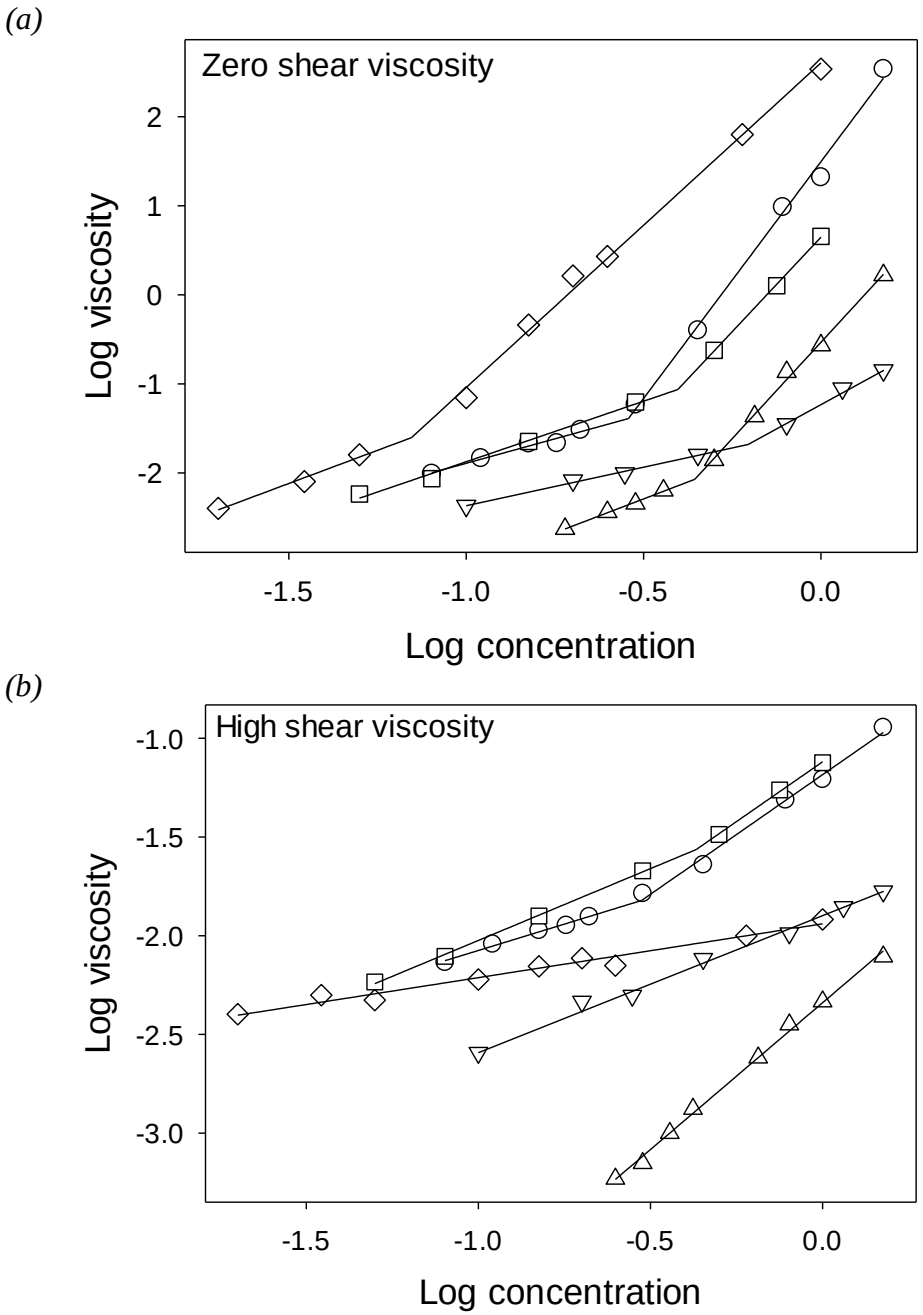

Fig. 5.2 Viscosity vs. concentration plots for guar gum (○), locust bean gum (□), λ-carrageenan (△), κ-carrageenan (▽) and scleroglucan (◇) at shear rate $\dot{\gamma}$ = 0 (a) and 3500 s^{-1} (b).

polymer chains to the formation of an entangled polymer network (Morris et. al. 1981).

In addition to identifying *C** values at zero shear, *C**s were also determined at a high shear rate to investigate the dependence of coil overlap on shear. This dependence will be used to understand the tribological behaviour of polysaccharides in a mixed regime where lubricants are subjected to high shear rates. High shear *C** values were calculated as before but with high shear viscosity (at $\dot{\gamma}$ = 3,500 s^{-1}) plotted against concentration. Fig. 5.2 (b) shows double logarithmic high shear viscosity versus concentration plots for each polysaccharide tested. Viscosities are lower at high shear throughout the concentration ranges for each polysaccharide, due to their shear thinning behaviour.

GG and LBG retain their marked transitions between dilute (single entity, $C < C^*$) and concentrated (entangled, $C > C^*$) regions at high shear *i.e.* two intercepting power law fits are observed (Fig. 5.2 b), as is the case at zero-shear (Fig. 5.2 a). This is in contrast to the behaviour of λC, κC and SCL which display single power-law relationships between concentration and high-shear viscosity throughout their concentration ranges. Table 5.1 gives values of zero and high shear *C** (obtained from Fig. 5.2 (a) and (b), respectively) and shows that the high shear *C** values for GG and LBG are greater than their zero shear *C** values; thus, indicating a greater critical concentration required to reach coil overlap due to partial polymer alignment in the shear flow.

Table 5.1
C values calculated from zero and high shear ($\dot{\gamma}$ = 3,500 s^{-1}) viscosity versus concentration plots (i.e. Fig. 5.2(a) and (b)).*

Biopolymer	Zero shear *C**/wt.%	High shear *C**/wt.%	Polymer conformation
Guar Gum	0.28	0.30	Random coil (Robinson et al. (1982))
Locust Bean Gum	0.40	0.43	Random coil (Launcy et al. (1997))
κ-carrageenan	0.62	N/A	Extended chain (Vreeman et al. (2004))
λ-Carrageenan	0.44	N/A	Extended chain (Rees (1969))
Scleroglucan	0.07	N/A	Rigid-rod (Gidley et al. (2009))

The fact that *C** behaviour is not observed at high shear for λC, κC and SCL indicates that the polymer alignment of extended and rigid-rod chains in shear flow is more facile than for random coil chains and that the shear induces complete disentanglement and a dissociation of chains thereby behaving in an analogous manner to dilute solution conditions.

This proposed mechanism of chain conformation influencing polymer alignment (shear thinning) and chain disentanglement is similar to that made by Peiffer *et al.* (1986). In their study the authors investigated polymer chain extensibility and disentanglement of random-coil and rod-like polymers using birefringence experiments in an elongational flow field created inside an opposing jet device. The authors demonstrated that random coil chains expanded to rod-like conformations in $C < C^*$ solutions (at high elongational rates) and oriented in the elongational flow but, the entanglements formed in $C > C^*$ solutions prevented maximum polymer extension, and complete orientation did not occur. Rod-like polymers, however, were easily orientated at concentrations below and above *C** due to the ease at which they can be oriented in extensional flow.

On the basis of the data observed and related literature, it can be concluded that for polysaccharide solutions where $C > C^*$, rigid-rod and extended-coil chains readily orient in shear and elongational flow becoming fully disentangled whilst random coil polymers retain their chain entanglements without full alignment (up to the high shear rate tested, $\dot{\gamma} = 3{,}500\ s^{-1}$). An explanation for this behaviour is that the polysaccharide chains become less flexible as their chain expansion coefficients increase which causes fewer intermolecular interactions (or contact sites) thereby facilitating disentanglement under shear.

5.2.2. Tribology

To investigate the dependence of tribological behaviour on lubricant structure, the effect of hydrocolloid chain expansion and coil overlap behaviour on friction was tested in regimes of both boundary and mixed lubrication. To achieve this, Stribeck curves at numerous concentrations of each polysaccharide were obtained. Stribeck curves in this study were generated from friction coefficient (μ) measurements at a range of different entrainment speeds using an elastomer-steel tribopair. This allowed the selection of conditions for subsequent studies: 1 mm s^{-1} was used as the speed for boundary regime friction as it is the slowest speed attainable on the MTM2 instrument. 251 mm s^{-1} was chosen as the speed for

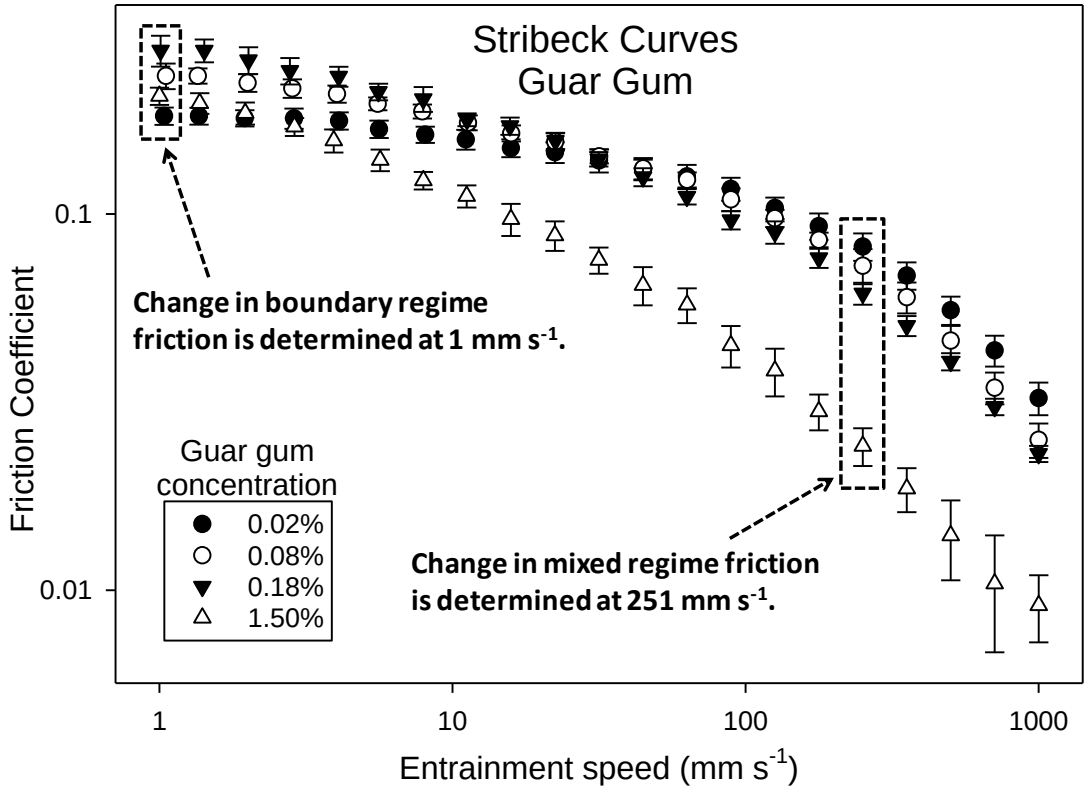

Fig. 5.3.Friction coefficient vs. entrainment speed plots (Stribeck curves) for guar gum solutions at various concentrations. From a series of such plots, the effect of concentration on friction coefficient is determined at two entrainment speeds, U = 1 and 251 mm s^{-1}, representing boundary and mixed regimes, respectively.

mixed regime friction as it is fast enough to be out of the boundary regime for all concentrations, but not too fast that a rise in friction begins as the hydrodynamic regime is approached. Thus, changes of μ with polysaccharide concentration at $U \sim 1$ and ~250 mm s^{-1} can be observed from Stribeck curves (an example is shown in Fig. 5.3 for four concentrations of GG) and will now be discussed in detail in the two subsequent sections.

5.2.2.1. Effect of polysaccharide concentration on boundary regime friction

To probe the influence of hydrocolloid conformation and concentration on tribology in a boundary regime of lubrication, μ at $U = 1$ mm s^{-1} was plotted against concentration of random coil (Fig. 5.4) and expanded chain (Fig. 5.5) polysaccharides. For Fig. 5.4 (random coils), the data points left of the dashed line are in a boundary regime of lubrication (surfaces are in full contact and the bulk fluid is excluded), whilst those right of the dashed line are in a

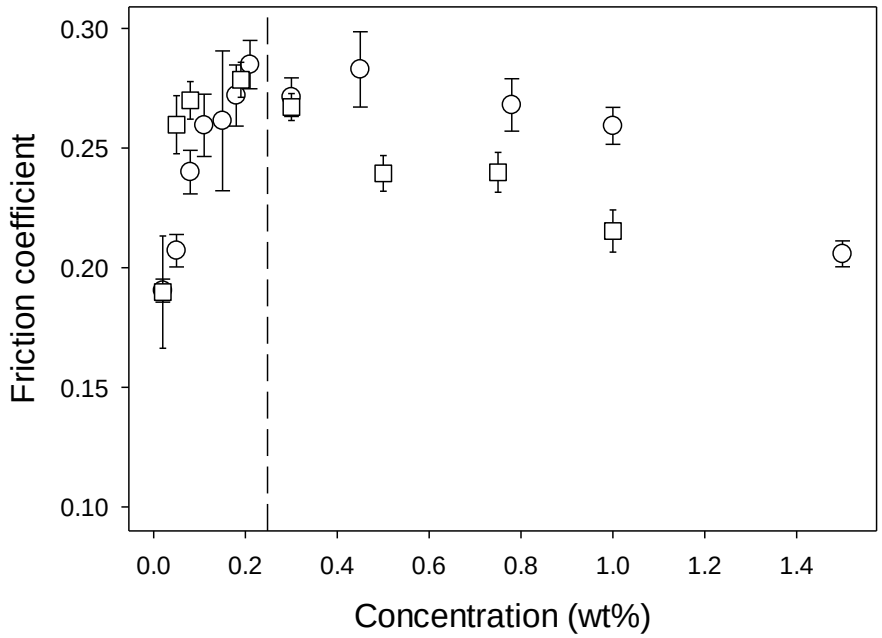

Fig. 5.4. Friction coefficient (at U = 1 mm s^{-1}) vs. concentration plots for random coil polysaccharides guar gum (○) and locust bean gum (□). Data points right of the dashed line are in a mixed regime of lubrication at U = 1 mm s^{-1}, all others are in boundary conditions.

mixed regime of lubrication (surface separation and fluid entrainment is of the same dimensional order as the size of the surface asperities). Boundary regimes were identified from a horizontal start to the Stribeck curves where μ is constant with U; mixed regimes however, were identified from μ decreasing with U from the onset of the speed range (Spikes, 1997). The data in Fig. 5.4 shows that at 1 mm s^{-1}, in boundary lubrication conditions, μ increases through an incrementally increasing concentration range of GG and LBG. Large boundary regime friction coefficients of galactomannans have previously been reported and were attributed to polymer blockage (de Vicente *et al.*, 2005) and exclusion (Zinoviadou *et al.*, 2008) at the ball and disc contact, however, an incremental increase in μ with concentration has not been shown before. In mixed lubrication conditions at U = 1 mm s^{-1} (right of the dashed line in Fig. 5.4) μ decreases with concentration of GG and LBG. This behaviour was expected because the bulk fluid is partially entrained during mixed regime conditions where the film thickness increases with viscosity due to a build-up of fluid pressure at the contact. Before providing an explanation for the observed rise in boundary friction with increasing random coil concentration, the effect with expanded-chain polysaccharides will be described.

The dependence of friction coefficient, at $U = 1$ mm s^{-1}, on concentration of polysaccharides with more expanded conformations (λC, κC and SCL) are reported in Fig. 5.5. Here, all concentrations of each polysaccharide displayed boundary regimes at $U = 1$ mm s^{-1} (*i.e.* their Stribeck curves initiated with μ being independent of *U).* Fig. 5.5 shows that μ decreases throughout concentration ranges of the carrageenans (extended-coil) and SCL (rigid-rod) polysaccharides.

A contrast, therefore, exists in boundary regime lubrication between random-coil polysaccharides (where μ increases with concentration) and those with more expanded conformations (where μ decreases with concentration). To provide an explanation of this behaviour, the ball and disc inlet and contact zones must be identified – as depicted in Fig. 5.6. The random coil polysaccharides are unable to fully align in shear and elongational flow fields (this was concluded in the previous section, 5.2.1) and therefore will possess high hydrodynamic volumes in the inlet zone thus restricting entrainment to the contact zone of the

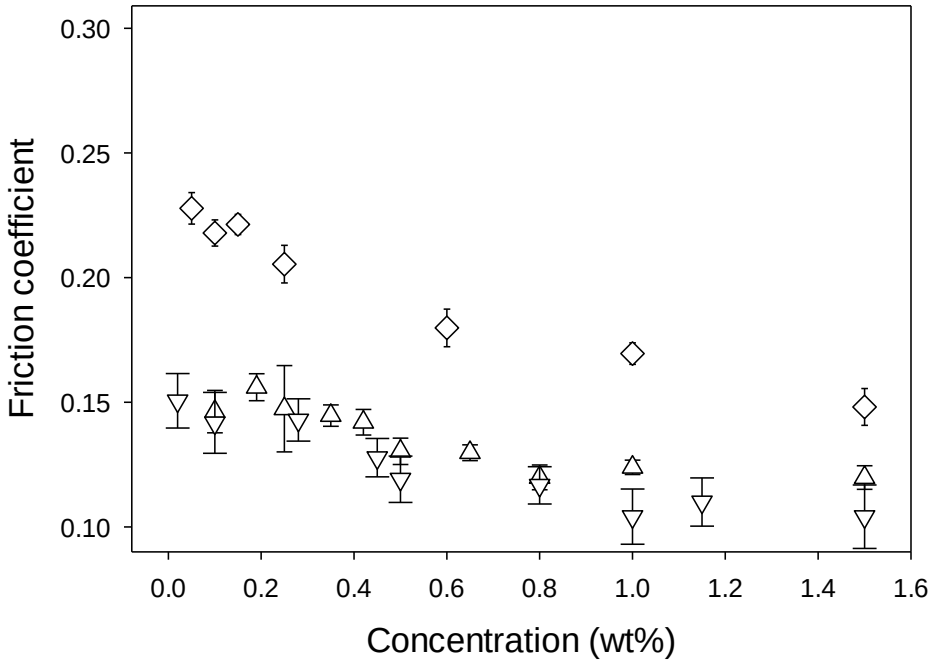

Fig. 5.5. Friction coefficient (at U = 1 mm s^{-1}) vs. concentration plots for extended-coil λ-carrageenan (△), κ-carrageenan (▽) and rigid-rod scleroglucan (◇) polysaccharides.

ball and disc. Conversely, polymers of a more expanded chain conformation are able to align in flow resulting in comparatively lower hydrodynamic volumes in the inlet zone and therefore being more able to entrain the contact zone and provide lubrication.

The discussed mechanism of structurally attributable polymer exclusion requires surface adsorption of polymers to the ball and disc to be considered because adsorption to the surfaces will facilitate entrainment. Polymer charge is expected to influence polymer adsorption; polyelectrolytes, for example λC, have been shown (Bongaerts *et al.*, 2009) to adsorb to PDMS surfaces where the hydrated polymer chains provide a water solvent layer at the surfaces capable of providing effective boundary films (Spikes, 1996). However, GG, which is non charged, does not adsorb to the surfaces used in this study; Cassin *et. al.* (2001) found no GG binding to silicone rubber surfaces using EWS (Evanescent wave spectroscopy)

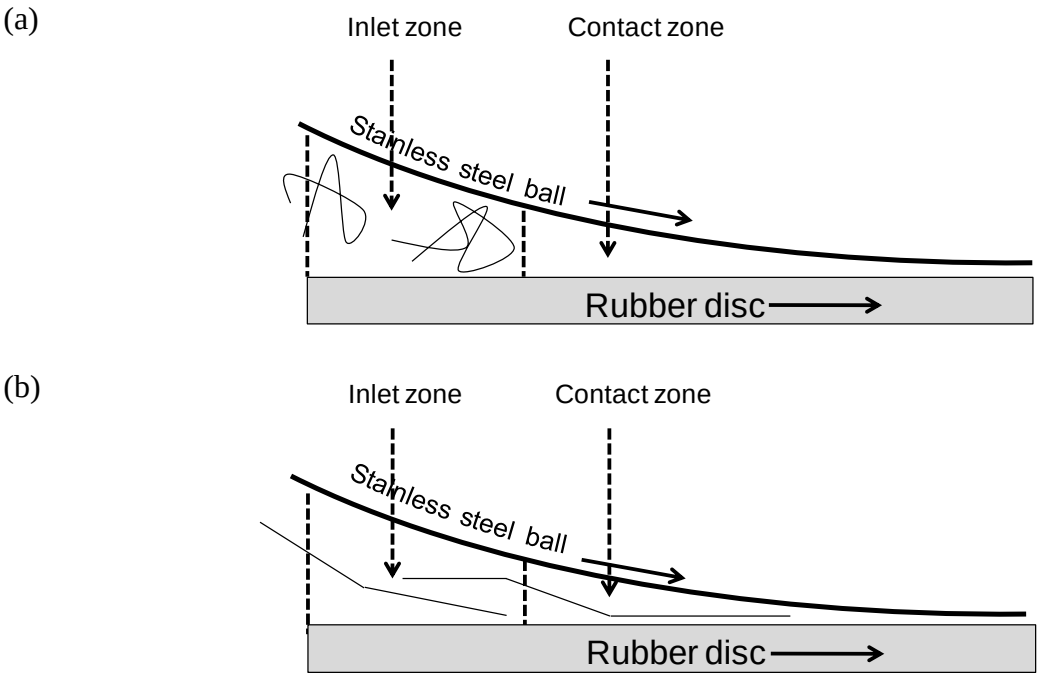

Fig. 5.6. Schematic representation of the behaviour of hydrocolloids at the ball-and-disc contact. Solid arrows indicate the direction of ball and disc movement. Due to alignment of polymer chains to flow, the hydrodynamic volume at the inlet zone to the ball and disc is lower for extended-coil and rigid-rod polysaccharides (b) than random-coils (a).

and this behaviour was subsequently confirmed by Malone *et al.* (2003) and de Vicente *et al.* (2005). The primary structure of GG is similar to LBG and SCL (Chapter 2.2.1) and so they all are expected to be non-adsorbing due to having weak chemical and electrostatic interactions with the surfaces. The fact that SCL (rigid-rod) is favourably entrained for lubrication whilst GG and LBG (random coil) are not, can, therefore, be attributed to polymer entrainment being influenced by conformation.

To summarise the investigation into the influence of hydrocolloid structure on boundary friction: random coil structures do not align in flow and are excluded from entrainment and therefore provide poor lubrication. On increasing their concentration, boundary friction coefficients increase due to decreased availability of fluid for entrainment. In contrast, hydrocolloids with more expanded chain conformations exhibit shear induced alignment to the contact. As a result, expanded chain hydrocolloids are entrained and provide boundary lubrication.

5.2.2.1.1. Effect of normal load on boundary friction

To determine if polysaccharide conformation influences the contact mechanics of the boundary regime, F_t versus W plots were formed by obtaining Stribeck curves at a range of applied normal loads (W). The measured tangential friction force ($F_t = \mu/W$) from Stribeck curves at U = 1 mm s^{-1} is plotted against W in Fig. 5.7 for GG, λC, κC and SCL. For all polysaccharide lubricants, F_t is shown to follow a dependence on normal load of $W^{2/3}$. As discussed in the literature review (section 2.4.3-Contact mechanics, and section 2.4.5-Soft-surface tribometry) an F_t dependency on load of $W^{2/3}$ has previously been observed in soft surface tribometry (Myant *et al.*, 2010; Stokes *et al.*, 2011) due to the formation of a fixed number of contact sites with an area that increases with load due to elastic deformation. The

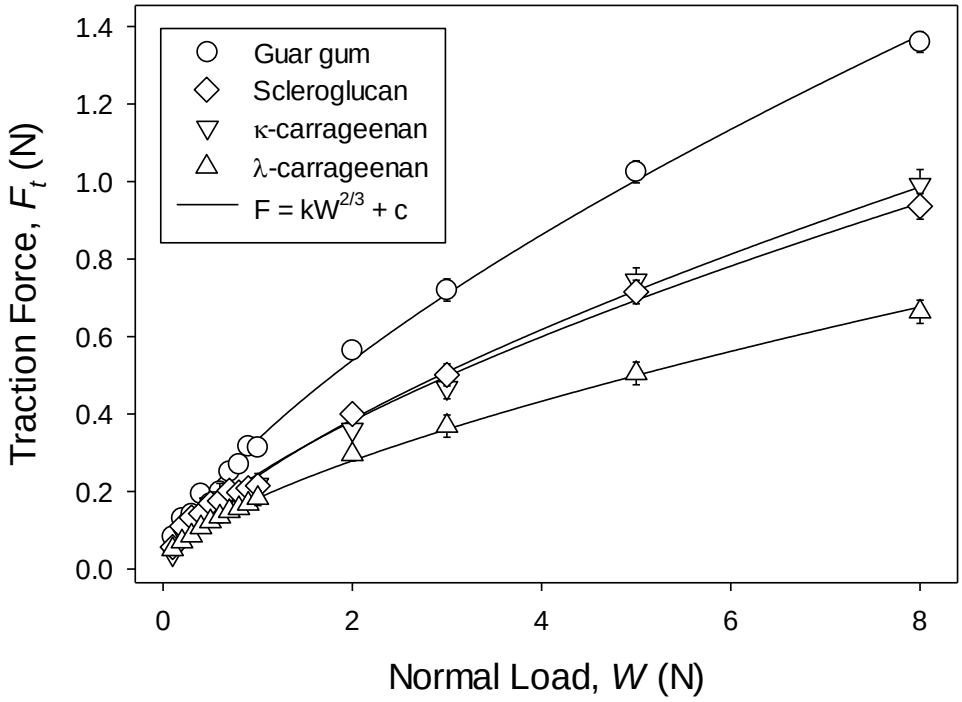

Fig. 5.7. Tangential friction force versus normal load plots for guar gum (○), λ-carrageenan (Δ), κ-carrageenan (▽) and scleroglucan (◇). Lines show fits to $F_t = kW^{2/3} + c$.

fact that a guar gum lubricated contact has a greater friction force than the extended chain polysaccharides over a range of applied loads demonstrates that the mechanism of structurally attributable polymer entrainment is a behaviour that is independent of the applied normal force. The fact that each polysaccharide follows $W^{2/3}$ is useful only for characterising the contact behaviour for preferentially entraining and excluding polymer thickeners – this characterisation will be referred to in Chapter 6 where the contact mechanics of fluid gel lubricated contacts are explained.

5.2.2.2. Effect of polysaccharide concentration on mixed regime friction

This section describes the influence of hydrocolloid chain conformation and coil overlap effects on tribology in a mixed regime of lubrication. As previously shown in Fig. 5.3, mixed regime friction coefficients were taken from Stribeck curves at $U \sim 250$ mm s^{-1}.

Friction coefficients (at $U \sim 250$ mm s^{-1}) were plotted against the concentration of expanded chain (Fig. 5.8) and random coil (Fig. 5.9) polysaccharides. The data in Fig. 5.8 which is for λC, κC and SCL shows that μ decreases linearly with concentration of the carrageenans throughout the range tested, despite passing the zero-shear C^* values of 0.44 and 0.62 wt.% for λC and κC, respectively. The fact that this relationship is linear throughout the concentration range that spans conditions that would, at rest, be described as progressing from dilute to entangled solutions indicates that this structural transition does not occur during a mixed regime of lubrication for expanded conformation polymers. This behaviour is consistent with the conclusions drawn previously on extended conformation polymer chains

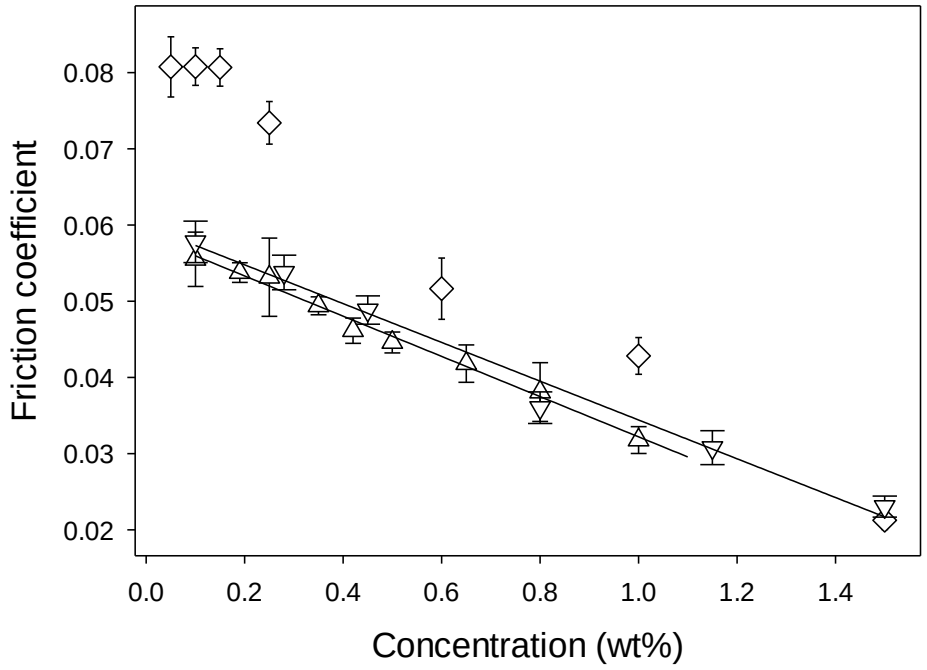

Fig. 5.8. Friction coefficient (at U ~ 250 mm s^{-1}) vs. concentration plots for extended-coil λ-carrageenan (Δ), κ-carrageenan (▽) and rigid-rod scleroglucan (◇) polysaccharides.

being able to fully disentangle in concentrated solutions under shear and elongational flow. Thus, the flow brought about by entrainment to the rotating ball and disc allows extended-coil chains to orient and become fully disentangled at $C > C^*$ allowing single entity polymer chain behaviour to occur throughout the concentration range. The tribological effect of passing the C^* value for SCL is not discussed here because the value is too low (C^* = 0.07 wt.%) to probe the behaviour of dilute conditions given the inherent error margins of the tribological setup.

The data for both GG and LBG (Fig. 5.9) can be modelled by two linear fits intercepting at a concentration denoted here as C_T^*, representing a critical tribological concentration. For GG and LBG, C_T^* = 0.24 and 0.43 wt.%, respectively, which are similar to their rheologically determined C^* values of 0.28 and 0.40 wt.%. The similarity of the rheologically and tribologically determined critical concentrations suggests that coil overlap behaviour influences entrainment for lubrication. This behaviour corresponds with the fact that random coil chains at $C > C^*$ do not disentangle at high shear rates (this was tested at $\dot{\gamma}$ = 3,500 s^{-1}) and thus, an entangled polymer network is expected in mixed regime conditions for random coil polysaccharides.

The mixed regime friction coefficients for GG and LBG show linear fits with a decrease in their gradient at concentrations greater than C_T^* (Fig. 5.9), conversely, the viscosity versus concentration plots for GG and LBG (Fig. 5.2) show an increase in gradient after C^*. More specifically, as the concentration of GG or LBG are progressively increased, the friction coefficient continually decreases, but its dependence on concentration is reduced beyond C_T^*. This is in contrast to their rheological behaviour on passing C^* which demonstrate a pronounced increase in the dependence of concentration on viscosity beyond C^*. To provide an explanation for the observed tribological behaviour of GG and LBG, the

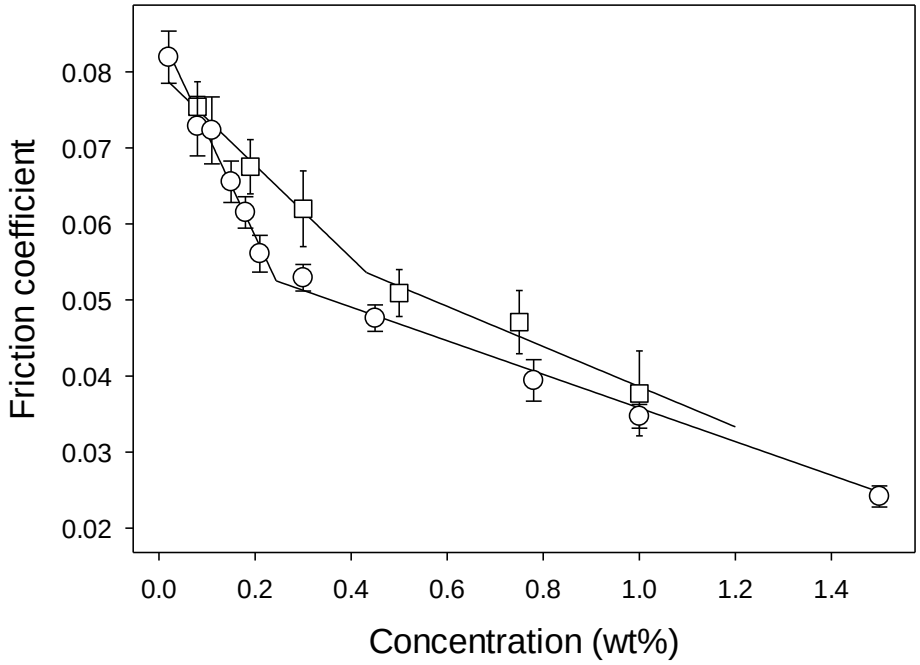

Fig. 5.9. Friction coefficient (at U ~ 250 mm s^{-1}) vs. concentration plots for random coil polysaccharides guar gum (○) and locust bean gum (□). Friction decreases with concentration following two linear relationships intercepting at C_T = 0.24 and 0.43 wt.% for guar gum and locust bean gum, respectively. The C_T* values are similar to their rheologically determined C* values of 0.28 and 0.40 wt.%, respectively.*

structure of the hydrocolloid solutions in relation to the ball and disc contact are required to be considered. At $C < C^*$ the polymer chains exist as single entities and so can pass through the gap at the contact zone. In these dilute concentrations, increasing C increases solution viscosity which is partially entrained (in mixed lubrication conditions) hence the observed frictional decrease. At $C > C^*$ an entangled network forms which hinders the rate of fluid entrainment to the contact due to large volumes of polymer occupying the inlet zone where the rotational freedom of the ball and disc are reduced as well as the availability of polymer chains for entering the contact zone.

A similar behaviour of depleting the contact zone of lubricant is observed during a test where κC is allowed to form a gel within the tribometer reservoir. The purpose of this gelation test was to advance the understanding of the influence of macroscopic polymer

network formation on mixed regime tribometry. Friction coefficients (at U = 500 mm s^{-1}, mixed regime) are shown in Fig. 5.10 as a function of temperature on cooling κC solutions at concentrations of 0.5, 1 and 2 wt.% (with 0.3 wt.% KCl) from 50 to 5 °C. At temperatures above gelation (> 35 °C), lower friction coefficients are observed with greater κC concentrations due to an increase in solution viscosity. After gelation, however, this dependence is reversed; more specifically, greater κC concentrations give greater friction coefficients. This behaviour is analogous to that described for entangled random coil solutions in that macroscopic biopolymer ordering hinders entrainment for lubrication despite providing a pronounced increase in viscosity. In the case of gelling κC, this is due to polymer chains forming an aggregated network of helices which occupy the inlet zone but deplete the contact zone of solvent (water) and polymeric material. In the case of concentrated random coil solutions, the flexible polymers make intermolecular contacts which are maintained in shear and elongational flow and hinder bulk fluid lubrication by restricting polymer availability for entrainment.

From the results obtained in this chapter thus far, it can be concluded that the

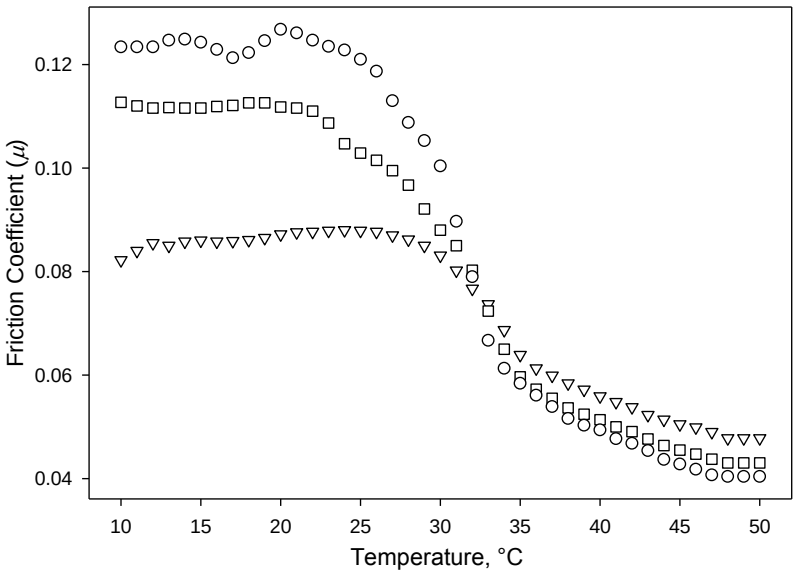

Fig. 5.10. Friction coefficient as a function of temperature on cooling solutions of 0.5% (▽), 1% (□) and 2% (○) κC with 0.3 wt.% KCl. Friction was measured at 500 mm s^{-1} (mixed regime).

converging geometry formed by the ball and disc contact can prevent bulk material entrainment which results in a disparity between hydrocolloid tribological and rheological behaviour. Furthermore, it can be concluded that the structure of hydrocolloids (in terms of solution conformation and coil overlap behaviour) influences tribological response.

5.2.3. Stribeck master curves

As discussed in the Literature Review (in section 2.4.6), Stribeck master curves can be formed by conducting Stribeck tests (μ versus U) on Newtonian lubricants at a range of viscosities (η) and plotting μ versus $U\eta$. The viscosity of Newtonian fluids is independent of the applied shear rate, and therefore entrainment speed, which allows $U\eta$ to be used as a scaling factor providing a superposition of data onto a single master curve. In light of the findings discussed in this chapter thus far, it seems that Stribeck master curves cannot necessarily be applied to hydrocolloid systems since the material being entrained and therefore measured tribologically, may not be equivalent to that tested rheologically. Thus, using rheological data (*i.e.*, η) to provide a superposition of Stribeck curves may not be appropriate for hydrocolloid lubricants. This hypothesis is discussed in this section.

Fig. 5.11 (a) shows a Newtonian Stribeck master curve for corn syrup prepared at a range of concentrations (and therefore viscosities) where all plots collapse onto a single curve which displays three lubrication regimes: boundary, mixed and hydrodynamic.

Fig. 5.11 (b and c) show attempted Stribeck master curves for λC and GG, respectively, by plotting μ versus UK where K is an arbitrary shift factor representing viscosity. The K values are constant throughout the entrainment speed range for each concentration and were determined by identifying values that allow the greatest degree of curve superposition. K values were used rather than viscosities because the hydrocolloid solutions are shear thinning and so identification of the η of the fluid in the contact requires the shear rate in the contact to be known. de Vicente et. al. (2005 and 2006) suggested that K can be used to represent the effective viscosity of the fluid in the contact and that the K values required to form maximum curve superposition correspond with apparent viscosities at shear rates of 10^4 -10^6 s^{-1} – thereby estimating the shear rate in the contact zone.

(a)

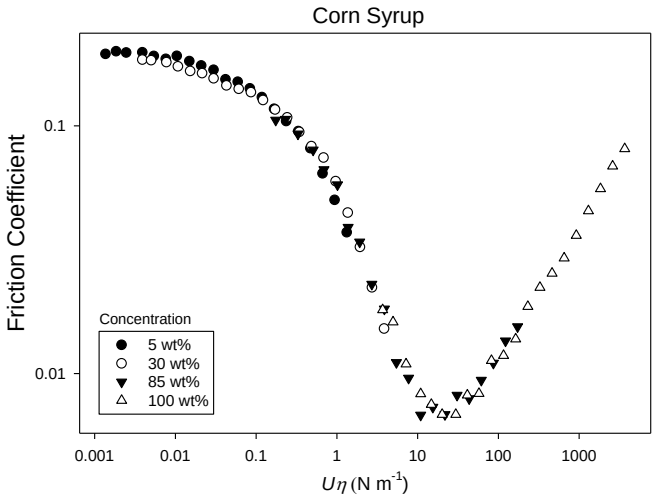

(b)

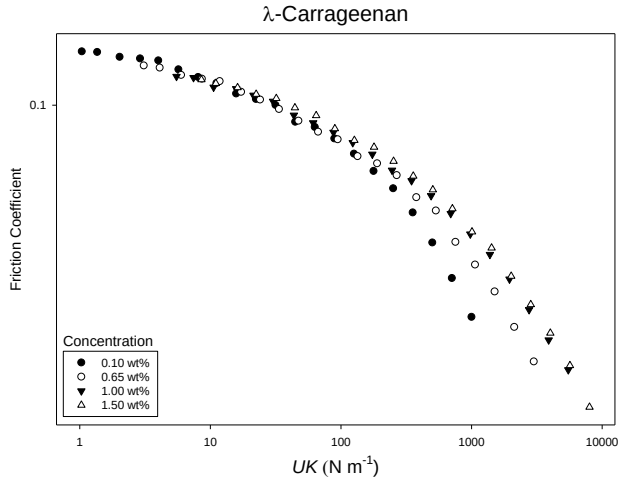

(c)

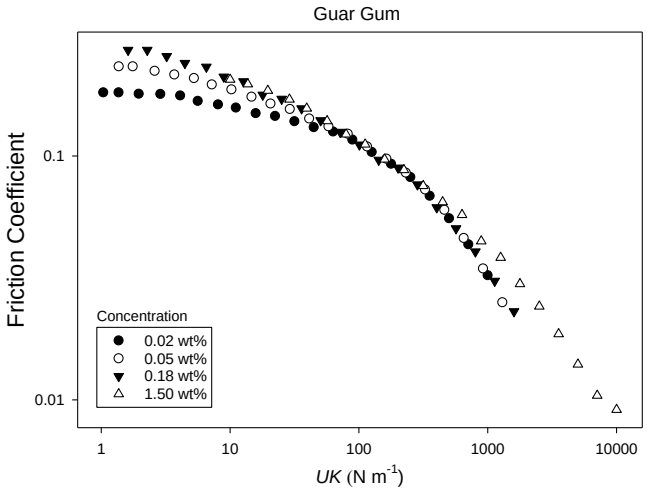

Fig. 5.11. Stribeck master curve (Friction coefficient vs. entrainment speed × viscosity) for Newtonian corn syrup (a). Attempts are made to form Stribeck master curves for non-Newtonian λ-C (b) and GG (c) with friction coefficient vs. entrainment speed × K curves, where K is a shift factor chosen to generate maximum curve collapse.

To form a complete Stribeck master curve, using $U\eta$, requires the viscosity of the fluid in the contact zone to be determined at each entrainment speed tested. However, since viscosity is a bulk property, and the bulk material of a hydrocolloid solution is not necessarily entrained due to polymer exclusion, rheologically determined viscosity values cannot provide full superposition, even if the shear rates are known at each speed. This is particularly notable in Fig. 5.11 (c) for GG which shows boundary friction coefficients increasing with concentration (and therefore viscosity), therefore, the boundary regimes will not superimpose regardless of the viscosity values used (viscosity will only shift the data along the *x*-axis). The result of this is that shear rates cannot be determined in the contact by identifying viscosities required to form superposition (and then determining the shear rate required to provide that viscosity) if the material being measured for its viscosity is not itself entrained due to structurally attributable polymer exclusion. As a consequence, Stribeck curves for hydrocolloids will not be superimposed to form master curves in this thesis.

5.3. The influence of sodium salts on lubrication

In this section, the influence of salt on the tribology of non-gelling hydrocolloid solutions is tested. The Hofmeister series of salts was employed to investigate the influence of salt type on tribometry throughout an extensive range, despite the fact that some of the tested salts are non-food grade. Salts were initially tested in water without hydrocolloids to test their influence on tribo-surface properties and then they were tested in GG solutions.

5.3.1. Sodium Salts in water

The lubricating properties of water and sodium salt solutions that span the Hofmeister series (Table 5.2) were investigated at concentrations ranging from 0.001 to 1 M using an elastomer-steel tribopair. Fig. 5.12 shows the Stribeck curves produced from water and 0.1 M solutions of sodium iodide (strongly chaotropic), chloride and citrate (strongly kosmotropic). For clarity of the data, only a sample of the entire tested range is shown in Fig. 5.12 **(**friction as a function of concentration for all tested salts will be displayed later). The Stribeck curves in Fig. 5.12 show boundary and mixed regimes only, where the boundary regime is

Table 5.2
Sodium salts used in this study, and their associated physicochemical properties. Lyotropic number (N)[a], Gibbs free energy of hydration ($-\Delta G_{hyd}$)[b]/kJ mol^{-1} and hydrated anion radius (R_{hyd})[c]/nm.

Anion	*N*	$-\Delta G_{hyd}$	R_{hyd}
Iodide, I^-	12.5	275	0.33
Nitrate, NO_3^-	11.6	300	0.34
Bromide, Br^-	11.3	315	0.33
Chloride, Cl^-	10.0	340	0.33
Fluoride, F^-	4.8	465	0.35
Phosphate, HPO_4^{2-}	3.2		
Citrate, $C_6H_5O_7^{3-}$	[d]		

Data from [a](Kunz et al., 2004b) and (Schott, 1984) [b](Lo Nostro et al., 2002), [c](Israelachvili, 2011), [d]citrate is more kosmotropic than phosphate (Hofmeister, 1888).

considerably influenced by ionic content, and the mixed regime is seemingly unaffected. Friction coefficients in the mixed regime are influenced partially by asperity contact and surface bound matter, and partially by the raised fluid pressure within the confined geometry. On increasing entrainment speed, the relative importance of the former over the latter diminishes. Thus, at speeds exceeding 100 mm s^{-1}, the friction coefficients collapse onto one another due to the fact that their viscosities, which largely determine friction at the high end of the mixed regime, are roughly equivalent. For that reason, this section is mainly concerned with tribological behaviour in the boundary regime. Hydrodynamic regimes were not observed on the Stribeck curves because the solution viscosities were not sufficient to fully separate the ball and disc.

To examine the boundary lubrication of aqueous salt solutions, the friction coefficients measured at $U = 1$ mm s^{-1} (from Stribeck tests) are shown as a function of sodium salt concentration, and type, for all solutions tested, in Fig. 5.13. At each concentration, boundary

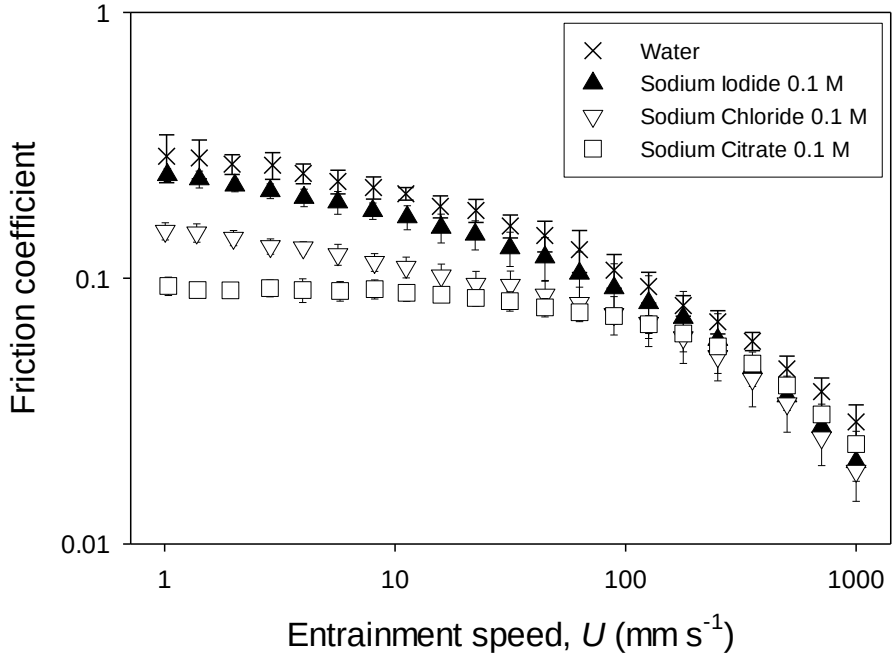

Fig. 5.12. Stribeck curves (friction coefficient versus entrainment speed) for water and aqueous solutions of sodium salts in a stainless steel/elastomer contact.

friction coefficients rank according to the Hofmeister series, with more kosmotropic salts providing the greatest lubrication. A very low concentration (0.001 M) of sodium citrate, the strongest kosmotropic salt tested, reduced the boundary friction coefficient from 0.28 (which was recorded with water alone) to 0.12 (> 50% reduction); thus, representing a substantial tribological influence.

In the literature review it was discussed that salts typically influence boundary friction by one of two methods (Chapter 2.4.8): (1) by influencing the conformation of surface polymer chains *e.g.* self-assembled monolayers (SAMs) and thereby influencing steric repulsion and surface separation, or (2) by hydrated salt ions binding to the surfaces and acting as 'molecular ball bearings'. It seems the behaviour described in the present study is not dominated by the solvent quality influencing the elastomer surface polymer solubility because one would then expect water, or chloride, to act as a neutral basis from which iodide

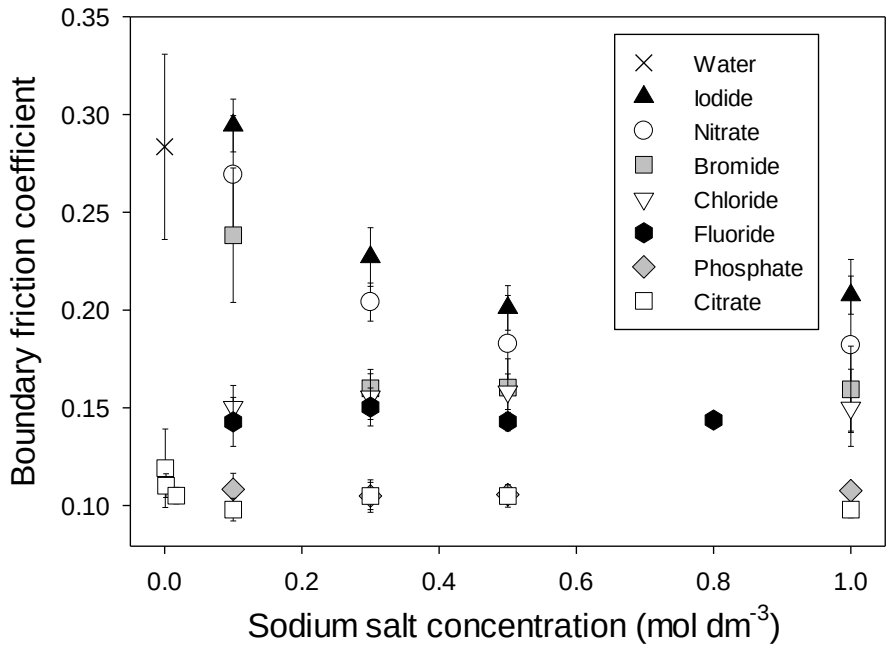

Fig. 5.13. Boundary friction coefficients at 1 mm s^{-1} in a steel/elastomer contact as a function of sodium salt type and concentration in aqueous solution. Salts in the legend are listed in order of appearance in the Hofmeister series (decreasing lyotropic number).

would have a specific effect on the surface polymer conformation, and therefore friction, and citrate would then have the opposite effect to that. The observed data, however, shows that both iodide and citrate reduce sliding friction when compared with water, that is, chaotropic and kosmotropic salts have the same directional influence on friction. Additionally, it would be expected that kosmotropic salts would reduce polymer solubility and therefore collapse the conformation and increase friction, as observed with SAMs (Heeb *et al.*, 2009). On this basis, the mechanism of lubrication by salt in the present system can be attributed to surface bound hydrated ions reducing surface-surface contact (Raviv and Klein, 2002) and increasing fluid viscosity at a close proximity to the surfaces (local-viscosity) by trapping water, thereby restricting flow. Thus, the influence of surface bound hydrated ions seems to dominate any effects to the elastomer's surface polymer conformation that may occur due to changes in solvent quality with salts. Both the effects of reductions in surface-surface contact and an increase in local-viscosity act to provide lubrication for the contacting surfaces and are increased on reducing lyotropic number where Gibbs free energies of hydration (Clarke and Lüpfert, 1999) tend to reduce (Table 5.2), and the adhesive force between approaching ion-bound surfaces is reduced (Vakarelski *et al.*, 2000). The tribological test is dynamic, thus surface-surface contact and local-viscosity will be more strongly related to the propensity for ions to retain hydration shells within the converging geometry (Gibb's free energy of hydration, which reduces with lyotropic number), than their hydration radius (which does not consistently change with reducing lyotropic number (Table 5.2)), hence the observed correlation of friction with the Hofmeister series.

The friction force associated with sliding solid surfaces in an aqueous medium was demonstrated in this study to reduce with ions, and this has previously been shown to result from bound hydrated ions increasing the minimum surface separation through repulsive

hydration forces, and a fast exchange of water molecules in the outer regions of neighbouring hydration shells which provides surface-bound hydration fluidity (Raviv and Klein, 2002). It is shown here, that this effect is strongly influenced by the anions' position within the Hofmeister series and is applicable to macroscopic systems with surface roughness dimensions (disc R_q = 801 nm, Table 5.2) far greater than the ionic hydration sheaths (radius ~ 0.34 nm, Table 5.2 (Israelachvili, 2011)) *i.e.*, the behaviour is not only relevant to atomically flat surfaces. It is expected, therefore, that the hydrated anions are able to form bound-water surface-monolayers as a result of being small enough to fit within the surface irregularities and provide complete surface coverage.

The effect of decreasing friction coefficient with increasing salt concentration reached a plateau for each salt tested, and the concentration at which this occurred was lower for more strongly kosmotropic salts. This plateau may relate to surface saturation of hydrated ions, where a lower molar content of ions is required for those with a lower lyotropic number as their hydration is more energetically favourable.

5.3.2. Sodium salts in guar gum solutions

To test the influence of salts of the Hofmeister series on hydrocolloid tribology, a similar test to that described in the previous section was conducted, but with the salts being added to 0.2 wt.% GG solutions rather than water. More specifically, a range of GG solutions with salts spanning the Hofmeister series was prepared and analysed by monitoring boundary friction coefficients as a function of salt type and concentration. GG was used because of its relevance to the food industry and its weak affinity for surface adsorption. The results of this test will now be discussed. Fig. 5.14 shows boundary friction coefficients (at U = 1 mm s^{-1}) of 0.2 wt.% GG solutions lubricating an elastomer-steel contact as a function of added salt type and concentration. Similarly to the behaviour described in the previous section for water/salt solutions, the addition of salt lowers boundary friction in a trend that follows the Hofmeister series. There is a stricking difference between water/salt and GG/salt solutions however, which lies in the relative impact of low salt concentrations: 0.1 M chaotropic iodide had no significant influence on boundary lubrication compared to water (Fig. 5.13), however, the addition of 0.1 M iodide to GG reduces μ from 0.285 to 0.233 (Fig. 5.14). Furthermore, citrate, which is strongly kosmotropic, plateaued with concentration at 0.015 M in water, compared to ~ 0.5 M in GG solutions. It seems, therefore, that surface bound hydrated ions, which are responsible for the behavior in water, do not explain the entire tribological behaviour in salt/macromolecule systems. Reduced anion diffusion through the viscous solution of GG may explain the continued reduction in friction with anion concentration. However, since nitrate has a stronger influence on friction in GG solutions than in water, despite the former having a greater viscosity, diffusion effects do not seem relevant. It seems more likely, rather, that the presence of salt allows surface adsorption of GG to take place, and/or manipulates the solubility of GG thereby influencing its polymer chain conformation.

GG's intrinsic viscosity was measured as a function of solvent quality to probe changes in chain conformation with salt. To monitor changes in surface adsorption, water-contact angles were measured on the hydrophobic elastomer surfaces after soaking in solutions of GG with salt for 20 mins (~ duration of a Stribeck test), rinsing in deionised water and drying. The effect of salt on GG intrinsic viscosity and GG adsorption will now be discussed, in turn.

Intrinsic viscosities, [η], give an indication of polymer hydrodynamic volume and are given by the Mark-Houwink relationship, Eq. 5.1, where *K'* is a constant, *M* is the polymer molecular weight, and α is the Mark-Houwink exponent. Intrinsic viscosities of GG in various solvents were obtained empirically by double extrapolation using equations by Huggins

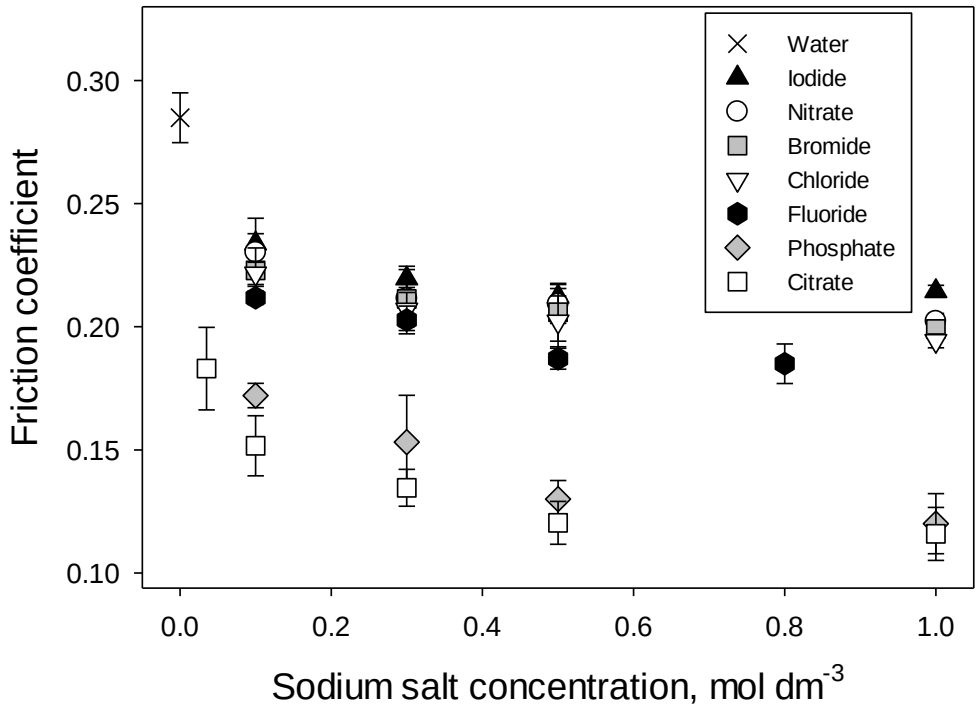

Fig. 5.14. Boundary friction coefficients at 1 mm s^{-1} in a stainless steel/elastomer contact lubricated by 0.2 wt.% GG solutions as a function of sodium salt type and concentration. Salts in the legend are listed in order of appearance in the Hofmeister series (decreasing lyotropic number).

$$[\eta] = K'M^{\alpha} \qquad \textit{Eq. 5.1}$$

$$\frac{\eta_{sp}}{c} = [\eta] + k_H[\eta]^2 c \qquad \textit{Eq. 5.2}$$

$$\frac{\ln \eta_{rel}}{c} = [\eta] + k_K[\eta]^2 c \qquad \textit{Eq. 5.3}$$

(Huggins, 1942) and Kraemer (Kraemer, 1938) (Eq. 5.2 and Eq. 5.3, respectively), where η_{sp} and η_{rel} are the solution's specific and relative viscosities, and k_H and k_K are Huggins and Kraemer constants, respectively. Fig. 5.15 shows such fits to demonstrate the method used for determining $[\eta]$ values; in this Figure, which is for GG in water, $[\eta]$ = 14.50.

To identify the influence of chaotropic and kosmotropic solvents on GG's intrinsic viscosity, this double extrapolation procedure was repeated for GG in water with various concentrations of sodium iodide (chaotropic) and citrate (kosmotropic); the results of which are shown in Fig. 5.16. This Figure shows that the intrinsic viscosity of GG is reduced in low

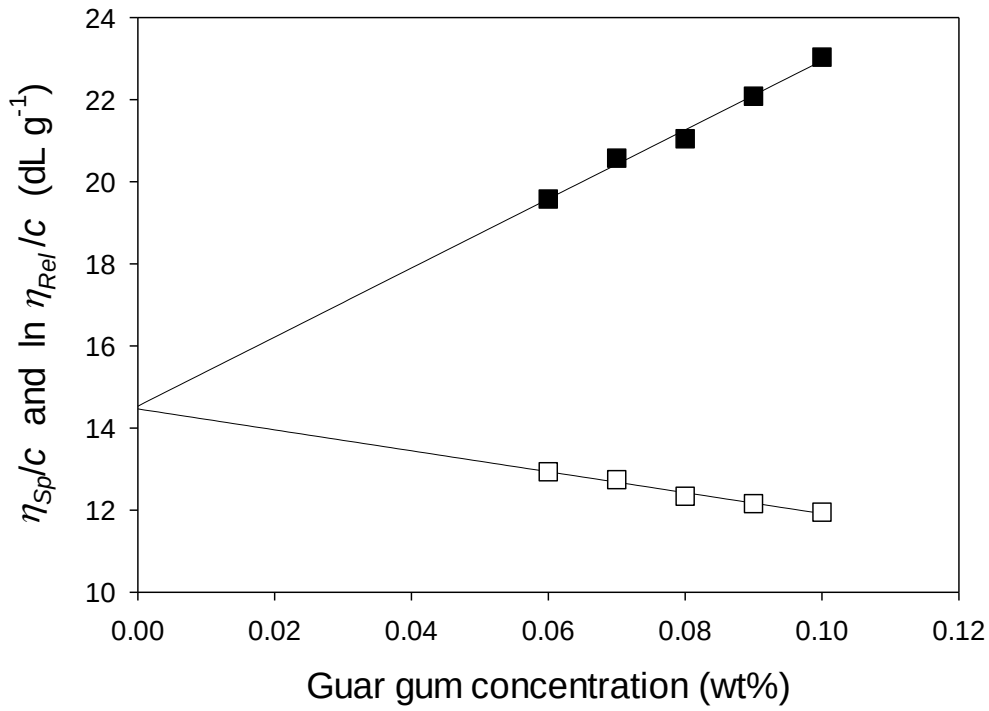

Fig. 5.15. Huggins (■) and Kraemer (□) extrapolations to infinite dilution identifying the intrinsic viscosity of GG by determining the y-axis intercept. In this case, the solvent is water with no added salt, and the intrinsic viscosity is 14.50.

electrolyte concentrations (≤ 0.3 M) of both kosmotropic and chaotropic salts suggesting a decrease in GG's solubility. The effect however, is not monotonic, that is, the addition of salt does not continue to have the effect of reducing [η] throughout the concentration range, *i.e.*, 1 M salts gave higher [η]'s than at 0.3 M, and sodium citrate actually increased the [η] of GG compared to no added salt.

The observation of decreasing GG's [η] with low salt concentration may have one of two effects on entrainment for lubrication: the hydrodynamic radii of the random coil structure is reduced, thus entrainment might be assisted if the change in radii is significant compared with the surface roughness dimensions. However, the chain would adopt a more collapsed conformation, *i.e.* change shape, which may not align to the contact as well as a more expanded conformation polymer. Thus, the effect that intrinsic viscosity has on entrainment is not clear, and since alterations to solvent quality influence friction so

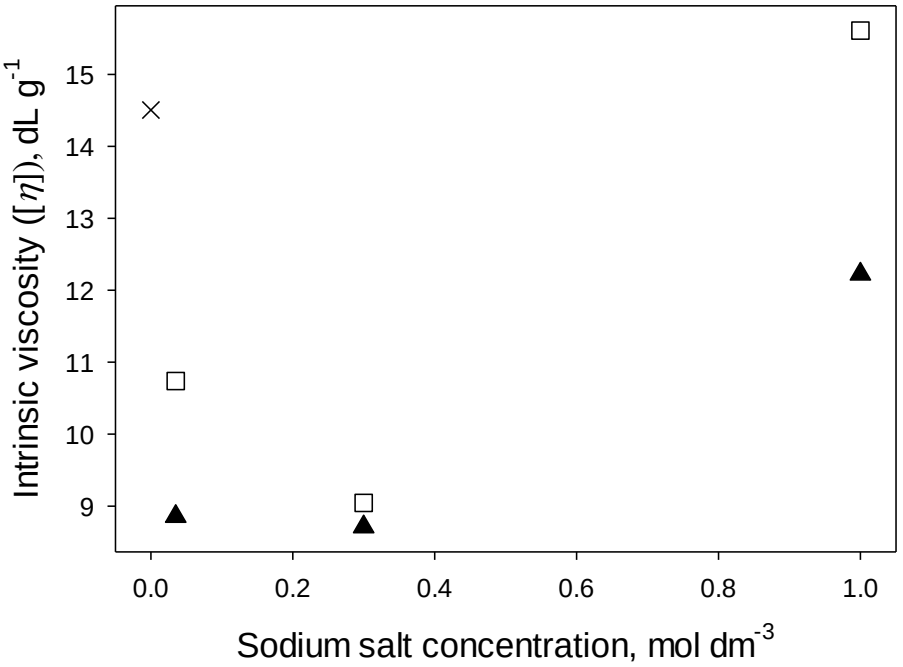

Fig. 5.16. Intrinsic viscosity of GG in water alone (×), and as a function of chaotropic (sodium iodide (▲)) and kosmotropic (sodium citrate (□)) concentration.

drastically (*i.e.* salt in water influences friction), it is difficult to elucidate. Nevertheless, the reduction of [η] with concentration of chaotropic and kosmotropic salts does not follow a monotonic trend with salt concentration and therefore the influence of solvent quality on GG's chain expansion is unlikely to explain the tribological behaviour which is monotonically dependent on salt.

The degree of GG adsorption to the elastomer surface was analysed as a function of salt type and concentration to test if it is the mechanism driving GG's reduced μ with salt. This test was achieved using contact angle studies. The elastomer surface is hydrophobic (θ = 106.52 °), but will become more hydrophilic as the amount of surface-adsorbed GG increases. Water contact angles are shown in Fig. 5.17 as a function of the salt type and concentration in 0.2 wt.% GG. It should be noted that submersion of elastomer surfaces to salt/water solutions, after the rinsing and drying process, did not influence the surface wettability. This indicates that the surface bound ions responsible for the lubrication of water/salt solutions do not have an affinity for the surfaces strong enough to withstand the rinsing step. Likewise, GG (0.2 wt.%) with no added salt did not influence the wettability of the elastomer surface which indicates that GG has a low surface adsorption affinity, as previously discussed.

The data in Fig. 5.17 demonstrates that the addition of salts to GG solutions results in a significant increase in surface wettability and therefore GG adsorption. Chaotropic and kosmotropic salts lower the contact angle continually with concentration (up to at least 1 M) where kosmotropic salts have a greater influence than chaotropic salts. This trend is very similar to that observed tribologically (Fig. 5.14) where the boundary friction of GG solutions decreased with salt concentration continually, and followed the Hofmeister series where kosmotropic salts lubricated more effectively than chaotropic salts. Therefore, GG surface adsorption seems likely to explain the observed tribological behaviour. This proposed

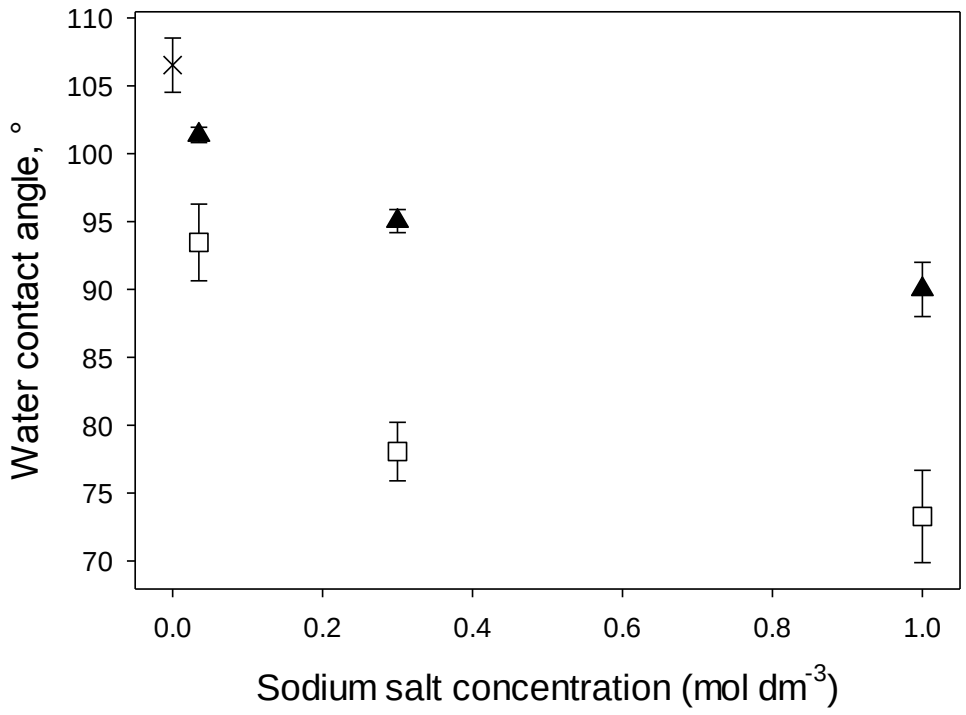

Fig. 5.17. Water contact angles of elastomer surfaces after immersion in 0.2 wt.% GG (×), and 0.2 wt.% GG with sodium iodide (▲) and sodium citrate (□).

mechanism for the lubrication of GG through surface adsorption with salts will now be discussed with reference to relevant literature.

Salt-promoted adsorption to surfaces is a well reported phenomena (Jerker, 1986); it is known to follow the Hofmeister series and is commonly observed during protein chromatography (Nishikawa and Bailon, 1975). The mechanism can be described using the hydration-shell hydrogen-bond model (Mancera, 1999). Mancera determined the Gibbs free energy of hydrogen bond formation to be positive between water molecules surrounding non-polar solutes. This promotes the non-polar solutes to aggregate in an effort to free water to the bulk, where hydrogen bonding is favourable (*i.e.* an enthalpic and entropic gain). This process is known as the hydrophobic effect and in salt solutions, the hydrogen bonds surrounding

non-polar solutes become even more unfavourable (greater enthalpies), thus increasing the driving force behind the hydrophobic effect.

Salt promoted adsorption of a polar polymer, poly (vinyl alcohol), onto a hydrophobic surface has also been observed (Kozlov *et al.*, 2003). Kozlov *et al.* tested polymeric adsorption using ellipsometry, surface roughness characterisations and contact angle studies, and determined that polymer-surface adsorption increased with salt concentration according to the Hofmeister series where chaotropic salts promoted some adsorption, and strongly kosmotropic salts showed the greatest effect. The correlation of adsorption data amongst the three techniques used also serves to verify the use of goniometry in this study for characterising polymer-surface adsorption.

To summarise the investigation carried out in this thesis into the effect of salt on GG solution lubricity: salt promotes the lubrication of GG solutions with a trend that is monotonic with concentration and significant for both chaotropic and kosmotropic salts, although the greatest effect is observed with kosmotropic salts. GG surface adsorption also follows the same trend with salts and so is expected to be the most significant mechanism promoting GG lubrication with salt. From the literature, GG adsorption seems likely to take place as a result of salts enhancing the hydrophobic effect. This creates surface bound hydrated polymers that are efficient at providing boundary lubrication.

5.4. Concluding remarks

With the significance of tribology in determining the oral perception of textural attributes, the role of food structure on tribological behaviour was investigated. Hydrocolloid solutions (with and without salt) were tested to represent simplified examples of liquid and semi-solid food types. From the results of these tests, it can be concluded that the structure of hydrocolloids (chain conformation and coil overlap behaviour) has a pronounced influence on tribology. Additionally, it can be concluded that salts influence boundary regime tribology as a result of forming surface-bound hydrated-ions, or, in the presence a polysaccharide, surface-bound hydrated-polymers, which act to provide lubrication.

The hydrocolloids used in this study were first analysed rheologically to characterise their coil overlap behaviour at low and high shear. It was determined that polymers with a random coil secondary structure retain their entanglements in concentrated solutions even at high shear rates. Conversely, under the same shear conditions, polymers with more expanded structures were shown to fully disentangle. This structurally attributable entanglement behaviour was then shown to influence tribology in a mixed regime of lubrication. Specifically, the entanglements of random coil structures restrict material entrainment to the contact zone for lubrication. Furthermore, in a boundary regime of lubrication it was shown that expanded chain conformation polymers are more preferentially entrained to the contact zone than random coil polymers due to their ability to align to the direction of flow.

Perhaps most importantly, the results described in this chapter demonstrate that the rheological behaviour of hydrocolloids does not necessarily correspond with their tribological behaviour and that their structures determine the response of both. This was most prominently demonstrated, firstly, with the presence of low kosmotropic salt concentrations having negligible impact on bulk rheology but significant tribological influence. And, secondly, an

incremental increase in polysaccharide concentration results in a continued increase in bulk viscosity for all polymer structures, but the effect of increased concentration on boundary friction is dependent on the conformation where friction is reduced with extended coil chains and increased with random coil polymers.

Chapter 6.

Tribology and rheology of hydrocolloid particulate fluid gels

6.1. Introduction

The aim of this chapter was to advance the understanding of both hydrocolloid tribology and fluid gel material properties. To do this, fluid gels were tested tribologically and rheologically as a function of particle stiffness and volume fraction. As discussed in the Literature Review (section 2.3.2), the volume fraction of suspensions controls their rheological behaviour with a dependence that can be used to characterise particle properties. Thus, the rheology of fluid gels as a function of volume fraction and particle stiffness, together with the findings from Chapter 4, will provide a comprehensive characterisation and understanding of their formation and material properties. Additionally, an understanding of the tribological behaviour of fluid gels is relevant for food systems with particulate or phase separated structures and so together with the findings in Chapter 5, will provide a detailed understanding of the influence of liquid and semi-solid food structures on lubrication.

The bulk of this Chapter is split into two main sections: fluid gel rheology and fluid gel tribology. Both sections characterise fluid gel properties as a function of their volume fraction and particle stiffness, although the aim of each section was very different. The aim of studying fluid gel rheology was to provide a comprehensive characterisation of κC fluid gel rheology and to advance the understanding of their behaviour and structures to allow for their incorporation into designed food formulation. The aim of characterising fluid gel tribology was to understand the tribology of particulate suspensions thus probing the influence of food structure on mouth-feel.

6.2. Fluid gel rheology

Having estimated the volume fraction of fluid gels produced with three κC concentrations (Chapter 4), their material properties on dilution were characterised using a

series of different shear and oscillatory rheological techniques to provide a detailed understanding of their behaviour. The results of this series of different rheological tests will progressively build a detailed characterisation and understanding of κC fluid gels. All fluid gel samples were sheared post-production, using an overhead stirrer, to break interparticle connections that may have resulted from quiescent ordering events.

6.2.1. Shear rheology

6.2.1.1. Shear viscometry

In order to characterise the rheological properties of fluid gels, their viscosities were investigated as a function of volume fraction for fluid gels with different particle stiffness's (*i.e.* produced from 0.5, 1 and 2 wt.% κC). To do this, flow curves were obtained from steady state flow experiments conducted in controlled stress mode. Results are shown in Fig. 6.1 (a) for fluid gels formed with 0.5 wt.% κC prepared at a range of dilutions with deionised water to control volume fractions, Φ_{FG}. The results shown are representative of the data obtained for all κC concentrations, that is, shear thinning over a broad range of volume fractions and a distinct yielding behaviour for samples with Φ_{FG} greater than about 0.2. The flow curves are typical for suspension rheology and can be fitted to the Cross model (Eq. 6.1) (Cross, 1965), as shown in Fig. 6.1 (b), where the same data as in Fig. 6.1 (a) is represented using shear rate ($\dot{\gamma}$) for the x-axis. Fitting the data to the Cross model allows zero and infinite shear viscosities (η_0 and η_∞, respectively) to be obtained, where *C* and *m* are Cross model constants.

$$\eta = \eta_\infty + \frac{\eta_0 - \eta_\infty}{1 + (C\dot{\gamma})^m} \qquad \textit{Eq. 6.1}$$

This procedure of fitting flow curves to the Cross model to identify η_o and η_∞ was repeated for fluid gels formed with 1 and 2 wt.% κC that were also prepared at a range of dilutions. This then allowed the influence of volume fraction and particle stiffness on fluid gel viscosity to be determined, as shown in Fig. 6.2 (a) for zero shear and Fig. 6.2 (b) for infinite shear viscosity. Fig. 6.2 (a) shows that fluid gel viscosities are strongly dependent on volume fraction with zero shear relative viscosities ~10^9 after production (apparent viscosity ~10^6 Pa s), a value typical for highly packed suspensions, *e.g.*, Flickinger and Zukoski (2002)). Before

(a)

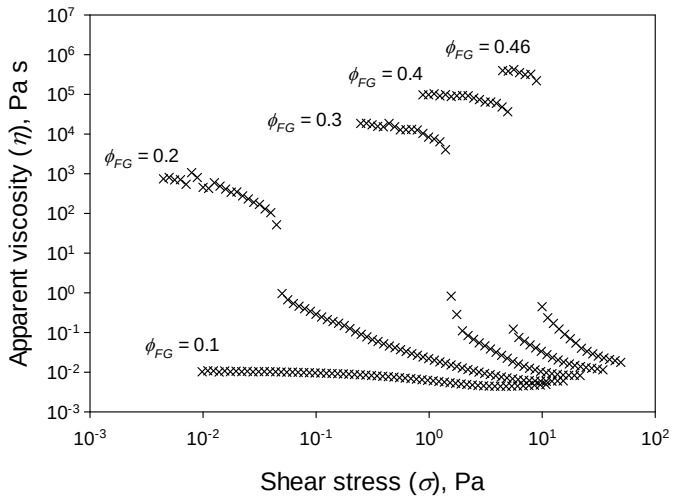

(b)

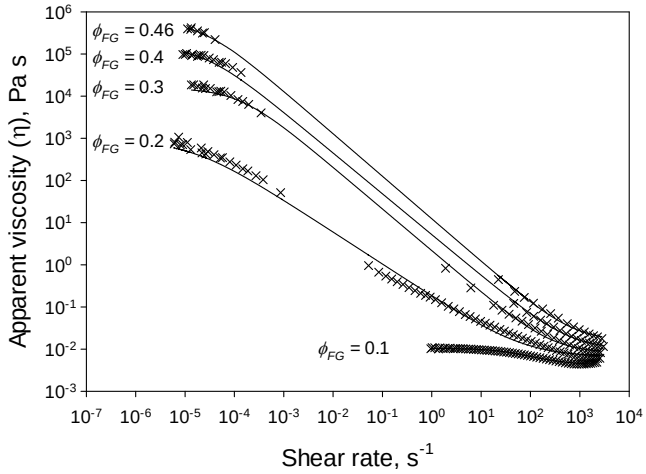

Fig. 6.1. Flow curves of fluid gels formed with 0.5 wt.% κC prepared at a range of dilutions. Data was collected in shear stress mode and is plotted as a function shear stress (a) and shear rate (b) where lines represent fits to the Cross model.

(a)

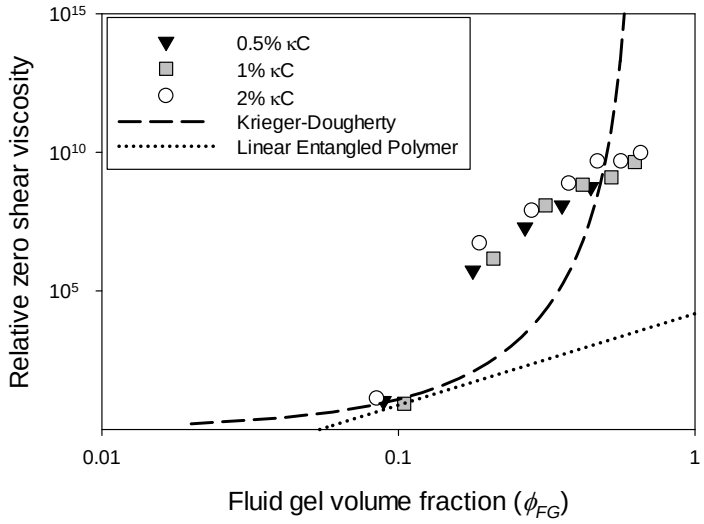

(b)

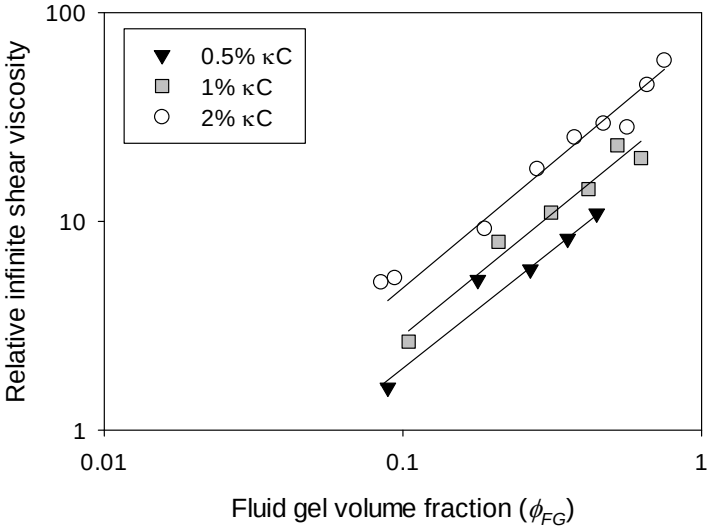

Fig. 6.2. Fluid gel volume fraction (Φ_{FG}) dependence on relative zero (a) and infinite (b) shear viscosity. Fits to the Krieger-Dougherty equation are shown assuming [η] = 23 dL g^{-1} and Φ_m = 0.64, and a power law dependence with exponent 3.4 is shown to model linear entangled polymers (a). Power law fits are also shown for the high shear data (b) with exponents of 1.17.

providing an explanation for the observed η_o trends, the high shear viscosity data will be discussed.

On increasing the concentration of κC used to form the fluid gels, the infinite shear viscosities became greater at each volume fraction (Fig. 6.2 b). This observed viscosity dependence on κC concentration can be explained by differences in deformability of the particles. Under high shear conditions the particles within the fluid gel samples are able to

move past one another and are deformed under the applied stress. Fluid gels produced with greater polymer concentrations produce less deformable particles (Chapter 4.3.3) which has the effect of increasing high shear viscosities, which was also observed with agarose microgels produced at a range of polymer concentrations using the w/o emulsion route (Adams *et al.*, 2004).

Coming back to the zero shear viscosity data presented in Fig. 6.2 (a), available models for describing viscosities of suspensions and linear polymer thickeners seem unsuitable for the behaviour of the κC fluid gels. One would typically expect the viscosities to asymptote to infinity as close packing fractions are approached (as modelled by Krieger-Dougherty, KD), a behaviour which is observed for uniform-microgel particles prepared with agarose (Adams *et al.*, 2004), and, indeed, kappa carrageenan (Frith and Norton, 2000). Therefore, there is a clear disparity in the rheology of kappa carrageenan gelled particles produced *via* sheared gelation (fluid gels) and those formed *via* the w/o emulsion route (uniform-microgels). This is despite the fact that both systems have equivalent components, that is, aqueous gelled carrageenan particles suspended in an aqueous medium. Since the fluid gel particles produced here are spherical, as are uniform-microgels, it seems that the viscosity dependence on Φ_{FG} is not due to particle shape so much as internal structure. This hypothesis will now be explored by discussing the internal structures of particles produced *via* the w/o route, and then sheared gelation.

A gelling biopolymer aqueous phase dispersed in oil, heated to above its gelation temperature, will produce, under shear, droplets with a relatively uniform internal polymer distribution and a distinct boundary between the droplet edge and the continuous oil phase due to the poor miscibility, or, high interfacial tension, at the oil/water interface. After cooling to allow droplet gelation and separation from the oil phase by aqueous dilution and

centrifugation, the resulting ‘hard sphere’ particles have a relatively uniform polymer density distribution throughout and a ‘hard edge’, or, distinct particle/continuous phase interface.

On sheared gelation, the fluid gel production process begins with the nucleation of gel particles which are segregated by the applied shear (Norton *et al.*, 2000). The nuclei then grow (Norton *et al.*, 1999) whereby non-gelled polymer chains in the continuous phase may contribute to the helix formation propagating from the nuclei (as well as coalescence and bridging events). During this process, the interfacial tension between the gelled and non-gelled carrageenan aqueous phases will not be sufficient to provide a hard edge and so the polymer density distributions will not be uniform within particles, rather, the polymer density is expected to tail-off progressively from the centre of particles to their surfaces.

Thus, the formation process of κC fluid gels is expected to produce ‘soft edge’, or, ‘hairy’ particles that are largely responsible for the viscosity data in Fig. 6.2 (a), which shows a clear disparity to κC uniform-microgels that behave similarly to hard spheres. The suggestion of κC fluid gels having hairy structures supports the findings in Chapter 4 (Formation and characterisation of fluid gels) which determined fluid gel particles to have fewer helical regions (*i.e.* a greater amount of polymer in the coil state, thus constituting ‘hairs’) than quiescently cooled gels due to the applied shear interfering with the molecular ordering process. It is worth noting that the agarose fluid gels prepared by Norton *et al.* (1998 and 1999) did follow the KD model because those particles were not ‘hairy’ after production since the applied shear during formation did not reduce the number of helical residues. Furthermore, a ‘hairy surface’ of the κC fluid gel particles was suggested from the fact that stopping the shearing process partway through cooling acts to bridge neighbouring particles together by allowing surface polymer chains, or ‘hairs’, to order between particles (Chapter 4.5).

In order to explain the observed η_o trends with Φ_{FG}, the Krieger-Dougherty equation will now be examined along with examples of similar rheological behaviour that were discussed in the literature review, section 2.3.2). The Krieger-Dougherty (KD) equation (Eq. 6.2) can be used to describe the dependence of the viscosity of suspensions upon their particle

$$\eta_{rel} = \left(1 - \frac{\Phi}{\Phi_m}\right)^{-[\eta]\Phi_m} \qquad \textit{Eq. 6.2}$$

volume fraction (Krieger and Dougherty, 1959) where, for hard spheres, the maximum volume fraction, Φ_m, is 0.64 and the intrinsic viscosity, $[\eta]$, is 2.5 dL g^{-1}. In soft microgel systems an effective volume fraction term, $\Phi_{eff} = kc$, can be used where c is the solid (dried) mass concentration of particles and k denotes particle specific volume. Φ_{eff}'s can then be calculated from fits to the modified KD equation (Eq. 2.7) which was achieved for agarose uniform microgels (that data is shown in the Literature Review, Fig. 2.11, page 29).

The data in Fig. 6.2 (a) cannot be fitted to the KD equation since the gradient does not progressively increase, which is required in the model, indicating that close packing behaviour is not approached. The observed viscosity increase is, however, with a greater concentration dependence than expected for linear entangled polymers which would have a power law dependence with exponent ~ 3.4 (Ferry, 1980; Morris *et al.*, 1981). Therefore, it is clear that the gelled structures have not unravelled to become linear chains after dilution. The value of Φ_m, in the KD model, is known to increase with polydispersity and particle deformability (Adams *et al.*, 2004); however, increasing the value of Φ_m still doesn't allow fits to KD for the κC fluid gels because the viscosities do not asymptote. This behaviour was also noted on analysis of polyacrylamide-based particles produced from emulsion polymerisation (Omari *et al.*, 2006) where the KD fit became increasingly worse at describing the behaviour as the crosslink density was reduced (this data shows a strong resemblance to

that here in Fig. 6.2 (a) and is displayed in the literature review - Fig. 2.12 (a), page 30). Omari *et al.* suggested that their observed behaviour was due to a progressive transition existing between entangled polymers and hard-spheres as the cross-link density of the particles is increased. There is also a strong resemblance in the η_o versus Φ_{FG} trends shown here with those of Senff and Richtering (2000) on the same polyacrylamide-based microgels formed with a very high cross-link density. In their study, the deviation from hard-sphere behaviour at high cross-link concentrations was attributed to the cross-linker having a greater polymerisation rate than the monomer, which in high relative concentrations has an effect of forming inhomogenous networks with the cross-linker concentration varying from particle centre to edge (Duracher *et al.*, 1999). This formed 'star-like microgels' with a highly cross-linked core and long polymer chains at the surface (this data is also displayed in the literature review - Fig. 2.12 (b), page 30)).

The similarity of the viscosity data in Fig. 6.2 (a) to low cross-link density particles (Omari *et al.* 2006) and tailing off polymer density particles (Senff and Richtering *et al.* 2000) suggests that the κC fluid gels behave rheologically as starlike, or, soft edge, microgel particles with structures lying between that of linear polymers and hard spheres. These structures would then be expected to allow particle compression and interpenetration (or particle overlap) to occur to an extent such that close packing behaviour is not observed.

The κC fluid gel viscosity data in Fig. 6.2 (a and b) is presented with confidence because, as mentioned in the Materials and Methodology chapter, the viscometry trends were verified by repeating tests numerous times using several geometries including roughened parallel plates and a cone-and-plate, using controlled rate and controlled stress tests, and by using data from ramped-down as well as ramped-up shear profiles.

6.2.1.2. Intrinsic viscosity

The intrinsic viscosity of linear polymers is a function of molecular weight and chain conformation, whilst for hard sphere particles the Einstein theoretical value is 2.5, as often used in the KD equation. Therefore, to probe the specificity of the tendency for fluid gels to act as polymers and particles, their intrinsic viscosities ([η]) were calculated by rheological analysis at dilute volume fractions ($\Phi_{FG} < 0.1$). The [η]'s were calculated empirically from viscosity measurements of dilute samples whose mass concentration was determined by gravimetric analysis after drying in a vacuum oven. Fits to the Huggins equation are shown in Fig. 6.3 where the reduced viscosity at infinite dilution (intrinsic viscosity) is obtained from the y-axis intercept. [η] values are 14, 19 and 23 dL/g for fluid gels prepared with 0.5, 1 and 2 wt.% κC, respectively.

Thus, the fluid gel [η] values are greater than 2.5 and increase with κC concentration.

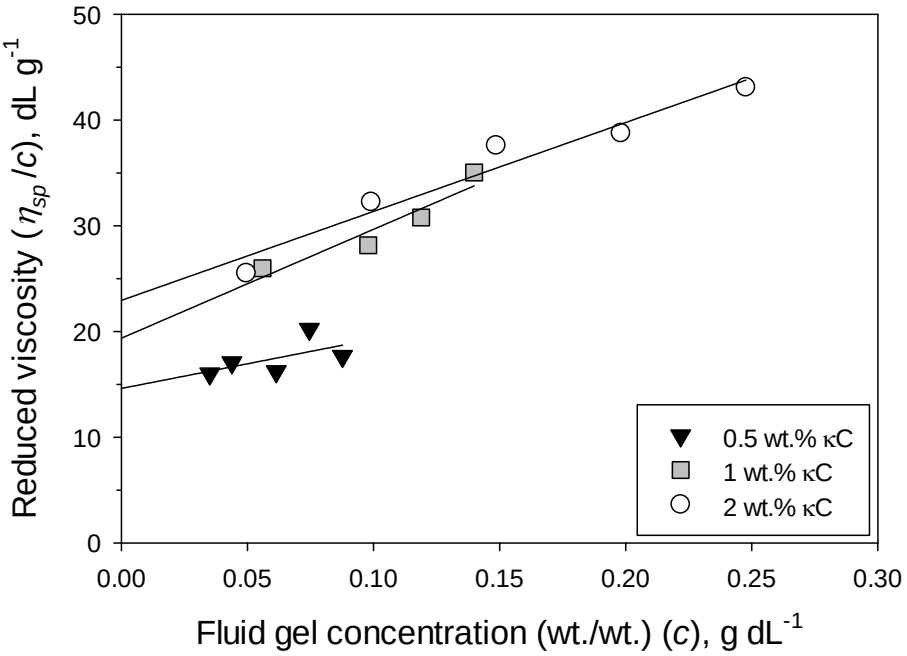

Fig. 6.3. Determination of fluid gel intrinsic viscosities from fits to the Huggins equation. When data is fitted to this equation, the intercept at the y-axis gives the intrinsic viscosity ([η]).

It has been shown that decreasing particle crosslink concentration increases [η] due to increasing particle deformability and a tendency towards linear polymer behaviour (Omari *et al.*, 2006; Wolfe and Scopazzi, 1989). Thus, the fluid gel [η] data supports their particle structures as being hairy since they have linear polymer tendencies.

Unravelling of the κC particles on dilution was not observed and nor was it expected given that it was not the case with agarose fluid gels, however, since the κC particles contain K^+ and were diluted with deionised water, it is perhaps necessary to clarify evidence indicating this:

- Microscopy was conducted on particles diluted with deionised water and clearly revealed the presence of particles (Fig. 4.7).
- The η_0/Φ_{FG} gradient is greater than expected for linear polymers.
- There was no change in the rheological properties of diluted fluid gels in the time from initial dilution to over 3 month's storage.
- Quiescently cooled κC gels stored in deionised water revealed no change in mechanical properties throughout more than 3 months of storage.
- The DSC studies (Chapter 4.3.2) were conducted on non-diluted κC fluid gels, thus indicating that the 'hairiness' results from disrupted molecular ordering by the applied shear, rather than from their dilution.

6.2.1.3. Thixotropy

Thixotropy tests can describe a materials time dependent rheological properties. This can be particularly insightful for suspensions that display interparticle ordering or aggregation. Thixotropy was measured in this work by conducting 'thixotropic loops' where the shear rate is ramped up, held constant, and then ramped back down constituting one sweep. A rest period is then endured and the process is repeated for a second sweep. This shear analysis is shown in Fig. 6.4 for fluid gels prepared with 0.5 and 2 wt.% κC at $\Phi_{FG} \sim 0.3$. Both fluid gels revealed a thixotropic behaviour since a hysteresis is displayed between tests ramping up and down, and between the first and second sweeps. This indicates a time dependant behaviour where the rate of structure breakdown is greater than that of rebuilding and where only partial recovery occurs during 10 min rest periods. The thixotropy is likely to be due to particle aggregation (or flocculation) caused by long-range inter-particle

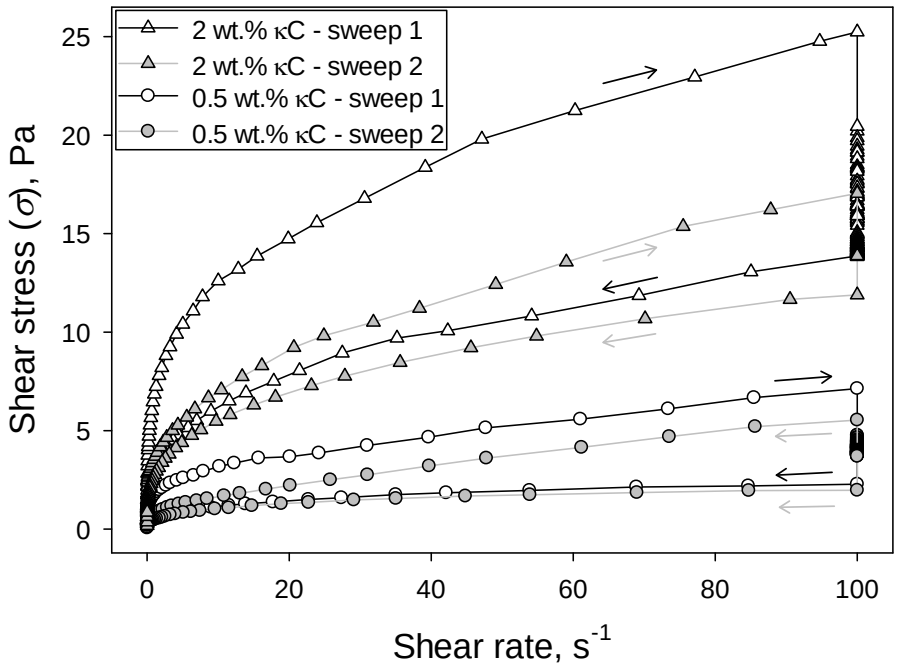

Fig. 6.4. Thixotropic loops for fluid gels prepared with 0.5 and 2 wt.% κC diluted to $\Phi_{FG} \sim 0.3$. Details on the procedure are described in Materials and Methodology, Chapter 3.4.9.4. Arrows indicate the direction of increasing and decreasing shear rate (ramping shear rates up or down).

ordering - a behaviour that was not observed for agarose fluid gels (Frith *et al.*, 2002). The fact that the κC fluid gels display thixotropy, whilst agarose fluid gels don't, suggests that fluid gel particle structures are responsible for determining their aggregation. Aggregation may result from particle charges (κC is polyanionic whilst agarose is neutral) or from interparticle entanglements (κC fluid gels are hairy whilst agarose are not) and warrants further investigation. To probe particle aggregation further, oscillatory rheological techniques were employed to identify the influence of particle stiffness and Φ_{FG} on the viscoelastic response, where elastic dominated behaviour is expected only at volume fractions exceeding close packing, or if an aggregated network is present. The results of oscillatory rheological tests are discussed in detail in the following section.

To summarise the rheological characterisation of κC fluid gels thus far, the incomplete molecular ordering during particle formation (which was determined from DSC studies, Chapter 4.3.2) gives the fluid gels a degree of linear polymeric tendency which prevents close packing behaviour on increasing phase volume.

6.2.2. Oscillatory rheology

Oscillatory rheology was considered for fluid gels to characterise their behaviour and also to probe particle structures and interactions. This was achieved from three investigations:

1. Storage moduli values were obtained, for the same range of fluid gels that were tested in the previous section, for analysis of its dependence on particle stiffness and packing fraction. This allowed particle properties to be probed by comparing the data with that from the models described in the Literature Review.
2. The particle volume fraction and stiffness required for an elastic response was identified to explore particle flocculation further.
3. Deformations required to initiate fluid gel flow were identified to probe the strength of the aggregates.

These tests, and their results, will now be described and explained in turn.

Dependence of storage modulus on particle stiffness and volume fraction

Fig. 6.5 shows the dependence of storage modulus (G') on Φ_{FG} and κC concentration, where data was taken at 0.1 Hz from frequency sweeps within linear viscoelastic regions (LVR). G' can be observed to increase with increasing κC concentration, an effect resultant from stiffer, less deformable, particles which was also demonstrated from the high shear viscosity plots (Fig. 6.2 (b)). However, the storage modulus is more strongly influenced by Φ_{FG}, a behaviour that fits well to a power law model with exponent 7 ($G' \sim \Phi_{FG}^{7}$). The same fit has previously been observed for soft microgel particles (Koumakis *et al.*, 2012) (data from that study is displayed in the literature review - Fig. 2.13 page 32) providing a strong indication that the fluid gels behave as a suspension of soft particles (rather than the other fundamental forms of particles described by Koumakis: hard spheres and ultra-soft micelles).

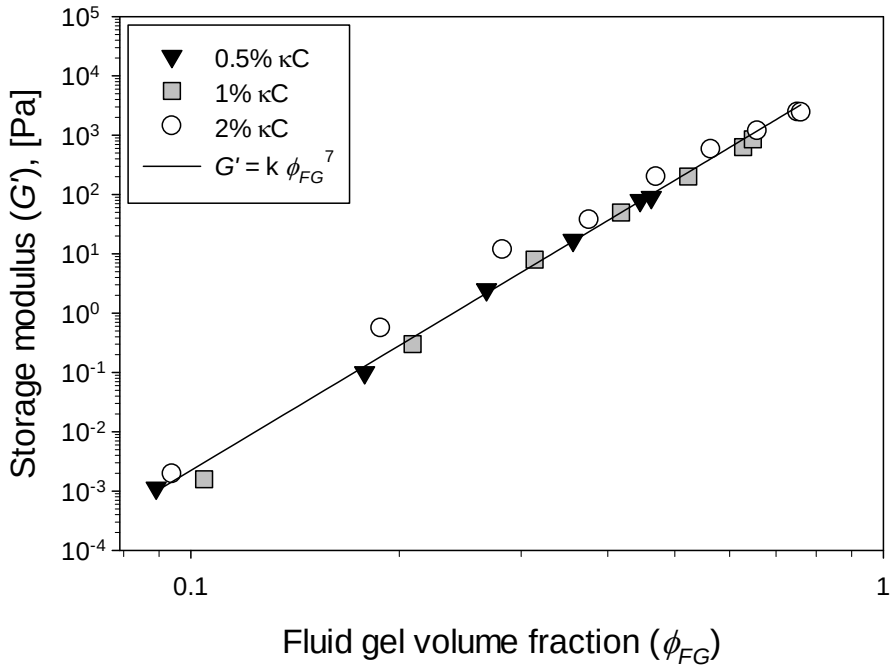

Fig. 6.5. Storage modulus at 0.1 Hz and within the LVR, as a function of Φ_{FG} for fluid gels prepared with 0.5, 1 and 2 wt.% κC. The straight line indicates a fit to $G' = k\,\Phi_{FG}^{7}$, where k is an arbitrary constant.

The fact that the particles are characterised as 'soft' provides further rationale for their deviation from hard-sphere behaviour that was described in the previous section (6.2.1).

Viscoelastic response

$\delta = \tan^{-1}(G''/G')$ values were evaluated, as a function of Φ_{FG}, to identify the onset of the elastic dominated response where $G' > G''$. Results are plotted in Fig. 6.6 where a dashed line is shown at $\delta = 45°$ to represent where $G' = G''$. Elastic dominated responses are observed with Φ_{FG}'s greater than ~ 0.3 which is lower than random close packing (RCP) which is ~ 0.64 for mondisperse hard spheres. The fact that there is an elastic dominated response at $\Phi_{FG} \sim 0.3$ suggests that particle interactions occur at low phase volumes which is in agreement with their thixotropic behaviour that was also observed for $\Phi_{FG} \sim 0.3$. Elasticities at low volume fractions have been reported for agarose fluid gels (Frith *et al.*, 2002) where the anisotropic particles allowed interactions and the formation of percolated networks at

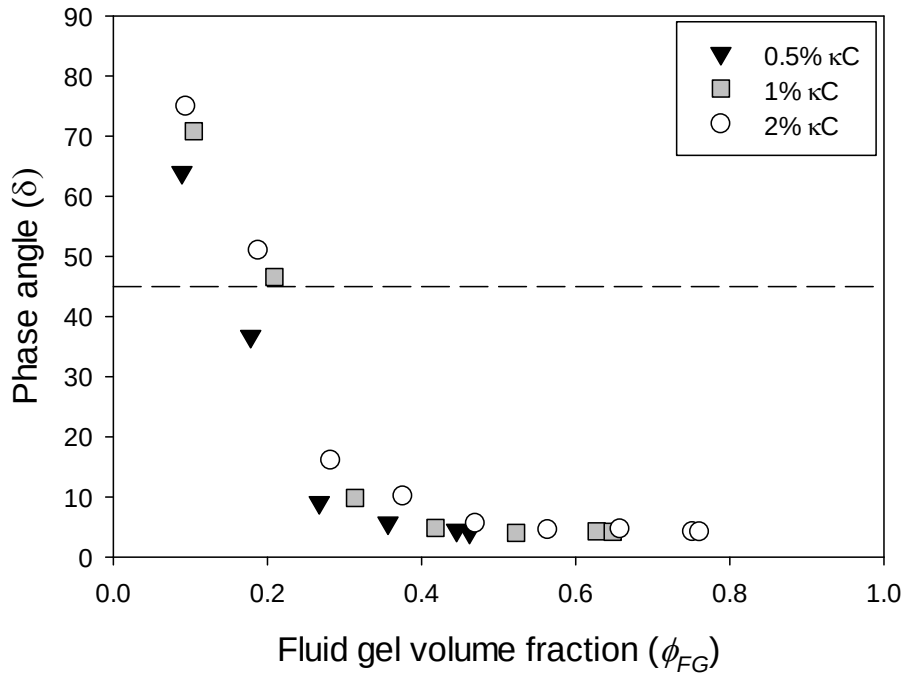

Fig. 6.6. Phase angle [$\delta = \tan^{-1}(G''/G')$] at 0.1 Hz and within the LVR, as a function of Φ_{FG} for fluid gels prepared with 0.5, 1 and 2 wt.% κC. The straight dotted line indicates where $\delta = 45°$, that is, where G' = G", thus representing the boundary between viscous (> 45°) and elastic (<45°C) dominated properties.

phase volumes lower than required for spherical particles; however, the agarose fluid gel particles were demonstrated to be non aggregated since they displayed no thixotropy. Anisotropy cannot be responsible for the elasticity observed here since the hydrated κC particles were shown to be spherical from optical microscopy. Thus, from the thixotropy and oscillatory rheological data, it can be determined that the κC fluid gel particles form percolated networks which are aggregated and require time to form; this behaviour is consistent with the 'hairy' particle model whereby penetrable chains form entanglements between neighbouring particles.

Strength of particle aggregates

The particle structures and interactions were further probed from strain sweep tests, at 1 Hz, where deformations required for flow can be examined. Fig. 6.7 shows normalised strain sweeps where the strain initiating flow (indicated by vertical lines on the figure, characterised by a 5% reduction in *G*') can be observed to increase with particle deformability, that is, softer particles deform to greater strains before flowing. Once flow is initiated, the particles with higher κC concentrations have a weaker dependence on strain (*i.e.* the curves become more horizontal with κC concentration). This behaviour is in contrast to that of uniform agarose microgels which demonstrate a stronger dependence on strain, after flow, on increasing agarose concentration. This behaviour of the κC fluid gels implies that increasing biopolymer concentration results in enhanced interparticle structuring and a

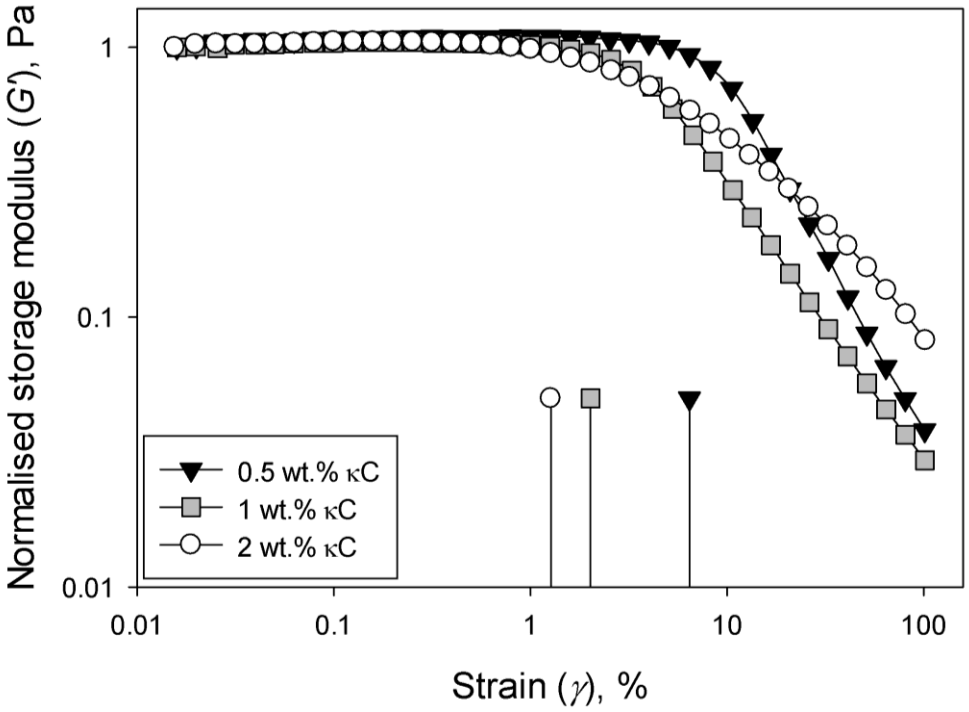

Fig. 6.7. Normalised storage modulus as function of applied oscillatory strain at 1 Hz for fluid gels prepared with 0.5, 1 and 2 wt.% κC, each diluted such that Φ_{FG}~0.4. Vertical lines indicate the strains at which the normalised G' plateau value decreases by 5%, thus suggesting a degree of fluid 'flow'.

tendency towards linear polymer behaviour which complements the observed increase in [η] with κC concentration. Thus, interparticle interactions provide percolated networks and therefore elasticity, even at low volume fractions, and those interactions take time to form and are most significant on increasing the linear polymer tendencies of the particles.

The final rheological test discussed in this section, is that on samples that were prepared by mixing particles of differing stiffness's. This experiment was conducted to identify the contribution of both stiff and soft particles to the rheology of fluid gels. Stress sweeps were employed for this test since they can provide both storage moduli and yield stress data from single experiments. Fig. 6.8 shows stress sweep data for a series of fluid gels varying in κC concentration (0.5, 1 and 2 wt.%) and a sample composed of a 1:1 mixture of fluid gels prepared from 0.5 and 2 wt.% κC (all samples were subjected to the same mixing procedure to eliminate the influence of pre-shear on rheological properties). It can be observed that increasing κC concentration has the effect of increasing *G*' and yield stress (the

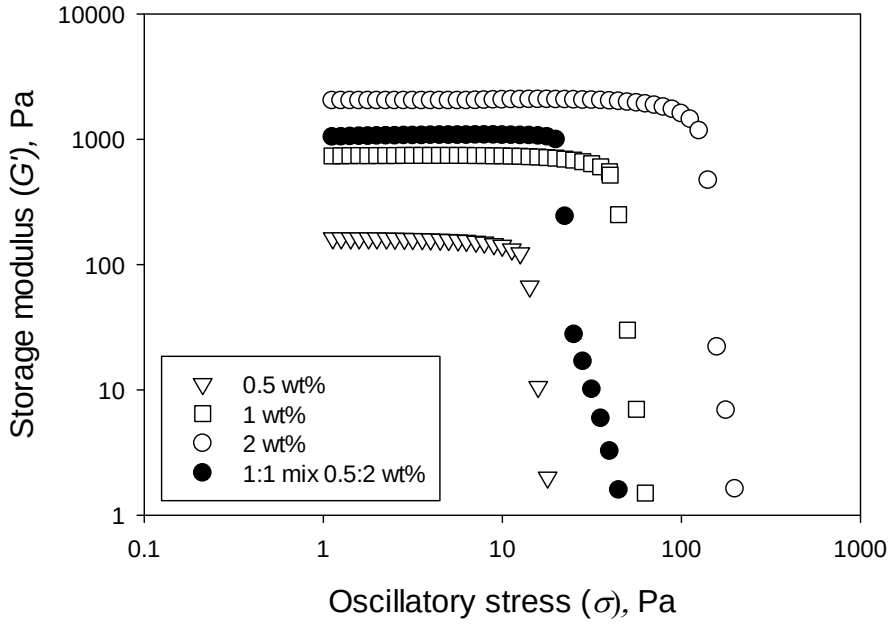

Fig. 6.8. Stress sweeps at 1 Hz for fluid gels prepared with 0.5, 1 and 2 wt.% κC. A stress sweep is also shown for a sample prepared from a 1:1 mix of 0.5 wt.% and 2 wt.% fluid gels.

latter can be inferred from the stress at which *G*' significantly reduces). The sample prepared from a mixture of different particle deformability's (black symbols on Fig. 6.8), however, shows a relatively high *G*' plateau and low yield stress. Thus, the elastic modulus of the mixed sample seems to be dominated by that of the stiffer particles, whilst the deformable particles act as fracture sites allowing the material to flow at low stresses. This ability to independently manipulate storage moduli and yield stresses by creating mixtures of particles with different physical properties can provide specific material responses and has previously been exploited (Bialek *et al.*, 1999). This technique of mixing particle stiffness's may be used to design structured fluids with a 'creamy' perception which has previously been associated with products that have a high storage modulus and low yield stress (de Wijk *et al.*, 2006) (de Wijk, Prinz, & Janssen, 2006).

The rheology of κC fluid gels characterised in this section has shown the particulates to form aggregated percolated networks at low volume fractions and to have linear polymer tendencies. This behaviour is hypothesised to arise from incomplete helix formation during gelation, which occurs for κC as a result of its slow gelation rate causing the applied shear to have a strong interference with the molecular ordering process.

6.3. Fluid gel tribology

The tribology of fluid gels was studied to complement the work in Chapter 5 which described the influence of the structure of polymeric thickeners on friction. This was assessed by obtaining Stribeck curves for the same range of fluid gels tested rheologically in the previous section (6.2). The tested range then allowed the influence of particle stiffness and volume fraction on lubrication to be explored. Fig. 6.9 shows Stribeck curves for a HL-PDMS tribopair lubricated with water and a selected range of the data obtained for the fluid gels. All the samples displayed boundary and mixed regimes and for 2 wt.% κC, a hydrodynamic regime begins at high speeds. In contrast to the tribology of agarose fluid gels (Gabriele *et al.*, 2010), the mixed regimes here do not show an increase in μ with U, or a 'bump', and have superimposable data from ramping speeds up and down. Gabriele *et al.* attributed their

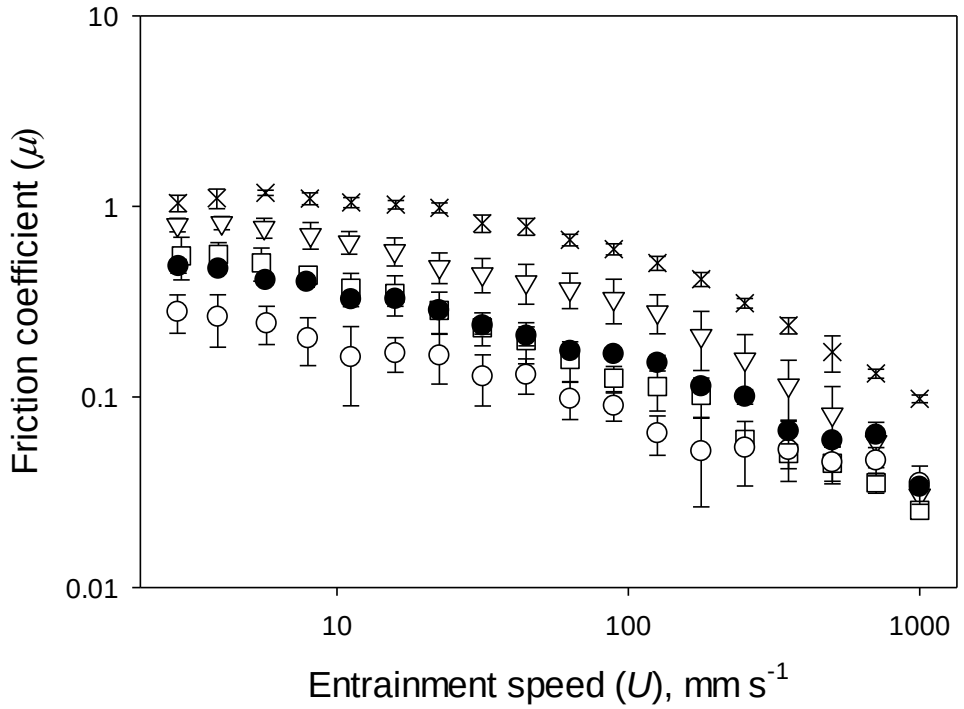

Fig. 6.9. Stribeck curves for HL-PDMS tribopair lubricated with water (×), fluid gels prepared from 0.5 (▽), 1 (□) and 2 wt.% κC (○) at their production volume fractions (see Table 4.1) and for a 2 wt.% κC fluid gel with Φ_{FG} ~ 0.4 (●). The data in this graph represents only a selection of the entire range of fluid gels tested.

observed increase in μ with U to particle exclusion of the ~ 100 μm particles from the ball and disc contact (see literature review, section 2.4.6). The data presented in Fig. 6.9, however, suggests particle entrainment to the ball and disc contact because the Stribeck curves are of typical shape without a 'bump' and, additionally, because increasing the number of particles (Φ_{FG}) and their stiffness's reduces the friction coefficients below the values obtained for the solvent (water) alone. Given that the fluid gel particle sizes (Table 4.1, page 109) are able to fit within the surface asperities (Fig. 3.10, page 87), particle entrainment at all speeds seems reasonable.

The tribology of the κC fluid gels was explored further by analysing the entire data set of boundary friction coefficients (at U = 3 mm s^{-1}) from the Stribeck curves obtained as a function of Φ_{FG} and particle stiffness; the results of which are shown in Fig. 6.10. There are two notable features of this Figure. Firstly, the data shows that boundary friction continually

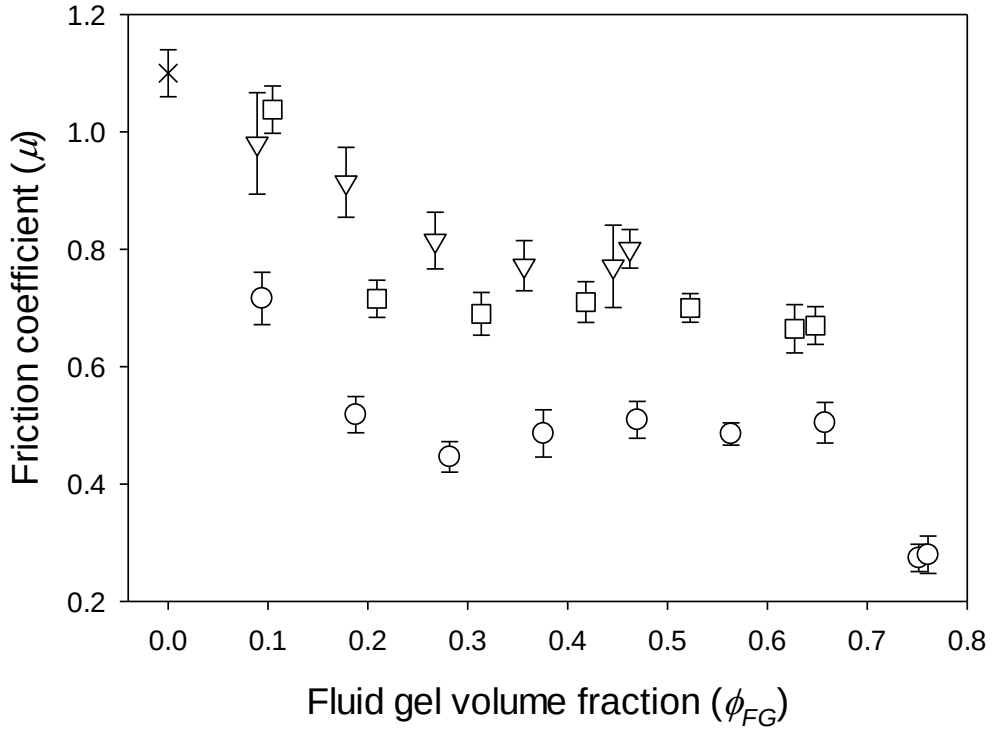

Fig. 6.10. Boundary friction coefficient (U = 3 mm s^{-1}) for κC fluid gels as a function of Φ_{FG} and particle stiffness. Data is shown for water (×) and fluid gels prepared from 0.5 (▽), 1 (□) and 2 (○) wt.% κC and represents the entire range tested.

reduces with increasing number of particles until reaching a plateaued effect from ~ 0.3 < Φ_{FG} < ~ 0.6; a further reduction in friction then occurs at Φ_{FG} > ~ 0.7. Secondly, it can be observed that over the range of volume fractions tested, increasing κC concentration, which increases particle Young's modulus, has an effect of reducing boundary friction. Explanations for these two observed trends will now be provided, in turn.

The plateau in boundary friction between Φ_{FG} ~ 0.3 and ~ 0.6 is despite the significant increase in viscosity (Fig. 6.2) and storage moduli (Fig. 6.5) that develop throughout this volume fraction range. The dependence of boundary lubrication on volume fraction, therefore, seems related to the number of particles within the contact, rather than particle-particle interactions or bulk rheological properties. It would then follow that the number of particles within the contact increases throughout the range 0 < Φ_{FG} < ~ 0.3, remains unaffected between ~ 0.3 < Φ_{FG} < ~ 0.6, and then at Φ_{FG} > ~ 0.7 a multiple particle entrainment mechanism allows numerous 'layers' of closely packed particles to entrain. This proposed

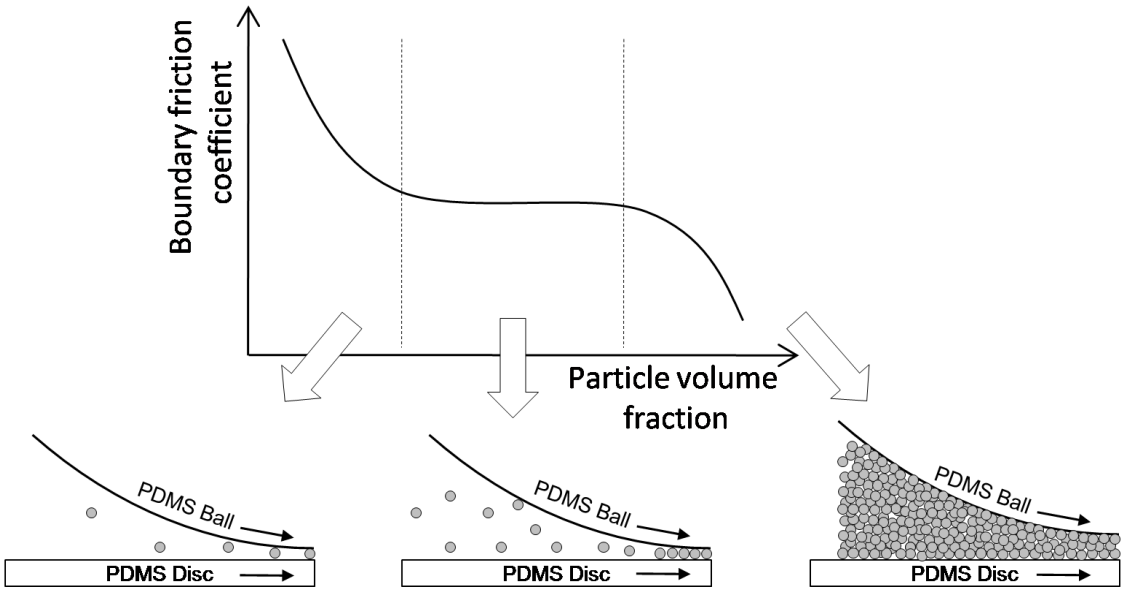

Fig. 6.11. Schematic representation of the particle entrainment at three distinctive regions of boundary friction coefficient with varying Φ_{FG}. Initially μ decreases with Φ_{FG} as the number of particles in the contact increases. Then, a plateau region occurs where changes in Φ_{FG} only influence the bulk and not the contact zone. Finally, at high volume fractions, multi-layer particle entrainment occurs.

mechanism is depicted schematically in Fig. 6.11.

Throughout the volume fraction range ~ 0.3 < Φ_{FG} < ~ 0.6, there is an effect of reducing boundary friction with increasing particle stiffness. This is despite the fact that the bulk rheology at rest (η_0 and G') shows a strong dependence on Φ_{FG}, due to particle interconnectivity, and a comparatively weak dependence on κC concentration through the same range (the influence of κC concentration was shown to be apparent under shear, *e.g.* η_∞, when the particle interactions are broken). Increased lubrication with particle stiffness is expected to be because the resistance of the particles to a compressive force influences friction, where greater particle Young's moduli reduce contact between the ball and disc, for a given normal load, and therefore reduce the sliding friction coefficient.

The implications of reduced friction on increasing particle stiffness will now be discussed. Whilst an increase in particle elasticity reduces boundary friction, particle detection on oral mucosa will occur on consumption of very stiff particles (particle detection is known to increase with particle material properties *e.g.* hardness (Tyle, 1993)). Additionally, as the hardness of the particles exceeds that of the ball and disc, three-body-abrasion will occur resulting in surface wear (Tylczak, 1992). Thus, the effect of reducing boundary friction with increasing particle stiffness is likely to occur only until the particle properties become similar to that of the rubbing bodies, which will depend on the use *e.g.* skin-creams, foods or mechanical parts.

6.3.1. Effect of normal load on boundary friction

To identify the contact mechanics of the fluid gel lubricated boundary regime, Stribeck curves were obtained at a range of normal loads (W) for deionised water and fluid gels prepared from 0.5, 1 and 2 wt.% κC. From these Stribeck curves, F_t (at $U \sim 3$ mm s^{-1}) was plotted as a function of W for each lubricant and is shown in Fig. 6.12. The water lubricated contact shows friction following a $W^{2/3}$ dependence, as expected for the highly compliant surfaces. The three fluid gel particulate suspensions, however, follow a linear dependence on W which is in contrast with the behaviour of κC as a non-gelled linear polymeric thickener which followed a $W^{2/3}$ dependence (see Fig. 5.7 in Chapter 5.2.2.1.1, page 130).

Before providing an explanation for the two trends of F_t/W data observed with κC as a polymeric and particulate thickener, the mechanistic cause of linear (W^1) and $W^{2/3}$

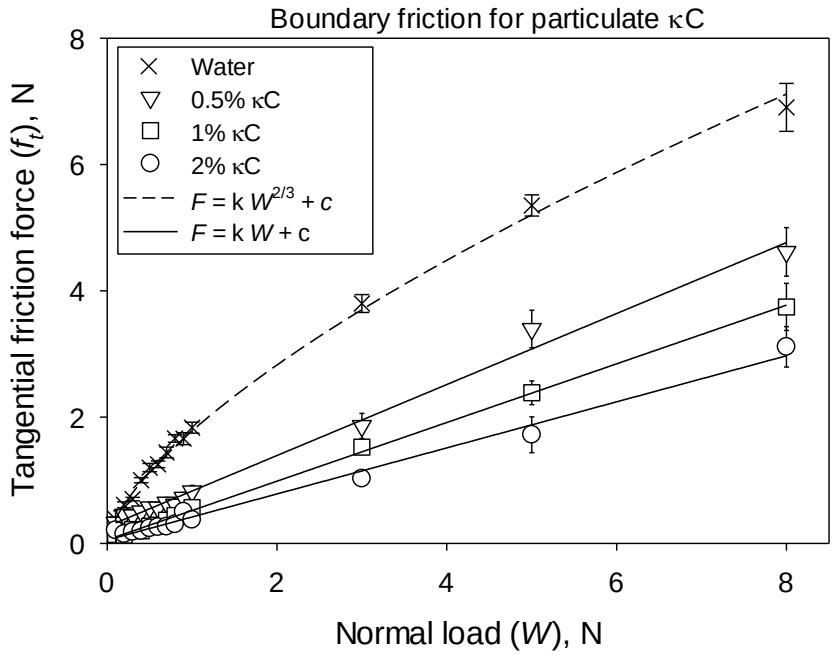

Fig. 6.12. The dependence of friction force on normal load for deionised water (×) and fuid gels prepared from 0.5 (▽), 1 (□) and 2 (○) wt.% κC.

dependencies will be discussed from a contact mechanics basis.

As discussed in the Literature Review and Chapter 5, an F_t dependency on $W^{2/3}$ is typically observed in soft surface tribometry (Myant *et al.*, 2010; Stokes *et al.*, 2011) and is due to the highly compliant surfaces providing a fixed number of contacts deforming elastically under load. Those contact sites have a contact area that increases with load proportionally to $W^{2/3}$ which is predicted by Hertz theory (Hertz, 1881); and since the friction force is known to be directly proportional to the real contact area (Ludema, 2001; Bowden and Tabor, 1954) it follows that F_t is proportional to $W^{2/3}$. For non-compliant surfaces (*e.g.* steel on steel), this behaviour is observed when there is a single asperity contact (and, therefore a fixed number of contact sites), such as that observed during friction measurements of an Atomic Force Microscope (AFM) (Szlufarska *et al.*, 2008). For multiple asperity non-compliant ('real') contacts, the contact area increases linearly with W due to an increasing number of asperity-contacts with increasing load (Archard's law); as observed experimentally and theoretically by Greenwood and Williamson (1966).

Transitions between linear and $W^{2/3}$ behaviour have been reported in AFM studies as wear modifies multiple-asperity contacts to single-asperities (Reitsma *et al.*, 2006) and for rough tips behaving as single-asperity contacts when contamination fills the voids between the mating surfaces (Putman *et al.*, 1995); this demonstrates that the contact type can be identified from the dependence of F_t on W.

An explanation for the linear dependence with the particulate fluid gel lubricants is that the system follows Archard's law (1957) where a load dependent number of contact sites mechanism prevails. In this model, increasing the normal load deforms the asperity contacts thereby allowing the fluid gel particles between neighbouring asperities of the same surface (which would be allowed given the PDMS ball and disc surface roughness's) to make contact

with the opposite surface, thereby increasing the number of contacting sites. Thus, in summary, κC as a polymeric thickener displays an F_t dependency of $W^{2/3}$ due to elastic deformation of a fixed number of contact sites at the interface of the soft conformable PDMS surfaces; and κC as a particulate thickener displays a linear dependence of F_t on W due to the entrained particles causing a load dependent number of contact sites.

The fact that κC formulated as a hydrocolloid solution without KCl (that is, a linear polymeric thickener) displays a different F_t dependency on load to κC fluid gels (particulate thickeners) provides further evidence that the fluid gel particles are entrained for lubrication at all speeds and that hydrocolloid structures dictate the tribological behaviour.

6.4. Concluding remarks

With particulate thickeners representing one of two classes of typical food thickeners, the tribology of fluid gels was investigated to complement the tribological study on linear polymeric thickeners that was discussed in the previous chapter. This was conducted by assessing fluid gel tribology as a function of volume fraction as well as particle stiffness. Since the rheological response of particulate suspensions, in relation to their particle phase volume, defines their characteristic behaviour, the bulk rheology of the same range of fluid gels was tested extensively to strengthen the understanding of their material properties.

On analysis of numerous rheological tests in comparison with model behaviour, it can be concluded that the κC fluid gels prepared here act as soft and hairy particles with linear polymeric tendencies that aggregate at low packing fractions. This behaviour is expected to result from an internal polymer network that decreases in density from the centre of particles to their edge that is formed from low interfacial tensions at the gel nuclei/matrix interface during particle formation and incomplete helix formation due to disruption from the applied shear during production.

The tribometry of fluid gels showed a reduction in friction (from that of water) that reduced on increasing particle volume fraction and Young's modulus. The boundary friction force followed a linear dependence on normal load as the particles act as surface asperities increasing in number of contacting points with normal load. Contrary to the bulk rheological behaviour of fluid gels which is dominated by particle-particle interactions and, hence, volume fraction, tribometry showed a strong dependence on particle Young's modulus. This is due to the particles being squeezed between the tribometry surfaces such that their strength against compression determines the ball-on-disc surface separation and, therefore, lubrication and the volume fraction determines the number of particles in the contact. Results in this

chapter, therefore, show a clear example of bulk rheological properties failing to translate to tribological trends, where a structural explanation is required to understand the behaviour of both.

Chapter 7.

Conclusions and Future Recommendations

The aim of this thesis was to advance the understanding of fluid gel formation and properties, and hydrocolloid tribology. Tribology was studied because previous research has shown strong correlations between tribological data and fat-related textural attributes. Hydrocolloids have previously been used in the formulation of reduced fat foods; thus understanding the influence of hydrocolloid structures on tribology will assist the design of texturally acceptable low-fat foods. This study is particularly relevant to Cargill who distribute hydrocolloids to food industries and therefore require a detailed understanding of how their ingredients influence lubrication and how they can be formulated by their customers to provide aqueous structures as alternatives to fat.

To conduct this study, fluid gels were prepared by sheared gelation and were characterised using a wide range of techniques. Their processing conditions were also manipulated to control the ratio of sheared to quiescent gelation thereby probing their formation process. Hydrocolloid tribology was considered in terms of polymeric and particulate structures. These structures are known to control flow properties and mixing efficiencies which can influence performance, texture and the perception of tastants and aromas. However, their structural influence on tribology, which is also relevant for texture perception, is not so well understood. To address this, a fundamental study was made to probe the influence of polymer chain conformation and concentration, and particulate volume fraction (identified through a novel technique employing centrifugation) and particle modulus, on aqueous soft-tribometry. The influence of salt on tribology was also investigated by testing a range of salts within the Hofmeister series with and without hydrocolloids. Additionally, the properties and formation of hydrophilic PDMS surfaces using a one-step modification was investigated. Furthermore, a preliminary study was conducted to identify input parameters and

tribopairs that minimise the error margins of tribometry data whilst maximising the discrimination between different lubricants.

The main conclusions from the results chapters of this thesis are summarised in the two subsequent sub chapters.

7.1. Understanding fluid gel formation and material properties

- **KCl concentration determines fluid gel particle size and storage stability.**

κC fluid gels prepared with high KCl concentrations consist of large particulates due to increased rates of gelation and therefore growth of particles. At low KCl concentrations, the fluid gel particulate structures are unstable against storage because the T_m is low enough to allow a significant degree of quiescent, and therefore inter-particle, molecular rearrangements. Thus, the production of κC fluid gels with small particulate structures that are stable on storage requires the KCl concentration to be within an appropriate range.

- **κC fluid gels have weaker polymeric gelled networks than quiescently formed gels.**

DSC tests demonstrated that fluid gels have lower enthalpies of melting and lower melting temperatures than their quiescently cooled counterparts. This is a result of fewer helical residues and smaller regions of aggregated helices causing a reduction in gel strength and an increase in κC saccharide units in the un-ordered domain *i.e.* providing lose polymer chains or 'hairs'. Crucially, κC fluid gel particles have different internal structures to quiescently formed uniform gels and therefore are not analogous to sheared (broken down) quiescent gels or particles formed within quiescently cooled w/o emulsions.

- **More than 98% of the molecular ordering process is required to take place under shear to produce κC fluid gels without large particulates.**

The temperature at which gelled material exits the sheared environment of a pin-stirrer was used to control the ratio of sheared to quiescent gelation. With > 98.4% of the gelation process taking place under shear, the exit temperature can then be used to control interparticle molecular ordering of surface 'hairs' which increase bulk storage modulus and yield stress. If these inter-connected particle fluid gels are then sheared, the bridges are irreversibly cleaved. Such properties could be useful for products requiring solid-like attributes at rest that can be sheared during application to yield a liquid-like response.

- **The volume fraction of fluid gels can be determined from their centrifugation provided the influence of centrifugation on particle compression is incorporated into the calculation.**

A method for determining fluid gel volume fractions was described, whereby fluid and quiescently formed gels are formed with identical ingredients and are then subjected to the same centrifugation process to identify the solid content of fluid gels and the stress induced compressibility of the gel networks.

- **κC fluid gels behave as soft and hairy particles that aggregate at low phase volumes.**

The hairy and deformable structures of fluid gel particles cause them to have a rheological behaviour that lies between that of linear entangled polymers and hard-spheres. This allows particle overlap to occur to an extent such that a close packing behaviour of the particles is not observed. Their structures also allow for elastic dominated responses and

thixotropy at low particle phase volumes whilst flowing with a shear thinning behaviour after yielding.

- **On increasing the κC concentration, fluid gel particle diameters decrease whilst particle phase volumes and Young's moduli increase.**

This has the effect of increasing bulk viscosity and storage modulus. This is largely due to the increased particle phase volumes with κC concentration. This was demonstrated by testing viscosity and storage modulus against volume fraction and κC concentration where it was observed that volume fraction was a more significant variable since particle-particle interactions dominate flow behaviour. Conversely, their tribological properties were strongly dependent on particle Young's moduli since particle compressibility influences surface-surface contact.

- **Mixing fluid gels of differing particle Young's moduli provides further control over their material response.**

Whilst the properties of fluid gels can be controlled through their exit temperature on production, κC concentration and volume fraction (and other parameters not studied here such as pin-stirrer shear rate, flow rate and salt concentration within the appropriate range), further control can be provided by mixing samples of different particle properties. This can allow products to have high storage moduli and low yield stresses due to the presence of stiff and soft particles, respectively, and is expected to provide a textural response tending towards 'creaminess'.

7.2. Understanding hydrocolloid tribology

- **The chain conformation that a polysaccharide adopts in solution is directly attributable to its ability to entrain for lubrication.**

This conclusion was made from a test conducted by assessing the boundary lubrication of a range of polysaccharides that vary in chain expansion coefficients from random coil to extended chain and rigid-rods. Whilst an incremental increase in concentration results in an increase in viscosity for all polysaccharides, the effect on boundary friction is dependent on polysaccharide conformation where it is increased for random coils and reduced for expanded conformations. This is due to the structure of long chain polymers influencing alignment to flow and therefore entrainment, and highlights the significance of ingredient structures on tribological response.

- **The presence of chain entanglements at high shear influences tribology in a mixed regime of lubrication.**

Random coil polysaccharides are unable to disentangle in concentrated solutions under high shear conditions ($\dot{\gamma}$ = 3500 s^{-1}) whilst more expanded structures under the same conditions of shear and concentration fully disentangle providing single entity polymer chain behaviour. This influences friction because entangled solutions restrict solvent and polymer entrainment for lubrication.

- **Salts have a significant influence on boundary friction.**

Salts in water reduce boundary friction by surface-bound hydrated-ions forming a boundary film. Salts also induce adsorption of polysaccharides to tribo surfaces thereby

providing lubrication *via* surface-bound hydrated-polymers. The influence of this on in-mouth perception remains to be seen and will be discussed in the following section on future recommendations. However, it is certain that salts strongly influence boundary friction; thus, this conclusion is an important factor to consider in the design of tribological experiments.

- **The particle elasticity of fluid gels influences ball-on-disc surface separation and volume fraction influences the number of particles entrained.**

On increasing the volume fraction of fluid gel particles the boundary friction initially decreases, then plateaus, then decreases again. These transitions represent the number of particles being entrained in the contact and do not correlate with rheological properties. Less deformable particles provide lower friction coefficients due to a reduction in ball-and-disc contact. Consequently, whilst the volume fraction strongly dictates rheological properties, particle deformability strongly influences tribological properties.

- **The influence of normal force on friction is dependent on thickener type.**

Polymer thickened systems display a friction force dependence on normal load consistent with a fixed number of contact sites whose area increases with load. Particulate thickened systems have behaviour consistent with a load dependent number of contact sites due to a greater number of particles being able to make contact with both surfaces as the load is increased.

- **Fluid gel particles smaller than the surface roughness dimensions are entrained for lubrication at all speeds.**

The κC fluid gels produced in this study had a diameter ~ 1 μm that were not detected on consumption and could fit within the surface irregularities of the tribo surfaces and so provide lubrication *via* entrainment at all rotation speeds.

- **The structures expected in the ball-and-disc contact determine tribological behaviour which cannot be predicted from rheological response.**

This is a key conclusion from this thesis and suggests that the microstructure of foods is important in determining textural attributes and that tribology is an important material property to study alongside rheology in the formulation of low-fat foods with acceptable mouth-feel.

7.3. Future recommendations

This section aims to suggest areas that warrant further research based on speculation and the conclusions made in this study.

- **Investigate the production and properties of mixed hydrocolloid fluid gel systems**

Mixing fluid gel samples composed of different particle stiffness's was shown to form products with interesting material properties and potential use in industrial application for generating a 'creamy' response from aqueous suspensions. This concept of mixing hydrocolloid systems in fluid gel applications should be extended to the following:

  - Fluid gels prepared separately, from *e.g.* κC and pectin, that are subsequently mixed together.
  - Fluid gels prepared from one hydrocolloid, *e.g.* κC, diluted with the solution of another non-gelling hydrocolloid. This would allow for control over the particulate volume fraction as well as the continuous phase viscosity. Furthermore, the effect of diluting with hydrocolloid solutions that are known to associate with κC, *e.g.* locust bean gum, could be compared to that of a hydrocolloid which doesn't interact with κC *e.g.* xanthan gum.
  - Fluid gels prepared from the sheared gelation of a mixture of two different heated and hydrated hydrocolloids. The hydrocolloids to be mixed could associate with κC, *e.g.* locust bean gum, or cause phase separation *e.g.* maltodextrin. The κC/LBG mixed fluid gels would be expected to form particles with increased stiffness due to their synergistic interaction. The κC/maltodextrin mixed fluid gels may separate forming new gel particle structures or reduce the κC gelation rate thereby decreasing their particle diameters.

- **Investigate the tribology of uniform κC microgels**

Whilst the rheology of the uniform κC microgels produced *via* the w/o emulsion route has been extensively studied, the tribology of these systems has not. In order to conduct this study, the oil and surfactants used for their formation will be required to be either sufficiently removed or show negligible impact on tribology. It is expected that they will behave similarly to fluid gels because the tribological behaviour of the latter was shown to be dependent on the number of particles in the contact and particle stiffness *i.e.* particle hairiness seems irrelevant to tribological behaviour, however, this needs to be confirmed.

- **Extend the tribological knowledge on the dependence of friction on the ratio of the surface roughness dimensions to particle diameters.**

In the present study the tribology of κC fluid gel particles smaller than the surface roughness dimensions were shown to entrain for lubrication at all speeds and the study by Gabriele *et al.* (2010) showed particle exclusion of agarose particles larger than the surface irregularities. However, this needs to be extended to particles that are far smaller than the surface roughness dimensions. This could be achieved by testing 100 nm fluid gel particles using the PDMS surfaces described in this thesis, or, more feasibly, testing the κC fluid gels described here with PDMS surfaces moulded onto sandblasted plates that provide a centre line average (R_a) roughness of ~ 10 μm. It is expected that a very high ratio of roughness/diameter will result in a boundary tribological behaviour where the particles are not excluded, and nor will they provide lubrication (at volume fractions lower than required for multiple particle entrainment). The reason for this prediction is that the particles will be too small to be in contact with both the ball and disc (given the irregularities) and, therefore, will not provide

surface separation in boundary conditions. Of course, at speeds great enough for a mixed regime of lubrication, the particles would reduce friction at all volume fractions due to the increased bulk viscosity.

A study in this area could potentially provide an explanation for the observed dependence of microparticulated whey protein concentrate diameter on oral perception which was studied by Singer *et al.* (1990). The study by Singer *et al.* showed a watery/empty perception for particles below 0.1 μm, a creaminess perception between 0.1 and 3 μm and powdery to gritty sensations for particles larger than 3 μm. Thus, the irregularities of the tongue and hard palate may be responsible for providing watery sensation with very small particles due to a lack of lubrication, whilst very large particles are detected as such on the oral mucosa, and intermediate diameter particles provide lubrication by partial separation of the tongue-palate without the perception of 'particulates'. This hypothesis should be tested tribologically.

- **Investigate the influence of hydrocolloid tribology on sensory perception**

This thesis has focused on the influence of ingredients and processing conditions on hydrocolloid microstructure, and the influence of those structures on tribology. The structure of hydrocolloids was shown in this thesis to influence tribology; and, since tribology has previously been shown to determine textural attributes, it is expected that hydrocolloid structures will influence texture perception. However, this needs to be tested to fully understand the significance of tribology in food formulation research.

The influence of polysaccharide chain conformation and salts on sensory perception needs to be identified. Additionally, the relevance of tribology on sensory perception could be

tested by preparing a range of fluid gels that vary in their tribological properties whilst having similar rheology. An example of such a test will now be briefly outlined.

A range of κC fluid gels can be designed where the samples vary in particle stiffness and have volume fractions such that their viscosities (at *e.g.* $\dot{\gamma}$ = 10 s^{-1}) or storage moduli (at *e.g.* 10 Pa, 1 Hz) are roughly equivalent. A screened panel trained in texture perception should then be asked to generate a list of identified textural attributes perceived during the first bite, mastication and residual/after-feel effects once swallowed. The attributes perceived during the latter stages of consumption are most likely to relate to tribological properties since the film thickness between the tongue and palate will then resemble that analysed instrumentally. A ranking test can then be used whereby the panel are asked to rank the samples according to an attribute selected from the attribute generation stage at a late stage of oral processing (this could be, for example, creaminess or slipperiness). The samples should be presented to the panel as a randomised complete block design (samples should not be presented in the same order of succession to each panellist in order to eliminate ordering effects) and the results analysed using Friedman's analysis of rank to determine if there are significant differences between any of the samples.

On the basis of the results presented in this thesis, it is expected that such a test would reveal a significant difference in the perception of boundary regime related textural attributes between the most and least deformable particles, despite the samples being designed to have similar rheological properties.

Chapter 8.

References

Adams, S., Frith, W. J. & Stokes, J. R. 2004. Influence of particle modulus on the rheological properties of agar microgel suspensions. *Journal of Rheology,* 48**,** 1195-1213.

Amonton, G. 1699. De la résistance causée dans les machines. *Memoires de l'Académie des Sciences***,** 275-282.

Archard, J. 1957. Elastic deformation and the laws of friction. *Proceedings of the Royal Society of London. Series A. Mathematical and Physical Sciences,* 243**,** 190-205.

Baines, Z. V. & Morris, E. R. 1987. Flavour/taste perception in thickened systems: the effect of guar gum above and below c*. *Food Hydrocolloids,* 1**,** 197-205.

Barbara, K. 1998. Properties and applications of xanthan gum. *Polymer Degradation and Stability,* 59**,** 81-84.

Batchelor, G. K. & Green, J. T. 1972. The determination of the bulk stress in a suspension of spherical particles to order c^2. *Journal of Fluid Mechanics,* 56**,** 401-427.

Bhushan, B. & Hsu, S. M. 2001. Section IV: Tribology of industrial components and systems. *In:* BHUSHAN, B. (ed.) *Modern tribology handbook.* CRC. 969-1644.

Bialek, J., Jones, M. & Norton, I. 1999. Pourable edible aqueous-continuous emulsions. *Patent WO/1999/002,047*.

Bongaerts, J. H. H., Cooper-White, J. J. & Stokes, J. R. 2009. Low Biofouling Chitosan-Hyaluronic Acid Multilayers with Ultra-Low Friction Coefficients. *Biomacromolecules,* 10**,** 1287-1294.

Bongaerts, J. H. H., Fourtouni, K. & Stokes, J. R. 2007. Soft-tribology: Lubrication in a compliant PDMS-PDMS contact. *Tribology International,* 40**,** 1531-1542.

Bowden, F. P. & Tabor, D. 1954. *The Friction and Lubrication of Solids,* Part 1, Oxford University Press.

Bowden, F. P. & Tabor, D. 1964. *The Friction and Lubrication of Solids,* Part 2, Oxford University Press.

Breslin, P., Gilmore, M., Beauchamp, G. & Green, B. 1993. Psychophysical evidence that oral astringency is a tactile sensation. *Chemical senses,* 18**,** 405.

Brown, C. R. T., Cutler, A. N. & Norton, I. T. 1996. *Liquid based composition comprising gelling polysaccharide capable of forming a reversible gel and a method for preparing such composition, EP0355908*.

Caggioni, M., Spicer, P. T., Blair, D. L., Lindberg, S. E. & Weitz, D. A. 2007. Rheology and microrheology of a microstructured fluid: The gellan gum case. *Journal of Rheology,* 51**,** 851.

Cargill. 2012a. *http://www.cargilltexturizing.com, Last accessed February 2013* [Online].

Cargill. 2012b. *https://www.cargill.com, Last Accessed February 2013* [Online].

Carvalho, W. & Djabourov, M. 1997. Physical gelation under shear for gelatin gels. *Rheologica Acta,* 36**,** 591-609.

Cassin, G., Appelqvist, I., Normand, V. & Norton, I. T. 2000. Stress-induced compaction of concentrated dispersions of gel particles. *Colloid & Polymer Science,* 278**,** 777-782.

Cassin, G., Heinrich, E. & Spikes, H. 2001. The Influence of Surface Roughness on the Lubrication Properties of Adsorbing and Non-Adsorbing Biopolymers. *Tribology Letters,* 11**,** 8.

Chalupa, W. F. 1997. *Concentrated gellan gum dispersion for use in fluid gel applications*. WO/1996/039047.

Chen, J. & Stokes, J. R. 2012. Rheology and tribology: Two distinctive regimes of food texture sensation. *Trends in Food Science & Technology,* 25**,** 4-12.

Chen, M., Briscoe, W. H., Armes, S. P. & Klein, J. 2009. Lubrication at Physiological Pressures by Polyzwitterionic Brushes. *Science,* 323**,** 1698-1701.

Chojnicka-Paszun, A., De Jongh, H. H. J. & De Kruif, C. G. 2012. Sensory perception and lubrication properties of milk: Influence of fat content. *International Dairy Journal,* 26**,** 15-22.

Chojnicka, A., De Jong, S., De Kruif, C. G. & Visschers, R. W. 2008. Lubrication properties of protein aggregate dispersions in a soft contact. *Journal of Agricultural and Food Chemistry,* 56**,** 1274-82.

Chronakis, L. S. & Kasapis, S. 1995. A rheological study on the application of carbohydrate-protein incompatibility to the development of low fat commercial spreads. *Carbohydrate Polymers,* 28**,** 367-373.

Clarke, R. J. & Lüpfert, C. 1999. Influence of anions and cations on the dipole potential of phosphatidylcholine vesicles: a basis for the Hofmeister effect. *Biophysical journal,* 76**,** 2614-2624.

Clegg, S. M. 1995. Thickeners, gels and gelling agents. *In:* BECKETT, S. T. (ed.) *Physico-chemical aspects of food processing.* Springer. 117-141.

Connelly, R. W. & Greener, J. 1985. High-Shear Viscometry with a Rotational Parallel-Disk Device. *Journal of Rheology,* 29**,** 209-226.

Conway, B. E. & Ayranci, E. 1999. Effective Ionic Radii and Hydration Volumes for Evaluation of Solution Properties and Ionic Adsorption. *Journal of Solution Chemistry,* 28**,** 163-192.

Cross, M. M. 1965. Rheology of non-Newtonian fluids: A new flow equation for pseudoplastic systems. *Journal of Colloid Science,* 20**,** 417-437.

De Vicente, J., Spikes, H. A. & Stokes, J. R. 2006a. Viscosity Ratio Effect in the Emulsion Lubrication of Soft EHL Contact. *Journal of Tribology,* 128**,** 795-800.

De Vicente, J., Stokes, J. R. & Spikes, H. A. 2005. Lubrication properties of non-adsorbing polymer solutions in soft elastohydrodynamic (EHD) contacts. *Tribology International,* 38**,** 515-526.

De Vicente, J., Stokes, J. R. & Spikes, H. A. 2006b. Soft lubrication of model hydrocolloids. *Food Hydrocolloids,* 20**,** 483-491.

De Wijk, R. A. & Prinz, J. F. 2005. The role of friction in perceived oral texture. *Food Quality and Preference,* 16**,** 121-129.

De Wijk, R. A., Prinz, J. F. & Janssen, A. M. 2006. Explaining perceived oral texture of starch-based custard desserts from standard and novel instrumental tests. *Food Hydrocolloids,* 20**,** 24-34.

De Wijk, R. A., Van Gemert, L. J., Terpstra, M. E. J. & Wilkinson, C. L. 2003. Texture of semi-solids; sensory and instrumental measurements on vanilla custard desserts. *Food Quality and Preference,* 14**,** 305-317.

Donose, B. C., Vakarelski, I. U. & Higashitani, K. 2005. Silica Surfaces Lubrication by Hydrated Cations Adsorption from Electrolyte Solutions. *Langmuir,* 21**,** 1834-1839.

Dresselhuis, D. M., De Hoog, E. H. A., Cohen Stuart, M. A. & Van Aken, G. A. 2008. Application of oral tissue in tribological measurements in an emulsion perception context. *Food Hydrocolloids,* 22**,** 323-335.

Dresselhuis, D. M., De Hoog, E. H. A., Stuart, M. a. C. & Van Aken, G. A. 2007a. Tribology as a Tool to Study Emulsion Behaviour in the Mouth. *In:* DICKINSON, E. & LESER, M. (eds.) *Food Colloids; self assembly and material science. Part V. Texture, Rheology and Sensory Perception.* Cambridge: Royal Society of Chemistry. 451-462.

Dresselhuis, D. M., Klok, H. J., Stuart, M. a. C., Vries, R. J., Aken, G. A. & Hoog, E. H. A. 2007b. Tribology of o/w Emulsions Under Mouth-like Conditions: Determinants of Friction. *Food Biophysics,* 2**,** 158-171.

Duracher, D., Elaïssari, A. & Pichot, C. 1999. Preparation of poly(N-isopropylmethacrylamide) latexes kinetic studies and characterization. *Journal of Polymer Science Part A: Polymer Chemistry,* 37**,** 1823-1837.

Einstein, A. 1906. A new determination of molecular dimensions. *Annalen der Physik (ser. 4),* 19**,** 289-306.

Eldridge, J. E. & Ferry, J. D. 1954. Studies of the Cross-linking Process in Gelatin Gels. III. Dependence of Melting Point on Concentration and Molecular Weight. *The Journal of Physical Chemistry,* 58**,** 992-995.

Ellis, A. & Jacquier, J. 2009. Manufacture and characterisation of agarose microparticles. *Journal of Food Engineering,* 90**,** 141-145.

Ferry, A. L., Hort, J., Mitchell, J. R., Cook, D. J., Lagarrigue, S. & Valles Pamies, B. 2006. Viscosity and flavour perception: Why is starch different from hydrocolloids? *Food Hydrocolloids,* 20**,** 855-862.

Ferry, J. D. 1980. *Viscoelastic properties of polymers,* John Wiley & Sons Inc.

Flickinger, G. & Zukoski, C. 2002. Rheology of aqueous polyurethane dispersions: Links between flow and particle interaction. *Journal of Rheology,* 46**,** 455.

Friedman, H. H., Whitney, J. E. & Szczesniak, A. S. 1963. The Texturometer—A New Instrument for Objective Texture Measurement. *Journal of Food Science,* 28**,** 390-396.

Frith, W. J., Garijo, X., Foster, T. J. & Norton, I. T. 2002. Microstructural origins of the rheology of fluid gels. *In:* WILLIAMS, P. A. & PHILLIPS, G. O. (eds.) *Gums and stabilisers for the food industry 11*. 95–103.

Frith, W. J. & Norton, I. T. 2000. Mechanical properties of model composites produced from food biopolymers: influence of biopolymer-biopolymer interfacial properties. *Supramolecular and colloidal structures in biomaterials and biosubstrates: proceedings of the Fifth Royal Society-Unilever Indo-UK Forum in Materials Science and Engineering,* Imperial College Press**,** 295–305.

Gabriele, A. 2011. *Fluid Gels: formation, production and lubrication.* Ph.D., University of Birmingham.

Gabriele, A., Spyropoulos, F. & Norton, I. T. 2009. Kinetic study of fluid gel formation and viscoelastic response with kappa-carrageenan. *Food Hydrocolloids,* 23**,** 2054-2061.

Gabriele, A., Spyropoulos, F. & Norton, I. T. 2010. A conceptual model for fluid gel lubrication. *Soft Matter,* 6**,** 4205-4213.

Gidley, M. J. & Nishinari, K. 2009. Physico-chemistry of (1,3)-b-glucans. *In:* BACIC, A., FINCHER, G. B. & STONE, B. (eds.) *Chemistry, Biochemistry, and Biology of 1-3 Beta Glucans and Related Polysaccharides.* Academic Press. 47-118.

Goodall, D. M. & Norton, I. T. 1987. Polysaccharide conformations and kinetics. *Accounts of Chemical Research,* 20**,** 59-65.

Greenwood, J. & Williamson, J. 1966. Contact of nominally flat surfaces. *Proceedings of the Royal Society of London. Series A. Mathematical and Physical Sciences,* 295**,** 300-319.

Guinard, J.-X. & Mazzucchelli, R. 1996. The sensory perception of texture and mouthfeel. *Trends in Food Science & Technology,* 7**,** 213-219.

Harding, S. E. 1997. The intrinsic viscosity of biological macromolecules. Progress in measurement, interpretation and application to structure in dilute solution. *Progress in Biophysics and Molecular Biology,* 68**,** 207-262.

Harding, S. E., Day, K., Dhami, R. & Lowe, P. M. 1997. Further observations on the size, shape and hydration of kappa-carrageenan in dilute solution. *Carbohydrate Polymers,* 32**,** 81-87.

He, Y., Shao, Q., Chen, S. & Jiang, S. 2011. Water Mobility: A Bridge between the Hofmeister Series of Ions and the Friction of Zwitterionic Surfaces in Aqueous Environments. *The Journal of Physical Chemistry C,* 115**,** 15525-15531.

Heeb, R., Lee, S., Venkataraman, N. V. & Spencer, N. D. 2009. Influence of salt on the aqueous lubrication properties of end-grafted, ethylene glycol-based self-assembled monolayers. *ACS Applied Materials & Interfaces,* 1**,** 1105-1112.

Hermansson, A.-M. 1989. Rheological and microstructural evidence for transient states during gelation of kappa-carrageenan in the presence of potassium. *Carbohydrate Polymers,* 10**,** 163-181.

Hertz, H. 1881. On the contact of elastic solids. *Journal für die reine und angewandte Mathematik,* 92**,** 156–171.

Hofmeister, F. 1888. Zur lehre von der wirkung der salze. *Naunyn-Schmiedeberg's Archives of Pharmacology,* 25**,** 1-30.

Holmlin, R. E., Chen, X., Chapman, R. G., Takayama, S. & Whitesides, G. M. 2001. Zwitterionic SAMs that Resist Nonspecific Adsorption of Protein from Aqueous Buffer. *Langmuir,* 17**,** 2841-2850.

Huggins, M. L. 1942. The Viscosity of Dilute Solutions of Long-Chain Molecules. IV. Dependence on Concentration. *Journal of the American Chemical Society,* 64**,** 2716-2718.

Hutchings, J. & Lillford, P. 1988. The perception of food texture: the philosophy of the breakdown path. *Journal of Texture Studies,* 19**,** 103-115.

Israelachvili, J. N. 2011. Interactions involving polar molecules. *Intermolecular and Surface Forces: Revised Third Edition.* 3 ed.: Academic press. 71-90.

Jerker, P. 1986. Salt-promoted adsorption: Recent developments. *Journal of Chromatography B: Biomedical Sciences and Applications,* 376**,** 331-341.

Kasapis, S., Morris, E. R., Norton, I. T. & Brown, C. R. T. 1993a. Phase equilibria and gelation in gelatin/maltodextrin systems - Part III: phase separation in mixed gels. *Carbohydrate Polymers,* 21**,** 261-268.

Kasapis, S., Morris, E. R., Norton, I. T. & Clark, A. H. 1993b. Phase equilibria and gelation in gelatin/maltodextrin systems - Part I: gelation of individual components. *Carbohydrate Polymers,* 21**,** 243-248.

Kilcast, D. & Clegg, S. 2002. Sensory perception of creaminess and its relationship with food structure. *Food Quality and Preference,* 13**,** 609-623.

Kim, Y. C., Kim, S.-H., Kim, D., Park, S.-J. & Park, J.-K. 2010. Plasma extraction in a capillary-driven microfluidic device using surfactant-added poly(dimethylsiloxane). *Sensors and Actuators B: Chemical,* 145**,** 861-868.

Kokini, J. L. 1985. Fluid and semi-solid food texture and texture-taste interactions. *Food Technology,* 39**,** 86-92.

Kokini, J. L. 1987. The physical basis of liquid food texture and texture-taste interactions. *Journal of Food Engineering,* 6**,** 51-81.

Koumakis, N., Pamvouxoglou, A., Poulos, A. S. & Petekidis, G. 2012. Direct comparison of the rheology of model hard and soft particle glasses. *Soft Matter,* 8**,** 4271-4284.

Kozlov, M., Quarmyne, M., Chen, W. & Mccarthy, T. J. 2003. Adsorption of Poly(vinyl alcohol) onto Hydrophobic Substrates. A General Approach for Hydrophilizing and Chemically Activating Surfaces. *Macromolecules,* 36**,** 6054-6059.

Kraemer, E. O. 1938. Molecular Weights of Celluloses and Cellulose Derivates. *Industrial & Engineering Chemistry,* 30**,** 1200-1203.

Krieger, I. M. & Dougherty, T. J. 1959. A Mechanism for Non-Newtonian Flow in Suspensions of Rigid Spheres. *Transactions of the Society of Rheology,* 3**,** 137-152.

Krzeminski, A., Wohlhüter, S., Heyer, P., Utz, J. & Hinrichs, J. 2012. Measurement of lubricating properties in a tribosystem with different surface roughness. *International Dairy Journal,* 26**,** 23-30.

Kunz, W., Henle, J. & Ninham, B. W. 2004a. 'Zur Lehre von der Wirkung der Salze' (about the science of the effect of salts): Franz Hofmeister's historical papers. *Current Opinion in Colloid & Interface Science,* 9**,** 19-37.

Kunz, W., Lo Nostro, P. & Ninham, B. 2004b. The present state of affairs with Hofmeister effects. *Current Opinion in Colloid & Interface Science,* 9**,** 1-18.

Launay, B., Cuvelier, G. & Martinez-Reyes, S. 1997. Viscosity of locust bean, guar and xanthan gum solutions in the Newtonian domain: a critical examination of the log $(\eta_{sp})_o$ - log $C[\eta]_o$ master curves. *Carbohydrate Polymers,* 34**,** 385-395.

Lee, S., Iten, R., Müller, M. & Spencer, N. D. 2004. Influence of Molecular Architecture on the Adsorption of Poly(ethylene oxide)−Poly(propylene oxide)−Poly(ethylene oxide) on PDMS Surfaces and Implications for Aqueous Lubrication. *Macromolecules,* 37**,** 8349-8356.

Lee, S. & Spencer, N. D. 2008. Poly(l-lysine)-graft-poly(ethylene glycol): a versatile aqueous lubricant additive for tribosystems involving thermoplastics. *Lubrication Science,* 20**,** 21-34.

Li, G., Cheng, G., Xue, H., Chen, S., Zhang, F. & Jiang, S. 2008. Ultra low fouling zwitterionic polymers with a biomimetic adhesive group. *Biomaterials,* 29**,** 4592-4597.

Liang, J. N., Stevens, E. S., Morris, E. R. & Rees, D. A. 1979. Spectroscopic origin of conformation-sensitive contributions to polysaccharide optical activity: Vacuum-ultraviolet circular dichroism of agarose. *Biopolymers,* 18**,** 327-333.

Lo Nostro, P., Fratoni, L., Ninham, B. W. & Baglioni, P. 2002. Water Absorbency by Wool Fibers: Hofmeister Effect. *Biomacromolecules,* 3**,** 1217-1224.

Lopez-Sanchez, P., Chapara, V., Schumm, S. & Farr, R. 2011. Shear Elastic Deformation and Particle Packing in Plant Cell Dispersions. *Food Biophysics***,** 1-14.

Ludema, K. C. 2001. Friction. *In:* BHUSHAN, B. (ed.) *Modern tribology handbook.* CRC. 205-234.

Malone, M. E., Appelqvist, I. a. M. & Norton, I. T. 2003. Oral behaviour of food hydrocolloids and emulsions. Part 1. Lubrication and deposition considerations. *Food Hydrocolloids,* 17**,** 763-773.

Mancera, R. L. 1999. Influence of Salt on Hydrophobic Effects: A Molecular Dynamics Study Using the Modified Hydration-Shell Hydrogen-Bond Model. *The Journal of Physical Chemistry B,* 103**,** 3774-3777.

Miller, J. L. & Watkin, K. L. 1996. The influence of bolus volume and viscosity on anterior lingual force during the oral stage of swallowing. *Dysphagia,* 11**,** 117-124.

Mitchell, J. R. 2008. Perception of starch and hydrocolloid thickened foods: Why mixing in the mouth is key. *Agro Food Industry Hi-Tech,* 19**,** 48-49.

Moro, T., Takatori, Y., Ishihara, K., Konno, T., Takigawa, Y., Matsushita, T., Chung, U.-I., Nakamura, K. & Kawaguchi, H. 2004. Surface grafting of artificial joints with a biocompatible polymer for preventing periprosthetic osteolysis. *Nature Materials,* 3**,** 829-836.

Morris, E. R., Cutler, A. N., Ross-Murphy, S. B., Rees, D. A. & Price, J. 1981. Concentration and shear rate dependence of viscosity in random coil polysaccharide solutions. *Carbohydrate Polymers,* 1**,** 5-21.

Morris, E. R., Rees, D. A., Norton, I. T. & Goodall, D. M. 1980a. Calorimetric and chiroptical evidence of aggregate-driven helix formation in carrageenan systems. *Carbohydrate Research,* 80**,** 317-323.

Morris, E. R., Rees, D. A. & Robinson, G. 1980b. Cation-specific aggregation of carrageenan helices: Domain model of polymer gel structure. *Journal of Molecular Biology,* 138**,** 349-362.

Myant, C., Spikes, H. A. & Stokes, J. R. 2010. Influence of load and elastic properties on the rolling and sliding friction of lubricated compliant contacts. *Tribology International,* 43**,** 55-63.

Nishikawa, A. H. & Bailon, P. 1975. Lyotropic salt effects in hydrophobic chromatography. *Analytical Biochemistry,* 68**,** 274-280.

Noīk, C. & Lecourtier, J. 1993. Studies on scleroglucan conformation by rheological measurements versus temperature up to 150 °C. *Polymer,* 34**,** 150-157.

Nordgren, N., Eronen, P., Österberg, M., Laine, J. & Rutland, M. W. 2009. Mediation of the Nanotribological Properties of Cellulose by Chitosan Adsorption. *Biomacromolecules,* 10**,** 645-650.

Nordgren, N. & Rutland, M. W. 2009. Tunable Nanolubrication between Dual-Responsive Polyionic Grafts. *Nano Letters,* 9**,** 2984-2990.

Norton, A. B., Cox, P. W. & Spyropoulos, F. 2011. Acid gelation of low acyl gellan gum relevant to self-structuring in the human stomach. *Food Hydrocolloids,* 25**,** 1105-1111.

Norton, I. T., Foster, T. & Brown, R. 1998. The science and technology of fluid gels. *In:* WILLIAMS, P. A. & PHILLIPS, G. O. (eds.) *Gums and Stabilisers for the Food Industry 9.* The Royal Society of Chemistry. 259-268.

Norton, I. T., Frith, W. J. & Ablett, S. 2006. Fluid gels, mixed fluid gels and satiety. *Food Hydrocolloids,* 20**,** 229-239.

Norton, I. T., Goodall, D., Austen, K., Morris, E. & Rees, D. 1986. Dynamics of molecular organization in agarose sulphate. *Biopolymers,* 25**,** 1009-1029.

Norton, I. T., Goodall, D. M., Frangou, S. A., Morris, E. R. & Rees, D. A. 1984. Mechanism and dynamics of conformational ordering in xanthan polysaccharide. *Journal of Molecular Biology,* 175**,** 371-394.

Norton, I. T., Goodall, D. M., Morris, E. R. & Rees, D. A. 1983a. Equilibrium and dynamic studies of the disorder-order transition of kappa carrageenan. *Journal of the Chemical Society, Faraday Transactions 1: Physical Chemistry in Condensed Phases,* 79**,** 2489-2500.

Norton, I. T., Goodall, D. M., Morris, E. R. & Rees, D. A. 1983b. Role of cations in the conformation of iota and kappa carrageenan. *Journal of the Chemical Society, Faraday Transactions 1: Physical Chemistry in Condensed Phases,* 79**,** 2475-2488.

Norton, I. T., Jarvis, D. A. & Foster, T. J. 1999. A molecular model for the formation and properties of fluid gels. *International Journal of Biological Macromolecules,* 26**,** 255-261.

Norton, I. T., Smith, C. G., Frith, W. J. & Foster, T. J. 2000. The production, properties and utilisation of fluid gels. *In:* KATSUYOSHI, N. (ed.) *Hydrocolloids part 2 – Fundamentals and Applications in Food, Biology and Medicine.* Elsevier Science. 219-227.

Nucci, N. V. & Vanderkooi, J. M. 2008. Effects of salts of the Hofmeister series on the hydrogen bond network of water. *Journal of Molecular Liquids,* 143**,** 160-170.

Omari, A., Tabary, R., Rousseau, D., Calderon, F. L., Monteil, J. & Chauveteau, G. 2006. Soft water-soluble microgel dispersions: Structure and rheology. *Journal of Colloid and Interface Science,* 302**,** 537-546.

Peiffer, D. G., Kim, M. W. & Lundberg, R. D. 1986. Influence of an elongational flow field on random coil and rod-like polymers in solution. *Polymer,* 27**,** 493-502.

Phillips, G. O. & Williams, P. A. 2009. Handbook of Hydrocolloids (2nd Edition). Woodhead Publishing.

Prinz, J. F., De Wijk, R. A. & Huntjens, L. 2007. Load dependency of the coefficient of friction of oral mucosa. *Food Hydrocolloids,* 21**,** 402-408.

Putman, C. a. J., Igarashi, M. & Kaneko, R. 1995. Single-asperity friction in friction force microscopy: The composite-tip model. *Applied Physics Letters,* 66**,** 3221-3223.

Ranc, H., Elkhyat, A., Servais, C., Macmary, S., Launay, B. & Humbert, P. 2006. Friction coefficient and wettability of oral mucosal tissue: Changes induced by a salivary layer. *Colloids and Surfaces A: Physicochemical and Engineering Aspects,* 276**,** 155-161.

Ratcliffe, I., Williams, P. A., Viebke, C. & Meadows, J. 2005. Physicochemical Characterization of Konjac Glucomannan. *Biomacromolecules,* 6**,** 1977-1986.

Raviv, U. & Klein, J. 2002. Fluidity of Bound Hydration Layers. *Science,* 297**,** 1540-1543.

Rees, D. A. 1969. Conformational analysis of polysaccharides. Part II. Alternating copolymers of the agar–carrageenan–chondroitin type by model building in the computer with calculation of helical parameters. *Journal of the Chemical Society B: Physical Organic,* 1969**,** 217-226.

Rees, D. A. 1970. Conformational analysis of polysaccharides. Part V. The characterization of linkage conformations (chain conformations) by optical rotation at a single wavelength. Evidence for distortion of cyclohexa-amylose in aqueous solution. Optical rotation and the amylose conformation. *Journal of the Chemical Society B: Physical Organic***,** 877-884.

Reitsma, M. G., Cain, R. G., Biggs, S. & Smith, D. W. 2006. Observed transition from linear to non-linear friction–load behavior using a lateral force microscope. *Applied Surface Science,* 252**,** 4964-4968.

Richardson, R. K., Morris, E. R., Ross-Murphy, S. B., Taylor, L. J. & Dea, I. C. M. 1989. Characterization of the perceived texture of thickened systems by dynamic viscosity measurements. *Food Hydrocolloids,* 3**,** 175-191.

Robinson, G., Ross-Murphy, S. B. & Morris, E. R. 1982. Viscosity-molecular weight relationships, intrinsic chain flexibility, and dynamic solution properties of guar galactomannan. *Carbohydrate Research,* 107**,** 17-32.

Rochas, C. & Rinaudo, M. 1980. Activity coefficients of counterions and conformation in kappa-carrageenan systems. *Biopolymers,* 19**,** 1675-1687.

Ross-Murphy, S. B. 1995. Structure–property relationships in food biopolymer gels and solutions. *Journal of Rheology,* 39**,** 1451.

Saunders, B. R. & Vincent, B. 1999. Microgel particles as model colloids: theory, properties and applications. *Advances in Colloid and Interface Science,* 80**,** 1-25.

Schott, H. 1984. Lyotropic numbers of anions from cloud point changes of nonionic surfactants. *Colloids and Surfaces,* 11**,** 51-54.

Senff, H. & Richtering, W. 2000. Influence of cross-link density on rheological properties of temperature-sensitive microgel suspensions. *Colloid & Polymer Science,* 278**,** 830-840.

Shama, F. & Sherman, P. 1973. Identification of stimuli controlling the sensory evaluation of viscosity II. Oral methods. *Journal of Texture Studies,* 4**,** 111-118.

Shewan, H. & Stokes, J. 2012. Biopolymer Microgel Suspension Rheology as a Function of Particle Modulus and Effective Phase Volume. *In:* WILLIAMS, P. A. & PHILLIPS, G. O. (eds.) *Gums and stabilisers for the food industry 16.* The Royal Society of Chemistry. 165-174.

Singer, N. & Dunn, J. 1990. Protein microparticulation: the principle and the process. *Journal of the American College of Nutrition,* 9**,** 388.

Singer, N. S., Yamamoto, S. & Latella, J. 1988. Protein product base. US Patent 4,734,287.

Smith, W. V. & Ewart, R. H. 1948. Kinetics of Emulsion Polymerization. *The Journal of Chemical Physics,* 16**,** 592-599.

Spikes, H. A. 1996. Direct Observation of Boundary Layers *Langmuir,* 12**,** 4567-4573.

Spikes, H. A. 1997. Mixed lubrication - an overview. *Lubrication Science,* 9**,** 221-253.

Stachowiak, G. W. & Batchelor, A. W. 2005. Physical properties of lubricants. *Engineering Tribology.* Butterworth-Heinemann. 11-50.

Stokes, J. R. 2011. Rheology of Industrially Relevant Microgels. *In:* FERNANDEZ-NIEVES, A., WYSS, H., MATTSSON, J. & WEITZ, D. A. (eds.) *Microgel Suspensions: Fundamentals and Applications.* Wiley-VCH. 327-353.

Stokes, J. R., Macakova, L., Chojnicka-Paszun, A., De Kruif, C. G. & De Jongh, H. H. J. 2011. Lubrication, Adsorption, and Rheology of Aqueous Polysaccharide Solutions. *Langmuir,* 27**,** 3474-3484.

Stribeck, R. 1902. Die wesentlischen Eigenschaften der Gleit- und Rollenlager. *Zeitschrift des Vereines deutscher Ingenieure***,** 46 (37): 1341-1348 (pt I) & 46 (38):1432-1438 (pt II) & 46 (39): 1463–1470 (pt III).

Sworn, G., Sanderson, G. R. & Gibson, W. 1995. Gellan gum fluid gels. *Food Hydrocolloids,* 9**,** 265-271.

Szczesniak, A. S. & Farkas, E. 1962. Objective Characterization of the Mouthfeel of Gum Solutions. *Journal of Food Science,* 27**,** 381-385.

Szlufarska, I., Chandross, M. & Carpick, R. W. 2008. Recent advances in single-asperity nanotribology. *Journal of Physics D: Applied Physics,* 41**,** 1-39.

Tharwat, T. 2004. Application of rheology for assessment and prediction of the long-term physical stability of emulsions. *Advances in Colloid and Interface Science,* 108-109**,** 227-258.

Tombs, M. P. & Harding, S. E. 1998. Polysaccharides and their potential for biotechnology. *An introduction to polysaccharide biotechnology.* CRC. 1-46.

Torres, M. D., Moreira, R., Chenlo, F. & Vázquez, M. J. 2012. Water adsorption isotherms of carboxymethyl cellulose, guar, locust bean, tragacanth and xanthan gums. *Carbohydrate Polymers,* 89**,** 592-598.

Tylczak, J. H. 1992. Handbook, ASM, Friction, lubrication, and wear technology. *American Society for Metals,* 18**,** 184-190.

Tyle, P. 1993. Effect of size, shape and hardness of particles in suspension on oral texture and palatability. *Acta Psychologica,* 84**,** 111-118.

Vakarelski, I. U., Ishimura, K. & Higashitani, K. 2000. Adhesion between silica particle and mica surfaces in water and electrolyte solutions. *Journal of Colloid and Interface Science,* 227**,** 111-118.

Van Aken, G. A., Vingerhoeds, M. H. & De Hoog, E. H. A. 2007. Food colloids under oral conditions. *Current Opinion in Colloid & Interface Science,* 12**,** 251-262.

Vardhanabhuti, B., Cox, P. W., Norton, I. T. & Foegeding, E. A. 2011. Lubricating properties of human whole saliva as affected by β-lactoglobulin. *Food Hydrocolloids,* 25**,** 1499-1506.

Vreeman, H. J., Snoeren, T. H. M. & Payens, T. a. J. 2004. Physicochemical investigation of k-carrageenan in the random state. *Biopolymers,* 19**,** 1357-1374.

Walkenstrom, P. & Hermansson, A. M. 1998. Effects of shear on pure and mixed gels of gelatin and particulate whey protein. *Food hydrocolloids.,* 12**,** 77-87.

Wassén, S., Rondeau, E., Sott, K., Lorén, N., Fischer, P. & Hermansson, A.-M. 2012. Microfluidic production of monodisperse biopolymer particles with reproducible morphology by kinetic control. *Food Hydrocolloids,* 28**,** 20-27.

Williams, J. A. 2005a. Boundary lubrication and friction. *Engineering Tribology.* Cambridge University Press. 348-380.

Williams, J. A. 2005b. The friction of solids. *Engineering Tribology*. Cambridge University Press. 132-165.

Wolf, B., Frith, W. J. & Norton, I. T. 2001. Influence of gelation on particle shape in sheared biopolymer blends. *Journal of Rheology,* 45**,** 1141-1157.

Wolf, B., Scirocco, R., Frith, W. J. & Norton, I. T. 2000. Shear-induced anisotropic microstructure in phase-separated biopolymer mixtures. *Food Hydrocolloids,* 14**,** 217-225.

Wolfe, M. S. & Scopazzi, C. 1989. Rheology of swellable microgel dispersions: Influence of crosslink density. *Journal of Colloid and Interface Science,* 133**,** 265-277.

Yanaki, T. & Norisuye, T. 1983. Triple helix and random coil of scleroglucan in dilute solution. *Polymer Journal,* 15**,** 389-396.

Zinoviadou, K. G., Janssen, A. M. & De Jongh, H. H. 2008. Tribological properties of neutral polysaccharide solutions under simulated oral conditions. *Journal of Food Science,* 73**,** E88-94.